

Design, fabrication and
testing of miniaturized
neural recording
platform for robotic
applications in fly
sensorimotor research

PhD dissertation

Jiaqi Huang

Supervised by: Dr Holger G. Krapp

Department of Bioengineering

IMPERIAL COLLEGE LONDON

1/31/2014

Originality Declaration

The work presented in this dissertation is the result of my own work, unless otherwise specified in the text.

Jiaqi Huang

Copyright Declaration

The copyright of this thesis rests with the author and is made available under a Creative Commons Attribution Non-Commercial No Derivatives licence. Researchers are free to copy, distribute or transmit the thesis on the condition that they attribute it, that they do not use it for commercial purposes and that they do not alter, transform or build upon it. For any reuse or redistribution, researchers must make clear to others the licence terms of this work.

Acknowledgements

I feel so lucky to find Dr. Holger Krapp as my supervisor. I was completely impressed by his inspiring talk in my first lab visit. He not only gives me opportunity to live my dream, gave me the chance to do a PhD, but also patiently guided me from engineering world into the biology world. And he also taught me how to climb snow mountain, Snowdonia, which is a great experience and memory, although I was tired out in my first snow mountain climbing. I am deeply grateful for all his help during my PhD and especially recently for extremely patiently reading my thesis in such detail, and working till late in the night. Thanks Holger, I am not sure if I can find any better supervisor in the future.

It is great to have Dr. Kit Longden and Dr. Martina Wicklein as post-docs in the group. Martina taught me lots of basic knowledge in biology and showed me the electrophysiology technique of the blowfly experiment. And she is also the person initiated my project design. Her excellent schedule stopped me from getting into trouble several times. Thanks Martina! Should I have any hardcore research behaviours, they must have come from Kit. It is so great to have a super intelligent and thoughtful mentor, guided me through every detail of my project, in a way with humour and inspirations. Lots of late night experience sharing of experiments and evening conversation, discussion and encouraging would be part of my deepest imperial college memories. And a great appreciation to both of them for the review of my thesis, gave me precious feedback from my rough drafts. They are the best post-doc in lab that I met so far, as well as great parents at their own family.

Glad to have so many nice lab colleagues, Kris, Naveed, Daniel, Ben, Peter, as well as the members of mouse lab and ultrasonic on the other side of the lab space and office desk mates. We shared experiences every day and sometimes happy experiences during the night out, and an unforgettable

Snowdonia experience, the various party memories. Special thanks to Lise and Veronique's birthday encouragement talk.

Thanks to the bioengineer faculties for all the support, Kate, Brita, Allan, Martin, Laura, Gary, Simon, Aldo, Rob, etc. We had lots of fun in daily teaching, as well as Christmas party. And also thanks to my mentor Darryl Overby for all the supports.

Glad to meet all the friends in UK, shared lots of happy time in this place. That's the memories which never fade.

Eventually, thanks to my parents for bringing me to the world, raised me up, taught me independence and meaning of family. Special thanks to my cousin Yiyi.

Abstract

Blowflies are exquisite fliers and have long been established as models for sensorimotor research. Their flight performance crucially depends on both visual and mechanoreceptive feedback. Our understanding of how the nervous system integrates signals of these sensory modalities, however, leaves two important issues unresolved. First: As most experiments are performed on restrained animals, how are neural signals integrated when the animal actually moves? Second: Are neural mechanisms underlying optic-flow-based self-motion estimation modulated by mechanosensory modalities when controlling motor behaviour?

To address these questions, I have designed a mobile platform and miniaturized electrophysiological recording equipment. Here, I describe details of the platform's mechanical and electronic components, test its performance, and demonstrate that it enables high quality recordings from an identified interneuron in the fly motion vision pathway, the H1-cell, which is believed to process optic-flow, generate during self-motion. I compare the recordings obtained with my novel platform to those gathered with much bigger setups, which are orders of magnitude heavier, and characterize the responses of the H1-cell under various stimulus conditions. My results are mostly in agreement with earlier work but include new findings on pattern size-dependent responses of the cell, which are in contrast to theoretical predictions based on previous behavioural and physiological studies. To investigate how the fly uses signals from different sensory modalities to control various optomotor behaviours and potentially vision-based collision avoidance, I have established a brain machine interface on a small mobile robot that uses the neural activity of the H1-cell to control the robot's motor system.

In summary, I have created a platform for in vivo recordings of neural activity in flies on a small robot. This novel technology will enable further studies on

multisensory integration to gain new insights into the design of fly sensorimotor pathways involved in course control and collision avoidance.

Content

Originality Declaration.....	I
Copyright Declaration	I
Acknowledgements.....	II
Abstract.....	IV
Content	VI
List of figures	XI
List of tables.....	XIX
Abbreviations	XX
Prologue	1
1. Introduction.....	3
1.1. Blowfly neurobiology of flight control.....	3
1.1.1. Vision and motion.....	3
1.1.1.1. Optic flow and ego motion	3
1.1.1.2. Elementary motion detector	5
1.1.1.3. The aperture problem	7
1.1.2. The blowfly visual system.....	8
1.1.2.1. Retina	10
1.1.2.2. Lamina	11
1.1.2.3. Medulla	12
1.1.2.4. Lobula complex.....	13
1.1.2.5. H1-cell	14
1.1.3. Sensory integration	16
1.1.3.1. Inertial sensor: haltere	16

1.1.3.2.	Sensory integration for gaze stabilization	18
1.1.3.3.	Sensory integration in the neck motor system	19
1.1.3.4.	Adaptation	21
1.2.	Fly robot related work	21
1.2.1.	Robot in H1-cell closed-loop control.....	22
1.2.2.	H1-cell recordings on a rotating platform.....	23
1.2.3.	Other mobile neuron recording system	25
1.3.	Summary	25
2.	Miniaturized neural recording platform for robot applications	27
2.1.	Introduction	27
2.2.	Methods.....	30
2.2.1.	Robot selection	30
2.2.1.1.	ASURO® robot.....	31
2.2.1.2.	Lego® mindstorms NXT 2.0 robot	32
2.2.1.3.	3pi® robot with mbed® controller	33
2.2.1.4.	Summary	34
2.2.2.	Mechanical design of recording platform.....	35
2.2.2.1.	Chassis.....	35
2.2.2.2.	Fly holder.....	37
2.2.2.3.	MM1-CR-XYZ micromanipulator.....	39
2.2.2.4.	Electrode holder.....	40
2.2.2.5.	Micromanipulator holder and amplifier enclosure	40
2.2.2.6.	Stabilizing beam	42
2.2.3.	Electrical design of recording platform	43
2.2.3.1.	Amplifier design specification	43
2.2.3.2.	Amplifier system	44
2.2.4.	Systems for verification	45

2.2.4.1.	Stepper motor system.....	46
2.2.4.2.	Pattern cylinder clip and internal LED ring light	47
2.2.4.3.	Assembly and shielding of systems	48
2.2.4.4.	Blowfly preparation	49
2.2.4.5.	Programming and experiment sequences	49
2.3.	Results.....	51
2.3.1.	Instantaneous recording stability analysis	51
2.3.2.	Prolonged recording stability analysis	53
2.4.	Summary	56
3.	H1-cell response characterization using the miniaturized recording platform.....	58
3.1.	Introduction	58
3.2.	Experiment 1: H1-cell temporal frequency tuning	60
3.2.1.	Method	60
3.2.2.	Result.....	62
3.2.3.	Discussion.....	65
3.3.	Experiment 2: Halteres removed	66
3.3.1.	Method	67
3.3.2.	Result.....	68
3.3.3.	Discussion.....	70
3.4.	Experiment 3: Pattern size dependence	72
3.4.1.	Method	73
3.4.2.	Results	74
3.4.3.	Discussion.....	78
3.5.	Experiment 4: Bi-lateral H1-cells adaptation	79
3.5.1.	Method	79
3.5.2.	Result.....	80

3.5.3. Discussion.....	83
3.6. Summary	84
4. H1-cell to robot interface	87
4.1. Introduction	87
4.2. Experiment 1: robot angular velocity calibration	89
4.2.1. Method	89
4.2.2. Result.....	90
4.2.3. Conclusion	93
4.3. Experiment 2: bi-lateral neuron machine interface.....	94
4.3.1. Method	94
4.3.1.1. Dissection	95
4.3.1.2. Interface programming.....	95
4.3.1.3. System assembly.....	98
4.3.2. Results	99
4.3.3. Discussion.....	100
4.4. Summary	102
5. Summary and future work	103
5.1. Summary	103
5.2. Future work.....	104
5.2.1. Optomotor	105
5.2.2. Multi-sensory integration	106
5.2.3. Closed loop control.....	107
Bibliography	109
Appendix.....	115
Appendix 1. Schematic of miniaturized amplifier	115
Appendix 2. Source code.....	117
Appendix 3. Video link	117

List of figures

Figure 1. Self-motion and global optic flow. Top left: Optic flow generated during pure lift translation plotted as tangent vectors on a unit sphere that symbolizes the visual field. The direction of translation, A_t , defines the location of two singularities in the flow field, the focus of expansion and the focus of contraction, where no relative motion takes place. Local vectors in a translation flow field are aligned along great circles connecting the focus of expansion with the focus of contraction and point in the opposite directions to A_t . Bottom left: During pure rotation all flow vectors are aligned along parallel circles centered with the axis of rotation, A_r , and are thus oriented perpendicular to the rotation axis. The example shows a flow field as a result of a roll rotation around the longitudinal body axis. Plots on the right hand side show cylindrical projections of the flow fields into the 2-dimensional plane where each position in the visual field is defined by two angles: the (horizontal) azimuth and the (vertical) elevation. Note that the gray window in the right half of the visual field shows local flow vectors pointing in the same direction despite the fact they were generated by different ego-motions. Modified from (Krapp & Wicklein 2008).4

Figure 2. Elementary movement detector: (top left) half-detector with preferred direction stimulus moving to the right, first inducing a signal in the left then in the right input channel. The delayed signal from the first input channel coincides with the non-delayed signal from second input channel at a multiplication stage if the time it takes the stimulus to reach the second input channel corresponds to the delay, τ , in the first input channel. (top right) the same half-detector stimulated with motion in the anti-preferred direction. In this case the two inputs are de-correlated in time and no sizable output is generated. (bottom left and right) A fully directional EMD combines two mirror-symmetrical half-detectors. Motion in the detectors preferred and anti-preferred direction result in a positive and negative output of the detector, respectively. Figure modified from (Krapp & Wicklein 2008).....7

Figure 3. The aperture problem. Motion orthogonal to the edge is detected, motion parallel to the edge can not be detected.8

Figure 4. The blowfly visual system. The visual system includes: retina, lamina, medulla, lobula and lobula plate. The lobula plate receives retinotopic input from lobula and medulla, where the connecting axons cross over in the internal chiasm. In the external chiasm axons originating in the lamina cross over on their projection to the medulla. As the whole system is organized in a retinotopic way, a crossover of projections is equivalent to an inversion of the vertical image plane. Modified from (Borst and Haag, 2002a)9

Figure 5. The ommatidium. (Left) *Drosophila* photoreceptors R1-6 and R7, (right) structure of a single ommatidium with photoreceptors R1-6 (gray), R7 (purple) and R8 (green). Modified from (Yishai Michael Elyada 2009)..... 10

Figure 6. Signal transmission from photoreceptor to LMC. Transsynaptic signals are high pass filtered. Modified from (Laughlin 1984) 12

Figure 7. H1-cell preferred direction mapping. Cell morphology (inset at the bottom): The picture shows the cell's ipsilateral dendritic (input) arborizations on the left and its telo-dendritic (output) arborisations on the right. Input mediated by the left eye is propagating to the right lobula plate. The cell is viewed from the posterior side of the head. Receptive field: Local preferred directions and motion sensitivities of the H1-cell presented as motion vectors in a cylindrical representation of the spherical visual field. Azimuth = elevation = 0 degrees denotes the point in front of the animal. The H1-cell is excited mainly by back-to-front motion from around -150 deg to +15 deg in azimuth, and -45 deg to +45 deg in elevation. Modified from (Krapp et al. 2001) 15

Figure 8. Position and structure of halteres. The halteres are located at the rear of metathorax (a), one of the haltere is magnified in (b) to reveal its structural components in detail. Modified from (Hengstenberg 1993)..... 17

Figure 9. Sensory integration. (a) The blowfly is placed in a stationary pattern cylinder with white on top and black on bottom (spatial wavelength of the pattern = 360 deg). The blowfly is oscillated between $\pm 90^\circ$ at constant speed around the roll axis, for various angular velocities, where both visual system and halteres are stimulated. The head roll angle of the blowfly as a function of angular velocity was found to have a band-pass-like shape where the peak response (40 deg) occurred at around 600 deg/s. The trough value is around 50% of the peak value. (b) The blowfly was placed in a homogeneous white cylinder (no visual contrast). The animal was oscillated at constant velocity

around the roll axis for different angular velocities, where only the halteres were stimulated. The head roll angle peaked (70 deg) at around 1200 deg/s. The trough value is 0% of peak value. (c) The blowfly was kept stationary in an oscillation cylinder with black and white pattern (spatial wavelength = 30 deg). The cylinder was oscillated around the fly's roll axis at different angular velocities - under these conditions only the motion vision pathway was stimulated. The head roll angle peaked (40 deg) at around 80 deg/s. The trough value was around 30% of peak value. Modified from (Hengstenberg 1991)..... 19

Figure 10. Neck motor neuron responses to a combination of visual and haltere stimulations. In a,b,c,d. the top lines give the responses of neck motor neuron, the middle lines indicate the time course and direction of the visual stimulation, and the bottom lines show the time course of the haltere stimulus. Only in plot c the neck motor neuron generated action potentials where the fly experienced rightwards visual stimulation and haltere stimulation simultaneously. Modified from (Huston & Krapp 2009) 20

Figure 11. Closed-loop fly robot interface. (1) Two high speed cameras were mounted on a robot that was placed on a turntable. Turntable and robot were surrounded by a vertical visual grating pattern (spatial wavelength = 11 deg). (2) Rotations of the turntable generated horizontal optic flow, which was captured by the cameras and displayed on two CRT monitors. The blowfly H1-cell activity was recorded. (3,4,5) The cell's spike rate was processed and converted into a control signal, which drove the robot to compensate for the rotation of the turntable, stabilizing the visual input. Modified from (Ejaz et al. 2011)..... 23

Figure 12. Lewen's neural recording setup. The blowfly was waxed in a tube exposing only its compound eyes and proboscis. A tungsten electrode was inserted into the lobula plate from behind. The extracellular H1-cell signals were pre-amplified and passed to a second amplifier stage via a slip ring. The whole system was mounted on the shaft of a stepper motor. Modified from (Lewen et al. 2001) 24

Figure 13. ASURO robot. The robot is powered by four AAA batteries. It equipped with an ATmega8L RISC-processor (8 MHz resonator system clock), an optical line-tracer, six collision-detector switches and two odometer-

sensors. The processor can be programmed via a serial RS232 port or USB at baud rate of 2400 bps.	31
Figure 14. Lego Mindstorms NXT robot. The robot is controlled by Lego intelligent block which has an ARM core microcontroller inside. The processor is programmed via USB.	32
Figure 15. 3pi robot with mbed controller. The robot is powered by four AAA batteries. It is controlled by ATmega328 microprocessor. The internal voltage regulator boosts the motor voltage to 9.25V, guarantees its speed performance.....	33
Figure 16. Chassis disc. It determines the distance between fly and electrodes.	36
Figure 17. Chassis central rod. The component connects chassis and fly holder.....	37
Figure 18. Fly holder. The component is used to fix a fly. The two pins also act as reference electrodes.	38
Figure 19. NAI® MM1-CR-XYZ micromanipulator. This small NAI® micromanipulator is much smaller and lighter than the Narishige® MX-2 model used in our lab. But this micromanipulator is much more difficult to operate as its light weight and small scale design is achieved at the expense of its mechanical stability.	39
Figure 20. Electrode clip. (Left) This component clips the electrode holder and mounts onto the micromanipulator. (Right) The positions of electrode, electrode holder and electrode clip after assembled.....	40
Figure 21. Micromanipulator holder. This component is the connection between chassis and micromanipulator. It also serves as a faraday cage of miniaturized amplifier.	41
Figure 22. Amplifier enclosure lid. This component holds the miniaturized amplifier and mounts onto the micromanipulator holder.	42
Figure 23. Stabilizing beam. This component is used to tighten the central rod and two micromanipulator holders.	43
Figure 24. Pattern cylinder clip. This component clips paper pattern cylinder and mounts onto a stepper motor shaft.	47
Figure 25. Motor shaft connector. This component connects the platform chassis and pattern clip to the stepper motor shaft.....	48

Figure 26. Fully assembled recording platform. (A) The fly is mounted so that a recording electrode can be inserted to the lobula plate from back of the head. (B) Experimental test setup. The recording platform is mounted on top of a stepper motor shaft (bottom). The surrounding grating pattern (special wavelength = 30 deg) is connected to the shaft of the top stepper motor. (Huang and Krapp, 2013)48

Figure 27. Stimulation and response during a 10 second H1-cell recording. (A) The angular velocity curve of stimulation (here, positive and negative angular velocities refer to motion in the anti-preferred and preferred direction of H1-cell, respectively). (B) The action potentials generated by the H1-cell under stimulation as described in A. The red horizontal line indicates the threshold potential for the spike sorting. The black window marks the section of the data magnified in C. (C) The zoom-in plot of the H1-cell action potential sequence described in B. (D) The spike rate of H1-cell, calculated from the time interval (inter spike interval, ISI) between two consecutive action potentials.....52

Figure 28. Experimental stability analysis. (A) The sequence of temporal frequencies of the stimulus used in the experiment. (B) Mean and standard deviation of spike rate at 4 Hz temporal frequency. (C) Mean and standard deviation of spontaneous spike rates. (N=8) (Huang and Krapp, 2013)54

Figure 29. The H1-cell temporal frequency tuning curves under both fly rotation and pattern rotation conditions. The results are based on data from eight blowflies. Error bars give the standard error of the mean.....63

Figure 30. Extreme results obtained from individual animals: (A) The plot of individual trials of fly #1, where the variability of the spike rate is higher in pattern rotation condition. (B) the plot of individual trials of fly #2, where the variability of the spike rate is higher in fly rotation condition. (C) The boxplot of fly #1, showing similar mean spike rate to B. (D) the boxplot of fly #2, showing similar mean spike rate to C.64

Figure 31. H1-cell temporal frequency tuning curves obtained with vertical black and white stripe pattern with and without halteres. Plots A, B are trials of stimulations at various temporal frequencies. Plots C, D are means and standard deviations of the H1-cell temporal frequency tuning (N=1). Plots A, C are obtained from blowflies with halteres; Plots B, D are based on experiments in blowflies without halteres. Positive and negative temporal

frequencies correspond to visual stimuli in the preferred and anti-preferred direction of the H1-cell, respectively. The straight purple lines in plots C, D indicate the overall mean spontaneous spike rate.68

Figure 32. H1-cell temporal frequency tuning curves obtained with and without halteres in the laboratory environment. Plots A, B are trials of stimulations at various temporal frequencies. Plots C, D are means and standard deviations of the H1-cell temporal frequency tuning. Plots A, C show data from blowflies with halteres; Plot B, D present data for blowflies without halteres. As in the previous figure, negative and positive temporal frequencies indicate stimulation in the cell's preferred and anti-preferred direction, respectively. The straight purple lines in plots C, D indicate the overall mean spontaneous spike rate.69

Figure 33. Temporal frequency tuning curves as a function of angular extent of the grating during pattern rotation. Each ribbon represents the angular extent dependent spike rate for a given temporal frequency. The middle green ribbon at 0 Hz temporal frequency shows the overall mean spontaneous spike rate. Negative and positive temporal frequencies correspond to motion in the anti-preferred and preferred direction of the cell, respectively. (The plot include averages of data from 5 animals.)74

Figure 34. Side view of data shown in figure 33. Each curve shows the angular extent dependent response for one temporal frequency obtained upon pattern rotation. The blue lines give responses to null direction motion, where neurons are inhibited. The red lines give responses to preferred direction motion, where neurons are excited. (N=5).....75

Figure 35. Temporal frequency tuning curves as a function of angular extent of the grating during fly rotation. The data were gathered from the same animals (N=5) which were used to obtain the results presented in figure 33, but here the animals were rotated in the centre of the stationary pattern.76

Figure 36. The side view of the results shown in figure 35. It is the same way of presenting the data as in figure 34. Note that for angular extents greater than 32.12 deg, there is a linear relationship between pattern size and spike rate for all positive temporal frequencies.77

Figure 37. Motion adaptation experiments. The electrode was placed in the right lobula plate of the blowfly to record the activity of the contralateral H1-

cell. The first stimulation sequence consists of 0.5 second without motion, 3 seconds anticlockwise rotation (view from dorsal side of the blowfly), 3 seconds clockwise rotation and 3.5 seconds without motion. The second stimulation sequence has 0.5 second without motion, 3 seconds clockwise rotation, 3 seconds anticlockwise rotation and 3.5 seconds without motion. This protocol guarantees that both H1-cells are excited by motion in the anti-preferred direction before and after motion adaptation. “E” stands for excitation, “I” for inhibition, “a” for motion adapted. 80

Figure 38. Dual H1-cell recordings in asymmetric temporal frequency tuning curves after adaptation. The electrode is recording both H1 neurons in the right hand side of the lobula plate. Data presented in plots A, C were recorded under CCW-CW stimulation. The tuning curve of the contralateral (left) H1 (motion adapted) is plotted over positive temporal frequencies while the the tuning curve of the ipsi-lateral (right) H1-cell is plotted against negative temporal frequencies. Data presented in plot B, D were recorded under CW-CCW stimulation. The tuning curve of the contralateral (left) H1-cell is plotted against positive temporal frequencies. While the tuning curve of the ipsi-lateral (right) H1-cell (motion adapted) is plotted against negative temporal frequencies. The green line indicates the overall mean spontaneous spike rate in between pattern rotations, the magenta line shows the overall mean spontaneous spike rate in between fly rotation. 81

Figure 39. Dual H1-cell recordings show symmetric temporal frequency tuning curve with adaptation. Same experimental conditions as described in figure 38, but recorded from a different blowfly. 82

Figure 40. Input voltage levels for dynamic characterization of 3pi robot. The input voltage is regulated by an 8 bit PWM generator. Levels 0 to 255 are equivalent to 0V to 9.25V, which are applied to the DC motors driving the wheels of the robot. 90

Figure 41. Image processing for analysing angular orientation. The top left image is the original image, where the robot is in the middle of the image with the black dot indicating the rotating centre and the black cross marking the robot edge. The black triangle is the reference mark on the ground. The bottom left shows a high contrast (black and white) image after noise removal and contrast saturation. The image on the right shows the result of the

analysis where the angular orientation has been calculated with respect to the coordinates of the patterns. The vector from dot to cross represents the orientation of the robot. The vector from dot to triangle is the reference vector. The angle calculated is defined by the counter clockwise angle between the reference vector and the vector describing the robot orientation.91

Figure 42. Robot angular velocity calculation. (Top) The angular orientations of robot measured from frames captured by a high speed camera. (Middle) Continuous representation of angular rotation. It shows the cumulative rotation angle covered by the robot over time relative to its initial angular position. (Bottom) Angular velocity of the robot, obtained from the temporal derivative of the angular position. The red line indicates 0 deg/ms.....92

Figure 43. Angular velocity of the robot as a function of PWM voltage during acceleration and deceleration. The mean and standard deviation of each point was calculated from 100 angular velocity measurements.....93

Figure 44. Full assembled fly-robot interface system. The mini-micromanipulators are used for electrodes placement. The blowfly is fixed in the rotating centre of the recording platform. The platform is insulated from mechanical vibrations of the motors driving the wheels by a damping layer made from a piece of sponge. The 3pi robot (diameter 94 mm) serves as spatial scaling reference in this figure.98

Figure 45. Bilateral H1-cell action potential detection. (top) The blue and red signals are recorded from different H1-cells. The green line is the threshold voltage for spike sorting. In this experiment crosstalk between the two recording channels occurred. Based on the different spike amplitudes of generated by the two H1-cells. The signals of the two cells could be separated in software. (bottom) The accurately detected spikes of the two H1-cells. Blue and red vertical lines indicated the detection of spikes of the ipsilateral and contralateral H1, respectively..... 100

List of tables

Table 1. The eigen speed of blowfly, hawk moth and bald eagle (Bomphrey et al., 2009; Stevenson et al., 1995)	28
Table 2. Comparison of robots.....	34
Table 3. Angular extent of the stimulus grating	73

Abbreviations

EMD	<i>Elementary motion detector</i>
LPTC	<i>Lobula plate tangential cell</i>
H1	<i>A horizontal motion sensitive spiking LPTC</i>
PD	<i>Preferred direction</i>
ND	<i>Null direction (or anti-preferred direction)</i>
SNR	<i>Signal to noise ratio</i>
ADC	<i>Analog to digital converter</i>
DAQ	<i>Data acquisition</i>
PCB	<i>Printed circuit board</i>
MCU	<i>Microcontroller unit</i>
UART	<i>Universal Asynchronous Receiver/Transmitter</i>
PWM	<i>Pulse width modulation</i>

Prologue

Mankind was often inspired by biological design principles which have proven successful over millions of year of evolution, when developing technical applications. The adaptive way in which animals and humans control their movements in habitats ranging from deserts, to tropical forests and from mountains to the beaches at the sea is still unmatched by any manmade robot. Understanding the principles of animal motor control is the subject of neuroscience research which, over the last few decades, has significantly benefitted from interdisciplinary approaches involving theoretical and engineering methods. Whenever ground breaking discoveries in neuroscience had been made they were based on the development of new methodologies. And in many cases the new discoveries were then translated into novel technical applications.

One of the great fascinations for humans has been the ability to fly – or at least to engineer aerial vehicles that can do so. This is one of the areas where the interests of engineers and neuroscientists have converged in the last couple of years. Neuroscientists, trying to understand how the nervous system accomplishes the control of flight and engineers who are eager to design highly manoeuvrable aerial vehicles have started to combine their expertise in an attempt to extract and translate principles of sensorimotor control found in bird and flying insects (Zufferey Jean-Christophe Staff, 2008).

One of the most accomplished flyers in the animal kingdom, the common blowfly, has been a model system for sensorimotor research for many years. Its flight envelope, the combination of translations and rotations it engages on when airborne, is superior to the performance of any manmade air vehicle. And yet, despite several decades of research into the secrets of how sensor signals from different modalities are used to control its aerodynamic stability as well as avoiding collisions with obstacles are still not entirely understood

with respect to the underlying neural mechanisms. This is mostly because of methodological limitation: There is hardly any model system in which specific neural activity could have been recorded during flight and then correlated with the sensory input as well as behavioural output parameters.

In my project I have designed a miniaturized recording platform as a first step to overcome some of the methodological problems. I have developed a system that will eventually enable studies on multisensory signal integration under closed-loop conditions where a blowfly is mounted on a small-mobile robot the movements of which it controls by the activity of an identified visual interneuron. Although this approach has its own limitations as the trajectory of the robot will be confined to the 2-dimensional plane, it will go beyond any previous studies in that multiple sensor systems will be activated during the robot's movements.

The major challenges of my project were to (i) design a miniaturized recording platform that features full functionality to enable (ii) stable high quality recordings over extended periods of time and (iii) under conditions where the recording platform is exposed to angular velocities within the dynamic input range the fly experiences during flight. Finally, I tested the performance of the mobile recording platform under various stimulus conditions and established an interface between the neural activity of a visual interneuron and a two-wheeled robot.

1. Introduction

In this chapter, I will review the background literature on the sensors of the blowfly, and how these sensors contribute to flight control. I will also review work on brain machine interfaces, in the more general sense, applied to flies and other insects which inspired this thesis.

1.1. Blowfly neurobiology of flight control

The blowfly, *Calliphora vicina*, is a frequently seen two winged insect. It is a convenient model animal in the lab, due to its simple feeding requirements and short reproductive cycle. It reaches a flight speed of 2.5 m/s and rotates at angular velocities as high as 1700 deg/s when flying (Bomphrey et al., 2009). Its light weight, small size, and a sophisticated flight motor system in combination with a variety of sensor systems providing robust information on state changes (Taylor and Krapp, 2007), the blowfly accomplishes a degree of aerial manoeuvrability that is hardly matched by any other flying animal or man-made air vehicle.

The blowfly uses a combination of visual and mechanosensory systems to control its gaze and flight. During locomotion, the visual system supports course, altitude, and attitude control. The latter is augmented by mechanoreceptive systems indicating, for instance, air speed and body accelerations (Taylor and Krapp, 2007).

In this section, the function of the visual systems and mechanosensors in the blowfly will be introduced and how their signals may be integrated to support tasks such as gaze and flight stabilization.

1.1.1. Vision and motion

1.1.1.1. Optic flow and ego motion

During ego-motion, the eyes of the blowfly will move relative to its visual surroundings. The resulting panoramic image shifts are often called “optic flow”

fields (Koenderink and Doorn, 1987) which consist of local velocity vectors describing the direction and relative magnitude of retinal image motion. The global structure of optic flow fields is defined by the translational and rotational ego-motion components where the contribution of the translation component is inversely proportional to the distance between the eye and the objects in the environment.

There are six degrees of freedom in ego-motion. Three translational, thrust, lift, sideslip, and three rotational yaw, pitch and roll (Taylor and Krapp, 2007).

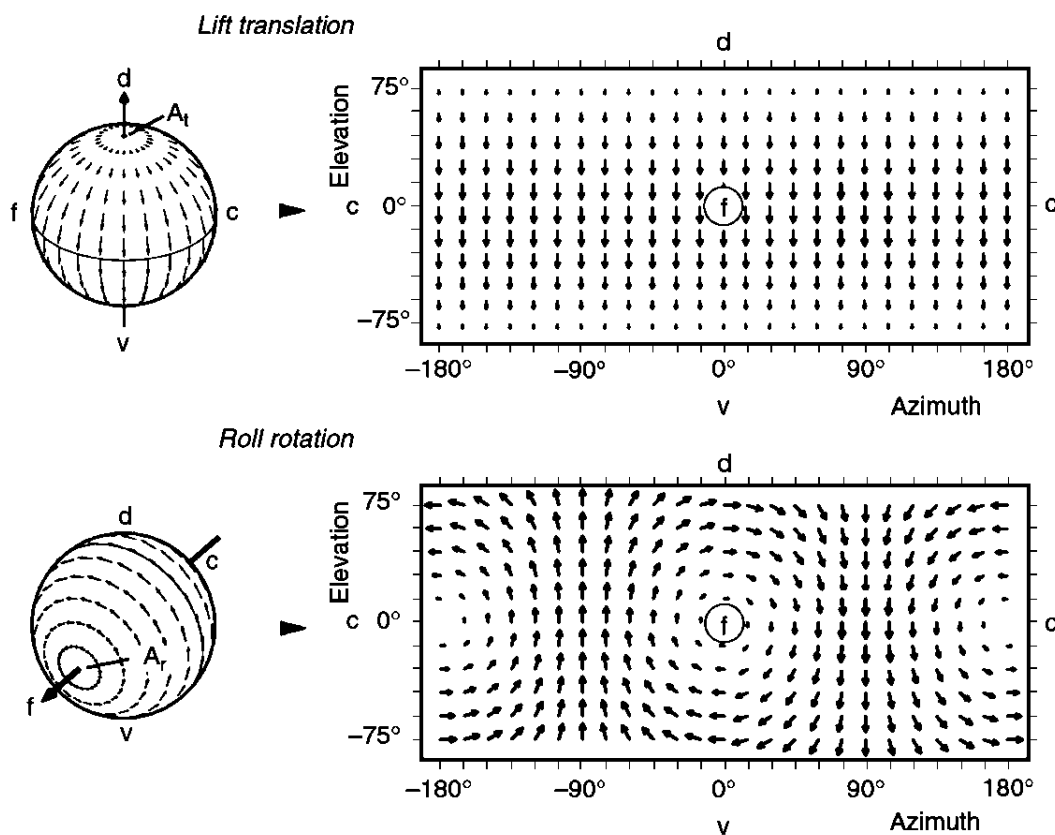


Figure 1. Self-motion and global optic flow. Top left: Optic flow generated during pure lift translation plotted as tangent vectors on a unit sphere that symbolizes the visual field. The direction of translation, A_t , defines the location of two singularities in the flow field, the focus of expansion and the focus of contraction, where no relative motion takes place. Local vectors in a translation flow field are aligned along great circles connecting the focus of expansion with the focus of contraction and point in the opposite directions to A_t . Bottom left: During pure rotation all flow vectors are aligned along parallel circles centered with the axis of rotation, A_r , and are thus oriented perpendicular to the rotation axis. The example shows a flow field as a result of a roll rotation around the longitudinal body axis. Plots on the right hand side show cylindrical projections of the flow fields into the 2-dimensional plane where each position in the visual field is defined by two angles: the (horizontal) azimuth and the (vertical) elevation. Note that the gray window in the right half of the visual field shows local flow vectors pointing in the same direction despite the fact they were generated by different ego-motions. Modified from (Krapp & Wicklein 2008).

Optic flow vectors generated by pure rotation do not contain distance information but only depend on the rotation vector and the azimuth and elevation upon which they are observed. The result is a pattern of coherent wide-field motion within the entire visual field. The velocity of optic flow is maximum at viewing directions perpendicular to the rotational axis, and gradually decreases to zero toward the axis of rotation, A_r . All local flow vectors are aligned along parallel circles which are centred on A_r . Their orientation is always perpendicular to the rotation axis.

Optic flow vectors generated during pure translation are aligned with great circles connecting the focus of expansion with the focus of contraction. Their orientation and magnitude depends on the difference between the translation vector and the projection of the translation vector into the different viewing directions defined by azimuth and elevation. As a result, and similar to rotation-induced flow vectors, their magnitude becomes maximum at viewing directions perpendicular to the translation axis, A_t , and zero at the singularities of the flow field. Other than during pure rotation, the magnitude of flow vectors in translation induced flow fields depends on distance. In terms of relative motion: objects close to a moving observer move faster than distant objects. Quantitative accounts on optic flow can be found in the literature (Dahmen et al., 2001; Koenderink and van Doorn, 1987).

The description of optic flow above holds true for an observer moving in a fixed environment where all objects are seen at a unit distance. Obviously, moving objects also cause image motion on the retinae of a stationary or moving observer. The direction and velocity of the resulting retinal image shifts is then given by the sum of the local velocity vectors. In case the observer is moving, external object motion introduces local discontinuities in the ego-motion-induced global optic flow field (Krapp and Wicklein, 2008).

1.1.1.2. Elementary motion detector

Optic flow is generated by ego-motion of an observer. Exploiting optic flow for visually guided behaviour requires a mechanism in the visual system that can analyses the direction and relative magnitude of the local velocity vectors. If this is done at a sufficient number of locations in the visual field, there is hope

that the ego-motion components, A_r and A_t , may be estimated and the resulting information can be used for gaze and flight control.

Nervous systems, in general, analyses directional motion by so-called Elementary Movement Detectors (EMDs) the functional properties of which Reichardt proposed (Reichardt and Egelhaaf, 1988). The EMD model is also called 'Reichardt detector'. This model describes the necessary and sufficient conditions required to distinguish between motions in opposite directions. It consists of: (1) Two spatially separated inputs. (2) Two different input transfer functions – one delayed, one without delay. (3) A non-linear combination of the delayed and non-delayed signals approximated by a multiplication operation. This basic structure of such a half detector is able to detect motion in one direction, called preferred direction, but cannot tell the difference between motion in the opposite, anti-preferred direction, and no motion. Two inputs and one output can only deal with two states, but two inputs and two outputs can deal with four states. By complementing the half detector with a mirror-symmetric version and then subtracting the output of the added half detector from the output of the original one on a common integration stage, the model is turned into a fully directional-selective EMD (Figure 2). The integration stage assumes four output states: (1) Generating positive output when motion passes across the inputs in the preferred direction of the detector. (2) Generating negative output for motion in the opposite direction. (3) No output is generated when there is no motion. (4) No output is generated when signals of the same amplitude from both half detectors reach the integration stage simultaneously.

This generic model is also named correlation-type motion detector, because it provides a spatiotemporal correlation of light intensities received at neighbouring sensors on the retina. The EMD output depends not only on the angular velocity of the given stimulus pattern, but also on the spatial wavelength of a pattern which contains periodic light intensity fluctuations. The ratio between angular velocity and spatial wavelength of a periodic pattern is called contrast or temporal frequency and has the unit 1/s. More information about motion detection models may be found in the literature (Borst and Egelhaaf, 1989; Egelhaaf and Borst, 1993; Reichardt, 1987).

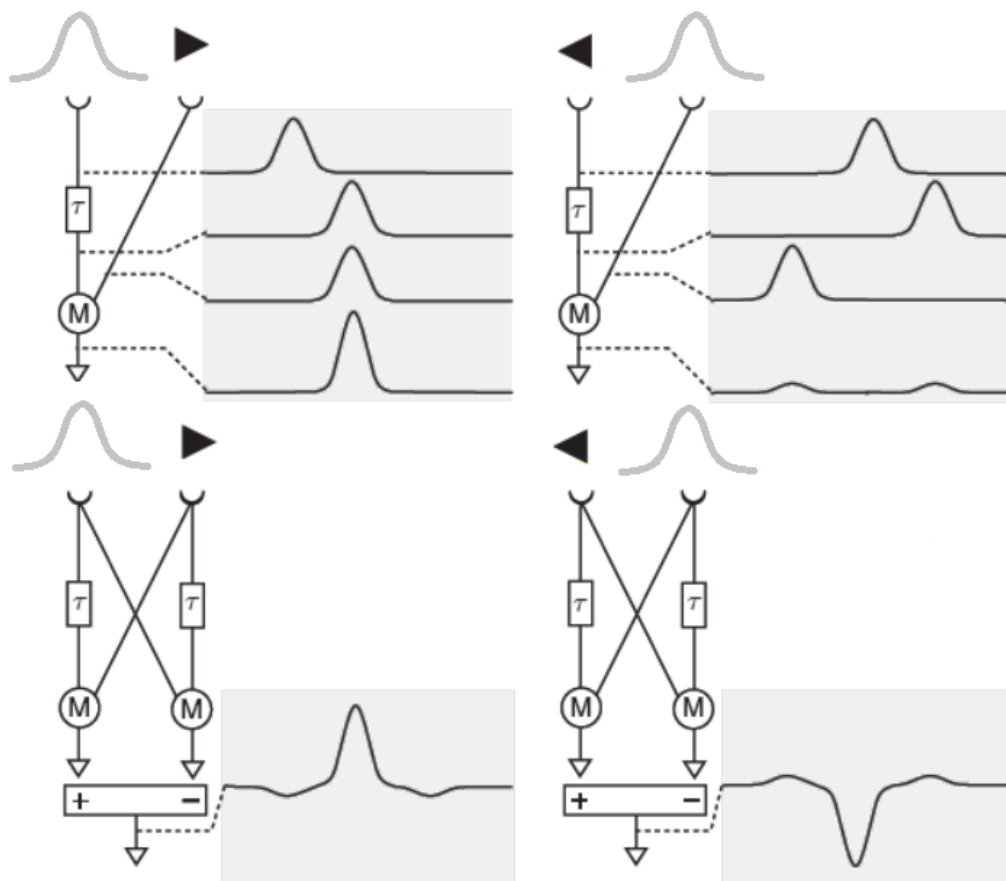


Figure 2. Elementary movement detector: (top left) half-detector with preferred direction stimulus moving to the right, first inducing a signal in the left then in the right input channel. The delayed signal from the first input channel coincides with the non-delayed signal from second input channel at a multiplication stage if the time it takes the stimulus to reach the second input channel corresponds to the delay, τ , in the first input channel. (top right) the same half-detector stimulated with motion in the anti-preferred direction. In this case the two inputs are de-correlated in time and no sizable output is generated. (bottom left and right) A fully directional EMD combines two mirror-symmetrical half-detectors. Motion in the detectors preferred and anti-preferred direction result in a positive and negative output of the detector, respectively. Figure modified from (Krapp & Wicklein 2008)

1.1.1.3. The aperture problem

As was described above, the EMD is able to measure the local image motion. But there is a theoretical issue called “aperture problem” which affects the measurement of the local image velocities. The direction of local visual motion viewed through a round aperture is ambiguous. Figure 3 shows a case, where only the motion component perpendicular to the pattern orientation can be measured while the parallel component is “invisible” for a local analysis. Identical responses in a motion sensitive neuron in the visual system can be

caused by a variety of contours of different orientations moving at different speeds (Shimojo et al., 1989).

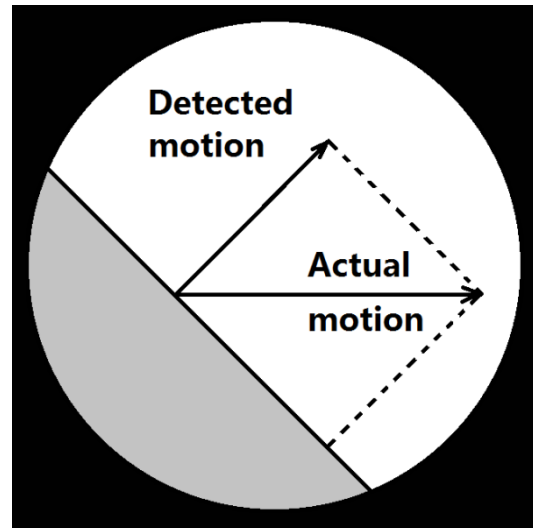


Figure 3. The aperture problem. Motion orthogonal to the edge is detected, motion parallel to the edge can not be detected.

In the visual system, neurons at peripheral stages along the motion vision pathway respond to local motion within their receptive field. Each local motion-detecting neuron may suffer from the aperture problem (Pack and Born, 2001). To overcome this problem the signals of many neurons with local receptive fields may be spatially integrated for a correct global motion estimate (Dahmen et al., 2001; Koenderink and Doorn, 1987).

1.1.2. The blowfly visual system

The blowfly visual system can be divided into four parts (Figure 4). The retina is the first part where changes in light intensity are transduced into time-varying electrical signal. At this stage visual processing takes place on a local basis with only a small amount of lateral processing. The retinotopic representation of visual information, i.e. light intensity changes at neighbouring locations in the visual field are mapped onto neighbouring elements in the visual system, is maintained (Strausfeld, 1976a).

The lamina is the second part. It is organized in a columnar structure and receives retinotopic inputs from the retina. Within each column local neurons are involved in some lateral processing.

The third part is called medulla, which consists of three regions: the outer medulla, the inner medulla and the serpentine layer (Krapp and Wicklein, 2008). The outer medulla receives inputs from lamina monopolar cells and other long visual fibres. The axons between the lamina and the medulla cross over to form the external chiasm.

The last part is called lobula complex, which consists of the anterior lobula and the posterior lobula plate. In both parts spatial signal integration takes place. The lobula plate tangential cells (LPTCs) spatially integrate local motion signals – which reflect the properties of EMD half-detectors. Many of the cells have extended receptive fields and respond to wide-field motion in a directional selective way. Certain sub-populations of LPTCs, the VS- and HS-cells (Hausen, 1984, 1993), were suggested to act as matched filters for specific optic flow fields (Franz and Krapp 2000). Some motion sensitive spiking cells have been well studied electrophysiologically, using small moving objects for visual stimulation including the H1-cell (Krapp and Hengstenberg, 1997).

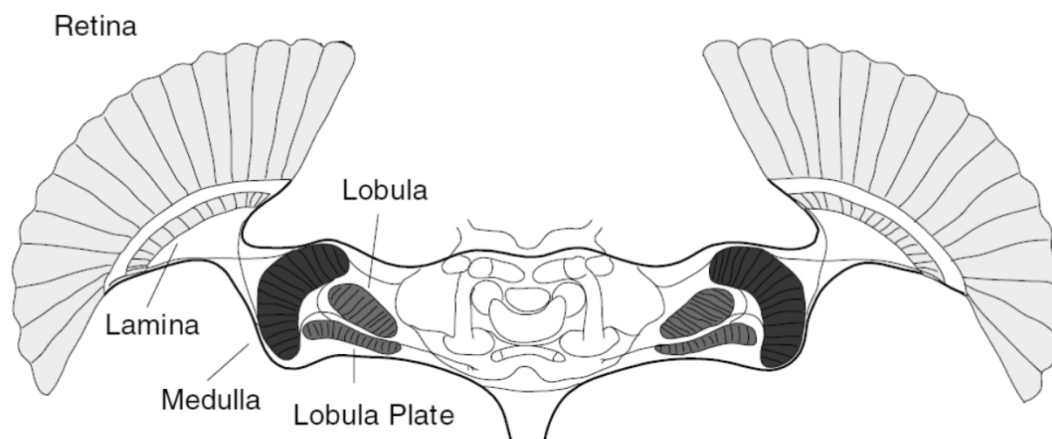


Figure 4. The blowfly visual system. The visual system includes: retina, lamina, medulla, lobula and lobula plate. The lobula plate receives retinotopic input from lobula and medulla, where the connecting axons cross over in the internal chiasm. In the external chiasm axons originating in the lamina cross over on their projection to the medulla. As the whole system is organized in a retinotopic way, a crossover of projections is equivalent to an inversion of the vertical image plane. Modified from (Borst and Haag, 2002a)

1.1.2.1. Retina

The retina is the first neuropil of blowflies' visual system.

The eye consists of around 5200 hexagonally arranged functional units in both compound eyes (Beersma et al., 1977), called ommatidia. Each ommatidium has its own lens focussing incoming light on eight photoreceptors in each ommatidium. The spatial resolution of the compound eye in *Calliphora* is about 1 to 2 degrees, restricted mainly by diffraction resulting from small lenses and by the geometry of the lens-photoreceptor arrangement (Land and Eckert, 1985).

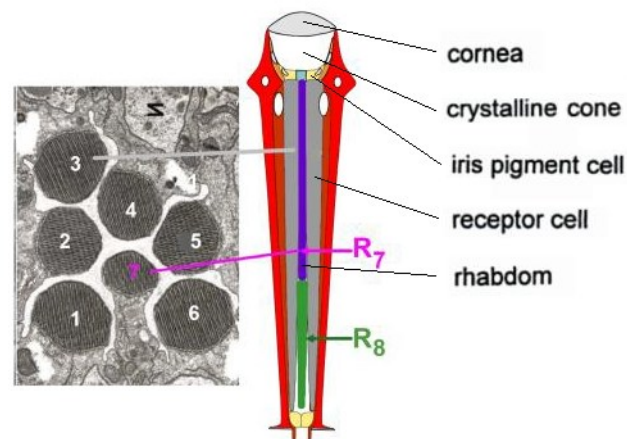


Figure 5. The ommatidium. (Left) *Drosophila* photoreceptors R1-6 and R7, (right) structure of a single ommatidium with photoreceptors R1-6 (gray), R7 (purple) and R8 (green). Modified from (Yishai Michael Elyada 2009)

Each ommatidium consists of the cornea, crystalline cones, rhabdom, receptor cells and pigment cells. The light passes through cornea and crystalline cones and is focused on the photoreceptors at the bottom of the crystalline cones, where the tip of the rhabdom is located. The rhabdom is a transparent crystalline receptive structure. It consists of rhabdomeres which contain a small number of photoreceptor cells. There are eight photoreceptors, R1-R8, which use light sensitive pigments to photochemically convert changes in photon flux into membrane potential changes. An increase in luminance is encoded by a depolarization of the membrane in insect photoreceptors (Laughlin, 1984). Neighbouring ommatidia are optically

insulated from one another by shieling pigments to reduce blurring of the images (Kirschfeld et al., 1977).

The R1-R6 photoreceptors have short axons that terminate in the cartridges of the first neuropil, the lamina. A 180 degree twist of the photoreceptor axons is required before they synapse on to the cells in the lamina to maintain spatial contiguity after the inversion of the image by each of the facet lenses. The R7 and R8 have longer axons, which bypass the lamina, and terminate at different levels in the medulla. It is believed that R1-R6 are important for motion detection and produce monochromic signals while R7/R8 mediates polychromic signals (Heisenberg and Buchner, 1977).

1.1.2.2. Lamina

The lamina is the most peripheral of the three optic neuropils. The inputs from the retina are grouped into retinotopic columns in lamina, called “cartridges”. The blowfly possesses a structure called “neural superposition eye”, where R1-R6 photoreceptors (short visual fibres) of each ommatidium in the retina project to different cartridges in the lamina. Each lamina cartridge contains five principle neurons, the large monopolar cells (LMC) L1-L5.

A depolarisation in the photoreceptors R1-R6 causes hyperpolarization in the LMCs. The sign of the signal is inverted in the lamina, compared to retina. The LMCs produce an impulse-shaped signal, when receiving a step-shaped input, which suggest them to function as some sort of high pass filter (Figure 6). The signal will decline to zero after the initial response peak.

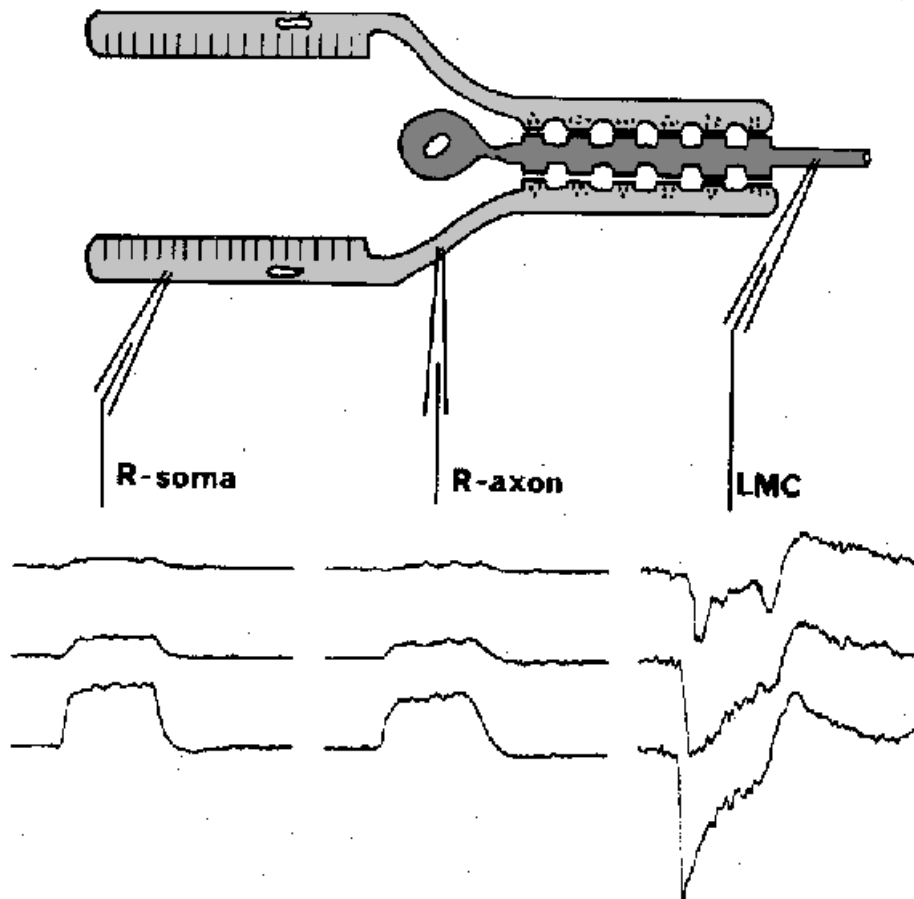


Figure 6. Signal transmission from photoreceptor to LMC. Transsynaptic signals are high pass filtered. Modified from (Laughlin 1984)

Among the Large monopolar cells, the L1 and L2 neurons are the principal neurons supporting motion vision (Tuthill et al., 2013). The motion vision pathway diverges into two pathways. The L1 neurons connect to Mi1 neurons in layers M1 and M5 of the medulla. The L2 neurons connect to Tm1 neurons in layer M2 of the medulla (Bausenwein et al., 1992).

1.1.2.3. Medulla

The medulla is the second neuropil in the visual system of the blowfly, receiving signals from laminar monopolar cells and directly from the photoreceptors R7, R8. The L1 monopolar cell axon ends in layers M1 and M5, connecting with the Mi1 cell, which connects or synapses with the motion-sensitive, direction-selective T4 cells in layer M10 (Bausenwein et al., 1992). These cells probably synapse onto tangential cells in the lobular plate (Strausfeld and Lee, 1991). The L2 monopolar cells connect to the M2 layer of the medulla and terminate on the transmedullary Tm1 cells. The Tm1 cells

connect T5 cells in the lobula, which are directionally selective and project to the lobula plate (Strausfeld and Lee, 1991).

1.1.2.4. Lobula complex

The lobula complex consists of two parts: the lobula (on the anterior side), and the lobula plate (posterior side of the lobula complex).

The lobula consists of six layers. The transmedullary Tm1 neurons, which originate in the medulla, contact the directionally selective T5 neurons on the posterior layer of the lobula. Different T5 neurons go to different layers of the lobula plate.

The lobula plate is located on the posterior side of the lobula complex and has indeed a plate-like shape. It receives retinotopic inputs from both the medulla and lobula. The lobula plate contains large motion-sensitive tangential neurons which have been characterized both anatomically and physiologically (Borst and Haag, 2002a; Hausen, 1984; Reichardt et al., 1983). They are called lobula plate tangential cells (LPTCs). LPTCs are thought to play a cardinal role in stabilization reflexes in flies supporting gaze and flight control. Local motion information from the retinotopically arranged arrays of directional-selective small field elements are selectively integrated onto the lobula plate (Krapp and Hengstenberg, 1996).

The lobula plate has four input layers. The layers are invaded by dendrites of different LPTCs which receive signals from one out of four separate retinotopically arranged input arrays each of which providing distinctly different directional information (Buchner, 1984).

The flat structure of the lobula plate, its location right underneath the cuticle of the animal's head capsule as well as the large two-dimensional morphology of the LPTCs make these neurons particularly accessible for electrophysiological studies. I have exploited those features of the LPTCs in this project.

1.1.2.5. H1-cell

There are around 60 identified lobula plate tangential cells in each hemisphere of the fly brain (Hausen, 1984). The LPTCs process motion information from retinotopic arrays of local motion sensitive units as well as information provided by networks of ipsilateral and heterolateral cells, before passing the integrated information on to downstream motor circuits (Borst and Haag, 2002a). The responses of LPTC are either graded membrane potentials (CH cells), action potential (H1-H2, V1-V2), or both (HS cells, VS cells, FD cells) (Borst and Haag, 1996; Hengstenberg, 1977). The LPTCs can also be classified by their primary direction selectivity, such as: horizontal motion sensitive cells (HS, CH, H and FD cells) and vertical motion sensitive cells (VS and V cells), although the preferred direction of receptive fields are more complex (Hausen, 1993; Krapp and Hengstenberg, 1996).

H1-cell is one of the horizontal motion sensitive cells in the lobula plate of the blowflies (Krapp and Hengstenberg, 1997). The blowfly has two H1 neurons, one in each hemisphere of the brain. The axon of the H1-cell is about 5 micrometres in diameter, 1200 micrometres in length and conducts action potentials at a speed of 1 m/s (Hausen, 1984). The diameter of the axons of most of these neurons enables both intracellular and extracellular recordings of their neural activity.

The dendritic arborisation of the H1-cell covers the entire anterior surface of the lobula plate, where it receives retinotopic input from local small-field neurons of the medulla and lobula. The telo-dendritic arborizations of H1-cells transmit the signals to the contralateral lobula plate. The H1-cell is a spiking neuron, which generates action potentials for signal propagation.

The receptive field of H1-cells as measured using local motion stimuli ranges from -165 degree to +15 degree along azimuth, and from -45 degree to +45 degree along elevation (Krapp and Hengstenberg, 1997), where the coordinate azimuth = elevation = 0 corresponds to the position seen by the eye equator right in front of the animal (Figure 7). The H1-cell is excited by back-to-front optic flow on the ipsilateral side, i.e. the side where its cell body is located. The response of the cell in terms of spike per second depends on

various stimulus parameters one of which is the temporal frequency of the stimulus pattern. It is inhibited by the front-to-back motion, where the spike rate can be reduced to zero. The H1-cells have a spontaneous spike rate of 20-50 spikes per second, when no visual motion is presented.

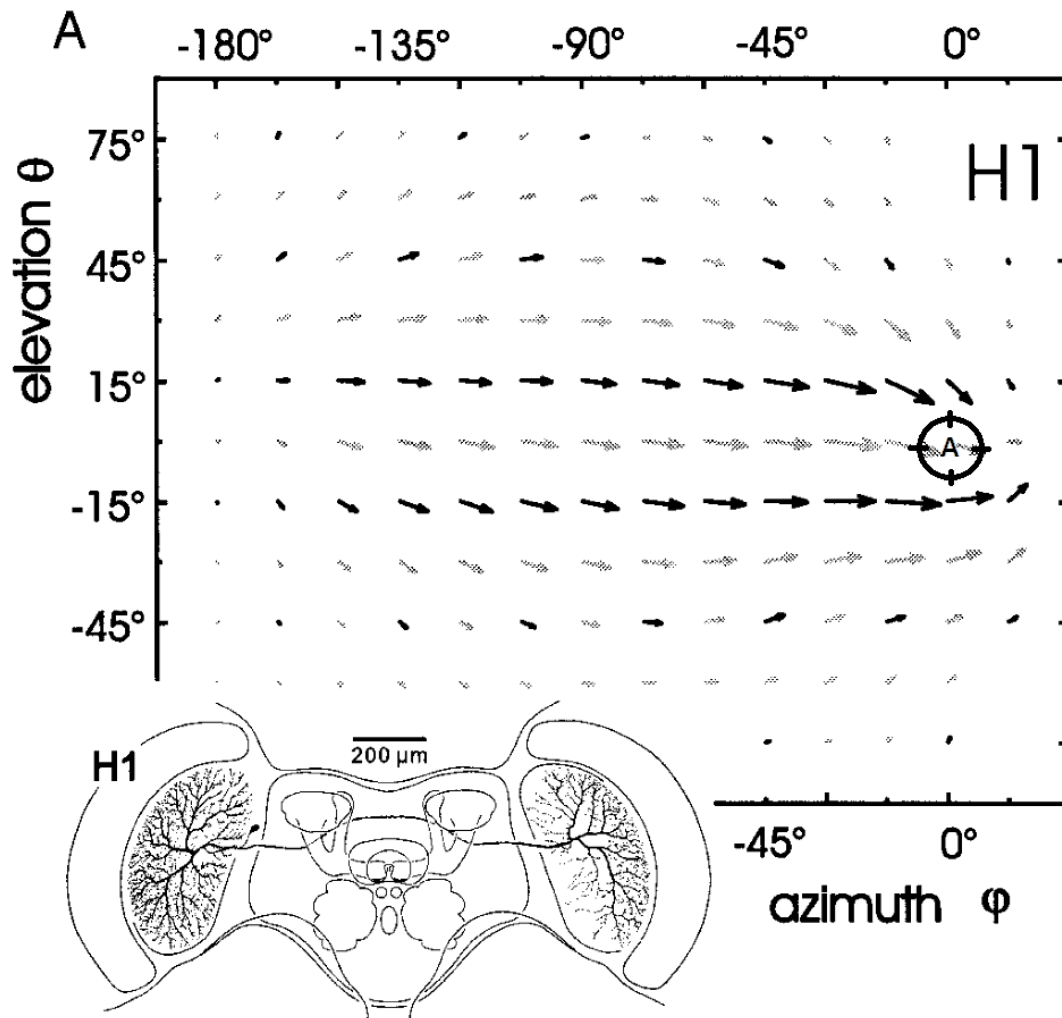


Figure 7. H1-cell preferred direction mapping. Cell morphology (inset at the bottom): The picture shows the cell's ipsilateral dendritic (input) arborizations on the left and its telodendritic (output) arborizations on the right. Input mediated by the left eye is propagating to the right lobula plate. The cell is viewed from the posterior side of the head. Receptive field: Local preferred directions and motion sensitivities of the H1-cell presented as motion vectors in a cylindrical representation of the spherical visual field. Azimuth = elevation = 0 degrees denotes the point in front of the animal. The H1-cell is excited mainly by back-to-front motion from around -150 deg to +15 deg in azimuth, and -45 deg to +45 deg in elevation. Modified from (Krapp et al. 2001)

The large receptive field of the H1-cell makes it suitable to process, and more importantly, to differentiate optic flow patterns. (1) A high degree of spatial integration averages out the fluctuations caused by the dependence of the motion detectors on local input features, as well as avoiding the aperture

problem. (2) The receptive field organization may fit behaviourally relevant optic flow patterns in order to contribute to the generation of appropriate behavioural responses. The H1-cell is the focus of my work for investigating sensory integration. Its spiking activity will eventually be used to control a 2-wheeled robot.

1.1.3. Sensory integration

Other than vision, mechanical (or inertial) sensors also play an important role in flight control (Taylor and Krapp, 2007). They trigger neck motor responses in combination with signals from the motion vision pathway mediating optic flow information (Huston and Krapp, 2009). The blowfly has many mechanosensory systems, for instance: filiform hairs on the antennae which sense changes in air speed, campaniform sensilla on the wings for sensing wing load, and the halteres which sense Coriolis forces during rapid attitude changes (Taylor and Krapp, 2007).

1.1.3.1. Inertial sensor: haltere

The haltere system is of interest in the context of this project because it helps generating stabilizing head movements and contributes to flight control when the thorax of the fly is rolled in featureless visual surroundings or in darkness.

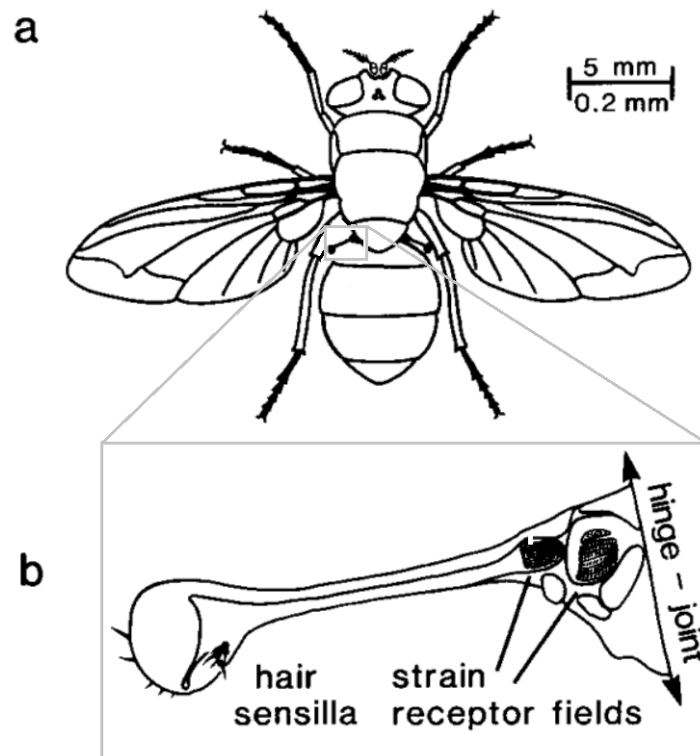


Figure 8. Position and structure of halteres. The halteres are located at the rear of metathorax (a), one of the haltere is magnified in (b) to reveal its structural components in detail. Modified from (Hengstenberg 1993)

The halteres are a pair of transformed hind wings in dipteran flies. These organs are used to sense the forces generated during body rotations and thus provide information about rapid attitude changes. The halteres are small club-shaped organs, located in between the thorax and the abdomen. A haltere consists of three parts: a distal knob, a thin stiff stalk, and a basal swelling on top of a hinge joint connected to the thorax. There are around 15 mechanoreceptive hairs on the knob, about 350 cuticular strain receptors in five distinct fields on the hinge and two internal stretch sense organs (Hengstenberg, 1993). The haltere beats vertically around 110-180 Hz in antiphase with the wings (Nalbach, 1993). The angular momentum of the halteres will be sensed if a body rotation occurs that is outside their plane of oscillation. The halteres measure angular velocity directly by its frequency, amplitude and phase relative to the wing beat (Nalbach, 1993). They are very sensitive to high angular velocity, and elicit compensatory head rotation with very short latencies (Hengstenberg, 1993).

1.1.3.2. Sensory integration for gaze stabilization

Insect gaze shifts can be classified as either voluntary or in response to a stimulus. Though the gaze may shift to an object of interest, it is normally aligned with the external horizon. Pitch and Roll movements of the head are related to equilibrium reflexes, for keeping the head upright with respect to the external environment (Hengstenberg, 1993).

The blowfly uses a variety of sensory mechanisms to keep its eyes level and for flight control. Visual and haltere subsystems have different dynamic characteristics. By combining information from the visual system and the haltere system, the gaze stabilization reflex covers both the low and high frequency range of possible stimulations.

Experiments highlighting the integration of individual sensing systems contributing to roll gaze-stabilization have been reviewed by Hengstenberg (Hengstenberg, 1991). Hengstenberg and colleagues tethered blowflies in a wind tunnel, where the wall of the tunnel was decorated with patterns. Both the fly and tunnel were connected to two electrical motors, respectively. The fly would, in tethered flight, perform compensatory head rotations to stabilize its gaze against either body rotations or rotations of the visual pattern. The head roll response during haltere stimulation kicked in at around 60 deg/s and reached its peak at 1000 deg/s. No response was observed below 10 deg/s (Fig 9b). When the pattern was rotated, and thus only the visual system but not the haltere system was stimulated, the head roll response was 40 degrees at a stimulation velocity of around 100 deg/s (Fig 9c). When both visual and haltere systems were stimulated, the peak head roll response at 1000 deg/s body rotation was reduced to 40 degrees and the head roll response in low body rotation velocities increased to about 20 degrees (Fig 9a). Based on his experimental results Hengstenberg (Hengstenberg, 1991) concluded that the overall response to haltere and visual stimulation was a linear (internally scaled) combination of the responses to the stimulation of either the halteres or the motion vision system. He also pointed out that multisensory integration increases both accuracy and response bandwidth in the gaze control system (Hengstenberg, 1991).

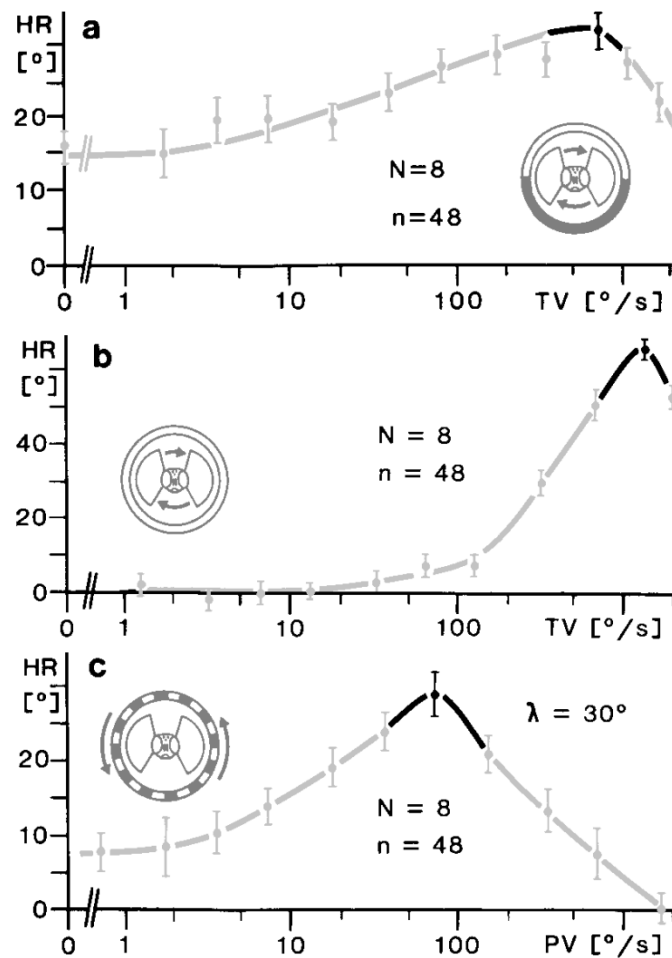


Figure 9. Sensory integration. (a) The blowfly is placed in a stationary pattern cylinder with white on top and black on bottom (spatial wavelength of the pattern = 360 deg). The blowfly is oscillated between $\pm 90^\circ$ at constant speed around the roll axis, for various angular velocities, where both visual system and halteres are stimulated. The head roll angle of the blowfly as a function of angular velocity was found to have a band-pass-like shape where the peak response (40 deg) occurred at around 600 deg/s. The trough value is around 50% of the peak value. (b) The blowfly was placed in a homogeneous white cylinder (no visual contrast). The animal was oscillated at constant velocity around the roll axis for different angular velocities, where only the halteres were stimulated. The head roll angle peaked (70 deg) at around 1200 deg/s. The trough value is 0% of peak value. (c) The blowfly was kept stationary in an oscillation cylinder with black and white pattern (spatial wavelength = 30 deg). The cylinder was oscillated around the fly's roll axis at different angular velocities - under these conditions only the motion vision pathway was stimulated. The head roll angle peaked (40 deg) at around 80 deg/s. The trough value was around 30% of peak value. Modified from (Hengstenberg 1991)

1.1.3.3. Sensory integration in the neck motor system

The results on gaze stabilization obtained at the behavioural level – suggesting a linear combination of sensory signals in the neck motor system – seem to be contrasted by work conducted at the neuronal level (Huston and Krapp, 2009). Sensory integration of compound eye and haltere signals had been recorded in neck motor neurons.

The blowfly's neck motor neurons (NMNs) connect to the neck muscles which ultimately control the gaze. One of the neck motor neurons was recorded, while it was stimulated by either the visual system, or the halteres, or both. Visual stimulation was supplied by a CRT monitor which displayed vertical bars moving horizontally either right-to-left or left-to-right. Haltere stimulation was achieved by periodic vertical movement of a magnet next to the haltere, where the tip of the haltere was treated with a mixture from paint and iron powder. The visual stimulation and haltere stimulation were applied in combination, which will produce four responses.

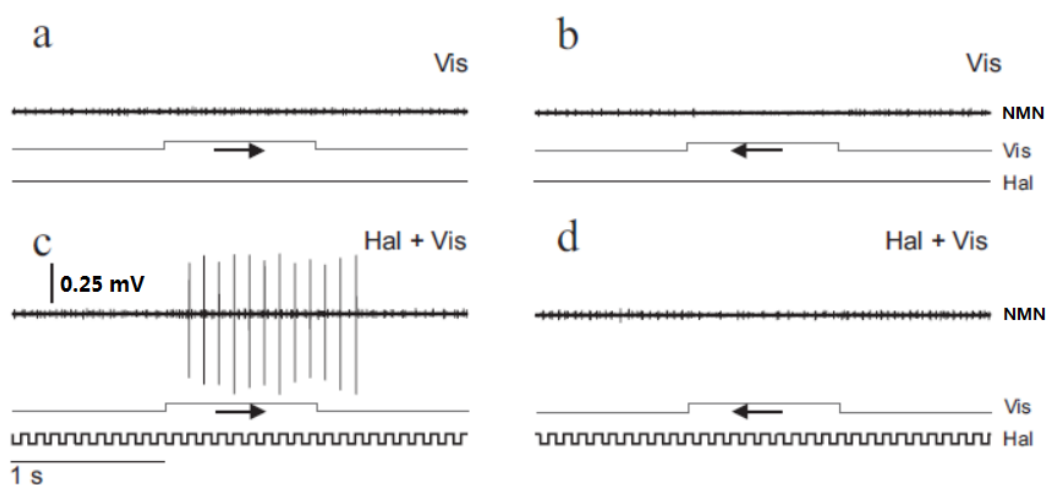


Figure 10. Neck motor neuron responses to a combination of visual and haltere stimulations. In a,b,c,d. the top lines give the responses of neck motor neuron, the middle lines indicate the time course and direction of the visual stimulation, and the bottom lines show the time course of the haltere stimulus. Only in plot c the neck motor neuron generated action potentials where the fly experienced rightwards visual stimulation and haltere stimulation simultaneously. Modified from (Huston & Krapp 2009)

The results (Fig. 10) show a gating-like nonlinear sensory integration at the level of the neck motor neuron. The neck motor neuron produced action potentials only when the visual stimulation in the cells preferred direction was combined with haltere oscillations.

Specific questions remain unanswered. (1) where is the integration happening, in cephalic ganglia or in thoracic ganglia? (2) Will the fly respond differently under more naturalistic stimulation conditions, e.g. wide-field optic flow stimulation or in a closed-loop regime? (3) how will other sensory modalities impact on multimodal signal integration in the context of gaze and flight stabilization? (4) Why has a linear interaction between different modalities

observed at the behavioural level although signal integration in the nervous system can be highly non-linear?

To find the answers to these questions, a novel approach will be required, that enables the monitoring of neural activity while the animal is actually moving in space and where more than one sensory modality is stimulated under closed-loop conditions.

1.1.3.4. Adaptation

Like other sensor system, visual sensors have a “dynamic range matching” problem. The dynamic response range within a neuron is rather limited compare to the dynamic range of sensory stimuli in nature. The solution is to shift and rescale the operating range of the cell with its set point centred to the mean stimulus intensity (Harris et al., 2000).

The adaptation of the H1-cell in blowfly has been investigated some time ago (Maddess and Laughlin, 1985). This study showed that the adaptation of the H1-cell was highly dependent on temporal frequency. Additionally, work from Harris et al. (Harris et al., 2000) shows adaptation does not only occur upon an adapting stimulus moving in the preferred direction.

Most of the physiological mechanisms of motion adaptation are not yet understood. Nonetheless, the adaptation is important so as to prevent the cells from saturation (Krapp and Wicklein, 2008).

1.2. Fly robot related work

Robotic technology is becoming more and more helpful in assisting researchers. It is particularly useful in several aspects of biomedical engineering, for instance when developing brain machine interfaces in the context of rehabilitation robotics and neuro-mechanical prosthesis (Warwick K et al., 2003). Robots can provide a useful platform to validate models derived from experimental data (Minegishi et al., 2013). They also benefit studies in neuroscience which may, in turn, inspire novel biomimetic engineering

solutions with respect to energy-efficient information processing and robust autonomous control design.

Due to improvements in semiconductor fabrication, electronics are becoming smaller in size and lower in power consumption. Conventional, normally bulky equipment can now be miniaturized to a size small enough to be embedded in some naturally behaving animals. For those animals too small to carry embedded systems, using a robotic system may be a first approximation of naturalistic closed-loop stimulus conditions while recording neural activities from the animal's nervous system. Such untether or half-tether methods may provide new possibilities for research that seeks to understand the design principles of biological sensorimotor control at the neuronal level.

In the next section, I will review a few systems related to insect brain machine interfaces, which inspired my work.

1.2.1. Robot in H1-cell closed-loop control

Ejaz and Peterson developed a fly robot interface (FRI) to study control laws for wide-field image stabilization using the activity of the blowfly H1-cells as feedback signal under closed-loop condition (Ejaz et al., 2011).

The robot was positioned on top of a turn table inside a cylinder with vertical black and white stripes pattern. Two high speed video cameras (200 fps) were fixed on top of the robot, oriented 45 degrees towards either side. When the turn table was rotated, it also rotated the cameras on top of the robot resulting in horizontal pattern motion. The pattern motion was captured by the high speed cameras and presented to a blowfly's compound eyes via two 200 Hz high speed CRT computer displays in front of the animal. The blowfly was stationary during the recording, located on a conventional recording setup (Figure 11).

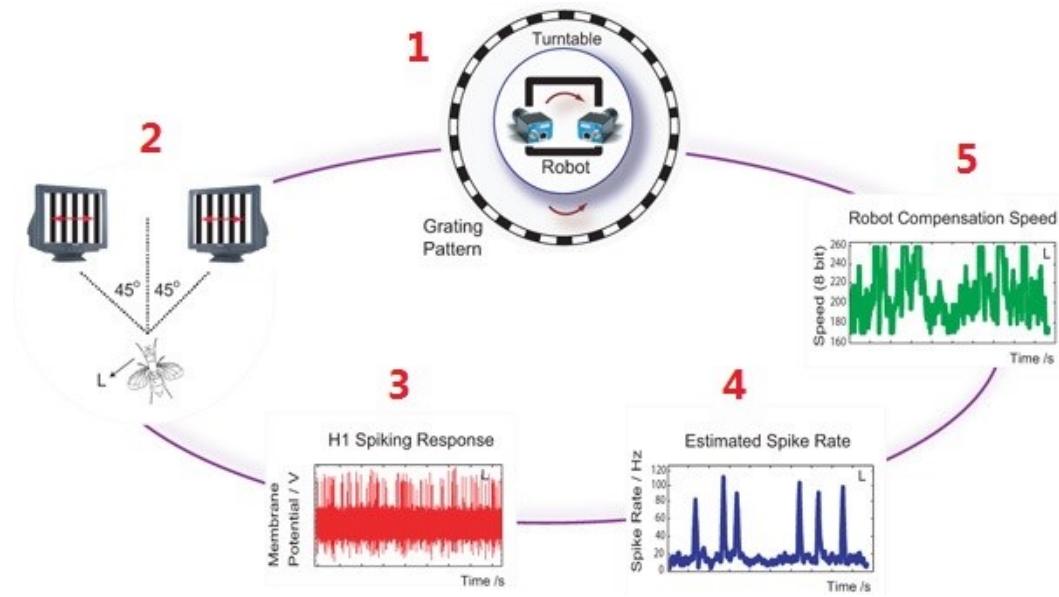


Figure 11. Closed-loop fly robot interface. (1) Two high speed cameras were mounted on a robot that was placed on a turntable. Turntable and robot were surrounded by a vertical visual grating pattern (special wavelength = 11 deg). (2) Rotations of the turntable generated horizontal optic flow, which was captured by the cameras and displayed on two CRT monitors. The blowfly H1-cell activity was recorded. (3,4,5) The cell's spike rate was processed and converted into a control signal, which drove the robot to compensate for the rotation of the turntable, stabilizing the visual input. Modified from (Ejaz et al. 2011)

The H1-cell activity of the blowfly was recorded extracellularly and its spike rate was used to control the robot rotation with a proportional controller to compensate of the turntable rotation, thus stabilizing the visual input. The results indicated a dependence of the FRI frequency response on the angular acceleration of visual motion. An adaptive controller was then used to control the robot, which dynamically scaled the feedback gain. The adaptive controller increased the bandwidth of the frequency response when compared with the performance of the fixed-gain proportional controller (Ejaz et al., 2013).

This system provided a starting point for studies into the neural mechanisms underlying a complementary combination of non-linear processes ultimately resulting in a linear performance of the overall system. The ultimate goal of this investigation will be to quantify the closed-loop dynamics of sensorimotor control at both the behavioural and neural level.

1.2.2. H1-cell recordings on a rotating platform

Lewen et al. have recorded blowfly H1-cell activity while the animal was rotating on the tip of a stepper motor shaft (Lewen et al., 2001). The setup

was designed so that the blowfly would experience naturalistic wide-field visual stimulation upon yaw rotations, without any pattern distortions. The experiments were carried out both indoors and outdoors under open-loop conditions. After comparing the response under natural light levels and lab light level, they found the noise entropy to be almost the same, while the signal entropy was a function of light level (Lewen et al., 2001).

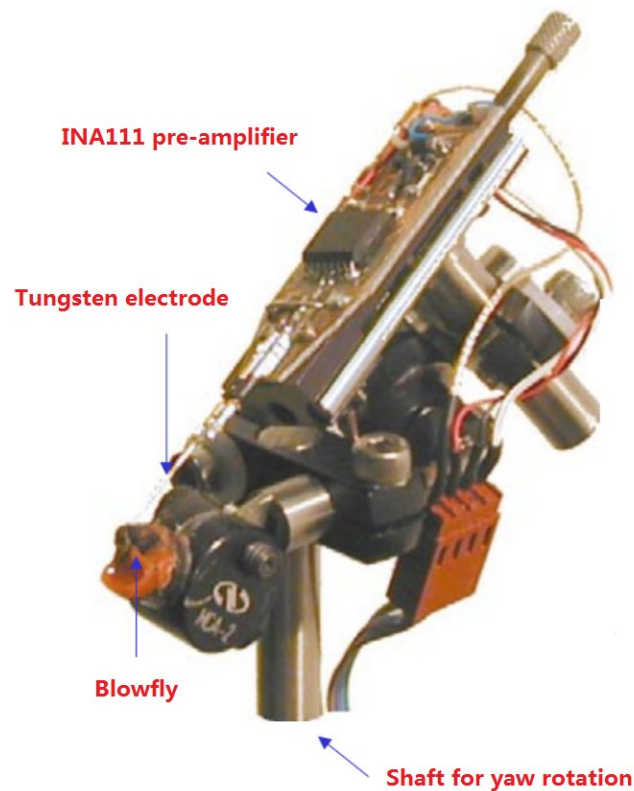


Figure 12. Lewen's neural recording setup. The blowfly was waxed in a tube exposing only its compound eyes and proboscis. A tungsten electrode was inserted into the lobula plate from behind. The extracellular H1-cell signals were pre-amplified and passed to a second amplifier stage via a slip ring. The whole system was mounted on the shaft of a stepper motor. Modified from (Lewen et al. 2001)

The thorax and abdomen of the blowfly were placed in a plastic tube and immobilized with wax. The compound eyes, proboscis, and the back of the head were left uncovered. A small feeding table was made by wax in front of the proboscis, from which the fly could access sugar water. A silver wire was contacting the body fluid as reference electrode while a tungsten microelectrode recorded the action potentials from the H1-cell extracellularly. The electrode signals were pre-amplified by a Burr-Brown INA111 integrated instrumentation amplifier. The pre-amplified signal then went through a slip

ring device, which allows the transmission of electrical signals from a stationary to a rotating structure, and amplified again by a second stage amplifier. A data acquisition card was used to digitize the signals for further data analysis in a computer.

The H1-cell of the fly was recorded under different indoor and outdoor light intensity conditions. The results suggested that the velocity tuning of the H1-cell depends on the absolute light level. At high light intensities the maximum responses occur at higher temporal frequencies – thus expanding the dynamic range of the H1-cell (Lewen et al., 2001).

1.2.3. Other mobile neuron recording system

Another platform is the brain-machine hybrid system built for closed-loop experiments in silkworms (Minegishi et al., 2013). The system was used to record from both cervical neurons of the silkworm on a robot, and showed that the moth could adjust its angular velocity by using sensory feedbacks caused by rotations of the robot which it was mounted on. This system enables stable extracellular patch recordings at angular velocities up to 86 deg/s, which is below the range required to effectively stimulate, for instance, the haltere in blowflies.

1.3. Summary

In this chapter, I firstly reviewed the organization of the blowfly visual system, including the function of most of its processing stages. Along the visual motion pathway local retinal image shifts are processed by arrays of retinotopically arranged elementary movement detectors and are finally integrated by wide-field directional-selective lobula plate tangential cells which indicate particular ego-motions. The H1-cell, one of the wide-field motion sensitive tangential cells in the lobula plate, is excited and inhibited by horizontal back-to-front and front-to-back optic flow, respectively. The spike rate of the H1-cell depends – besides other parameters – on the temporal frequency of the stimulus pattern

while generating spontaneous activity in the range around 30 spikes/s when no visual motion is presented.

One of the mechanical sensors, the haltere system, senses angular velocity of sudden attitude changes. Regarding multisensory integration, action potentials in neck motor neurons are triggered only if both visual and haltere stimulations are combined. In behavioural experiments, the halteres produce gaze stabilization responses at high roll angular velocities of the body. Together with visually induced head movements in the low angular velocity band, the integration of both sensors increases the bandwidth of the gaze stabilization system.

Robotic technology is becoming helpful in research on blowfly optomotor responses. For instance, H1-cell recordings on a stepper motor-driven platform have become feasible (Lewen et al., 2001). Further advance of robotic technology may enable a combination of behavioural and electrophysiological experiments on blowflies to study multisensory integration under closed-loop conditions.

Inspired by the work reviewed in this chapter, next I will outline the development of a miniaturized recording platform which is meant to be the core element of an experimental closed-loop system.

2. Miniaturized neural recording platform for robot applications

In this chapter, a miniaturized mobile recording platform will be introduced, on which a blowfly is mounted for electrophysiological recordings from identified motion sensitive interneurons in the fly visual system. The platform has been designed to accommodate all the equipment necessary to perform stable extracellular recordings while the platform is moved, either in terms of rotations on a stepper or a combination from translation and rotation of a small 2-wheeled robot. Here I will present the details of the design, both mechanical and electrical, as well as verifying the platform's performance.

2.1. Introduction

To study how the blowfly uses its various sensors for flight control, it is necessary that, whatever mobile platform is used, the dynamics of it at least overlap with the animal's flight envelop. This requires a purpose-designed solution which takes into account the small size of the insect.

The blowfly, *Calliphora vicina*, is a well-established model system for electrophysiological research on multisensory integration. It combines visual and mechanosensory information, achieving an aerobatic manoeuvrability that is unmatched by any man-made air-vehicle. The blowfly can achieve translational velocity of 2.5 m/s and angular rotation rates of 1700 deg/s in free flight (Bomphrey et al., 2009) with only about 10 mm of body length.

As we can see from table 1, the blowfly is not the fastest flying animal, but it has the highest Eigen speed (flight speed divided by body length) compared to the hawk moth and the bald eagle.

Table 1. The eigen speed of blowfly, hawk moth and bald eagle (Bomphrey et al., 2009; Stevenson et al., 1995)

	Blowfly	Hawk moth	Bald eagle
Body length (m)	0.01	0.06	0.96
Flight speed (m/s)	2.5	5.3	19.4
Eigen speed (body/s)	250	88.3	20.2

The blowfly's high Eigen speed is impressive, partly due to its small body length, which means less body weight, reduced inertial forces and less drag. On the other hand, small body length may come with limited muscle power, which means most of the muscle power is required for the fly to support its own weight rather than to produce lift for carrying additional payload

The conventional miniaturized 'on-board' recording systems which are designed for big insects, such as: locust (Harrison et al., 2011), hawkmoth (Wang et al., 2008), cockroach (Takeuchi and Shimoyama, 2004) are not suited to be fitted on a blowfly, due to its limited payload. Both size and weight of the system are important criteria, which will affect the aerodynamics of the blowfly, or even prevent it from taking off.

Schilstra and van Hateren (Schilstra and van Hateren, 1998) had designed coils which were mounted on top of the blowfly's head and thorax, to measure the orientation of the head and thorax while the blowfly was flying. The two coils were carefully designed to reduce interference with the blowfly's aerodynamics. They were both 2 mm in diameter, and weighted 0.8 mg and 1.6 mg respectively on head and thorax. Compared to the size and weight of the coils, Harrison's telemetry recording system for locust (Harrison et al., 2011) measures 13mm x 9 mm, and is almost 3 time bigger than a blowfly (the longitudinal and transvers dimensions of a blowfly are approximately 5 mm x 10mm). In terms of weight, Harrison's recording system including batteries amounts to 790 mg, while a blowfly is only 50 mg.

Because the approach from Schilstra and van Hateren (Schilstra and van Hateren, 1998) did not allow for in-flight recording of neuronal activity, more recently an AC-amplifier was designed for blowfly electrophysiological that

could be embedded into the blowfly's head capsule (Peterson, 2010). The dimension of the silicon die is around 1mm x 1.1mm. That is the smallest amplifier known so far. Full functionality of the system still requires the integration of micro power supply and electrode array before it may be used for recordings in freely flying blowflies.

Due to the fact that those miniaturized *on-insect* recording systems are not yet small enough to be applied to blowflies, a new solution is needed. Technically speaking, if a system can't be placed on a blowfly, then a blowfly has to be placed on a system. An alternative to in-flight recordings that still allows us to stimulate various sensors while monitoring the blowfly's neural activity would be a miniaturized electrophysiology setup placed on a robotic platform. Although limited in its dimensionality such system would be a first step toward studying multisensory integration under closed-loop conditions.

The work by Lewen and his colleagues (Lewen et al., 2001) I introduced earlier, comes close to my goal of recording neural activity in a freely-moving animal. Before their study, most of the electrophysiological experiments on blowflies were conducted when the animal was held stationary, to enable stable recordings.

A caveat of the otherwise excellent study by Lewen et al. (Lewen et al., 2001) was that, under natural conditions, blowflies don't only perform yaw rotations. They also engage on forward and backward translational movements. Both yaw rotation and translational movements will stimulate the H1-cells. For this reason, one stepper motor is not enough to generate naturalistic movements. A two-wheeled robot with independent wheel control, on the other hand, would more closely approximate the blowfly's movements in nature - certainly those of a walking fly.

Finally, there should be a stage in between the blowfly and the robot, which works as a transfer function that converts blowfly neural signals (input) into robot control signal (output). This transfer function is an essential part of the closed-loop condition, similar to the situation the fly would be in when moving through the environment. It requires to build an interface that uses visual feedback on the state changes of the fly generated by its own motion vision

system to control the movements of the robot, and thus its own trajectory in space. Such fly brain machine interface would require a signal chain through electrode, pre-amplifier, secondary amplifier, analog-to-digital converter and micro-controller along with its data transmission bus, such as a Universal Asynchronous Receiver/Transmitter (UART).

In this chapter, I will describe the mechanical and electrical details of a system I designed that will eventually be used to study multisensory integration in blowflies under closed-loop conditions.

2.2. Methods

2.2.1. Robot selection

One of the core elements required is an appropriate robotic platform. It will be used as a direct replacement of blowfly's own motor systems, and should enable the stimulation of the fly's sensors under closed-loop condition. There are, however, mechanical and electrical constraints regarding the robot selection and programming.

Mechanically, the robot needs to be able to carry the experimental setup without sacrificing its dynamic properties required to stimulate the fly's various sensor systems. Also, vibrations due to the action of the motors need to be sufficiently dampened to enable stable electrophysiological recordings. Closed-loop delays between measuring visual sensor signals and control of the motors driving the wheels of the robot will have to be short enough to stay within the biologically plausible range. The delay will be the result of microprocessor clock frequency, ADC sampling frequency, communicating baud rate and torque/speed characteristic of the motors.

Three types of two-wheeled robots were chosen as possible candidates. Their mechanics, electronics and processor capacity as well as software compatibility were taken into account when selecting the most suitable one for the project.

2.2.1.1. ASURO® robot

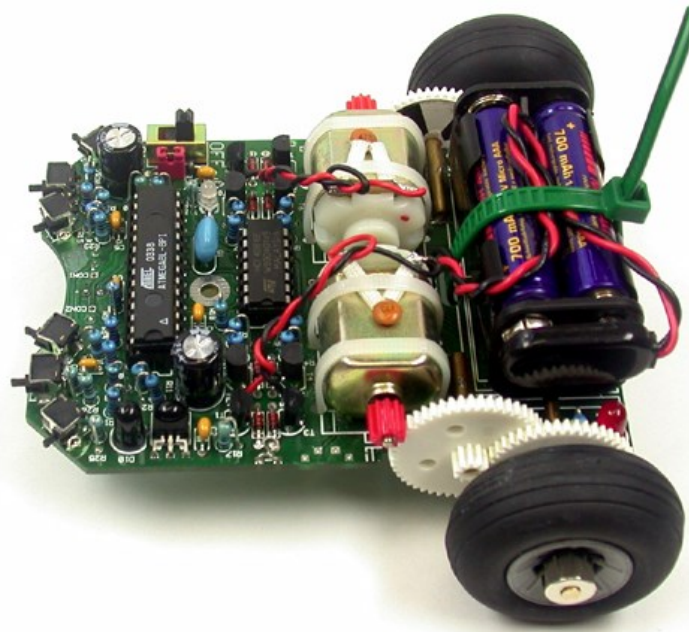


Figure 13. ASURO robot. The robot is powered by four AAA batteries. It equipped with an ATmega8L RISC-processor (8 MHz resonator system clock), an optical line-tracer, six collision-detector switches and two odometer-sensors. The processor can be programmed via a serial RS232 port or USB at baud rate of 2400 bps.

The ASURO robot is an educational robot, designed by the German Aerospace Centre (DLR). It was used in a study by Ejaz et al. (Ejaz et al., 2011) who exploited the activity of the H1-cell in a one degree of freedom visual stabilization task.

As we can see from the mechanical structure, the main PCB not only carries all the electronic components, but also acts like the chassis of the robot, locking the batteries, electrical motors, gears and wheels in position. The two independent controlled DC motors are driving two wheels through a 50:10 ratio gear-box.

The robot is powered by four AAA batteries and it is controlled by an ATmega8L RISC-processor, which has an 8 MHz resonator system clock. The ASURO is also equipped with an optical line-tracer, six collision-detector switches and two odometer-sensors. The robot is built using conventional through-hole electronic components, making it easy to assemble and repair. A pair of infrared transceivers - one set on the robot while the other one is in on a separate PCB which interfaces with a personal computer via serial RS232

port or USB - can be used to control the robot from a personal computer using serial port terminal software at baud rate of 2400 bps.

The ASURO robot can be programmed in C using freeware. The robot uses the same infrared channel for programming and updating the microprocessor memory remotely.

2.2.1.2. *Lego® mindstorms NXT 2.0 robot*

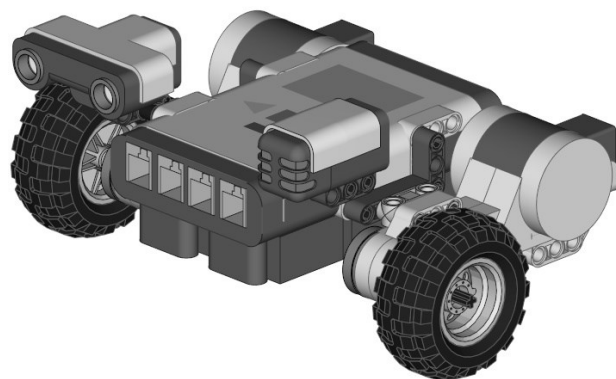


Figure 14. Lego Mindstorms NXT robot. The robot is controlled by Lego intelligent block which has an ARM core microcontroller inside. The processor is programmed via USB.

The Lego Mindstorms NXT 2.0 consists of robotics kits, which contains: an NXT intelligence block, various sensors (touch sensor, light sensor, sound sensor and ultrasonic sensor) and three identical servo motors with integrated gear box. The sensors and motors are connected to the intelligence brick via modified RJ12 cables. The brick can attach up to 3 motors and 4 sensors at the same time. The robot can be assembled in various shapes and sizes by using Lego blocks.

The intelligent brick contains most of the hardware, a 32-bit ARM7TDMI-core Atmel AT91SAM7S256 microcontroller with 256KB of FLASH memory, 64KB of RAM, an 8-bit Atmel AVR ATmega48 microcontroller, and Bluetooth support. The brick has a 100×60 pixel monochrome LCD display and four buttons that can be operated by the user through hierarchical menus. Power is supplied by six AA (1.5 V each) batteries in the consumer version of the kit and by a Li-Ion rechargeable battery and charger in the educational version.

2.2.1.3. 3pi® robot with mbed® controller

The 3pi is designed for line following and maze-solving competitions. It is small but powerful. The size of the 3pi robot is around 10 centimetres in diameter and it weighs 83 gram without battery, capable of moving at speeds up to 1m/second, which is in the range of what the blowfly produces.



Figure 15. 3pi robot with mbed controller. The robot is powered by four AAA batteries. It is controlled by ATmega328 microprocessor. The internal voltage regulator boosts the motor voltage to 9.25V, guarantees its speed performance.

The 3pi robot is controlled by an ATmega328 microcontroller, clocked at 20 MHz. ATmega328-based 3pi robots feature 32 KB of flash program memory, 2 KB RAM, and 1 KB of non-volatile EEPROM memory. Four AAA batteries supply power to the whole robotic system. In addition to the battery, there is a voltage booster module and regulator, which provides a regulated voltage of 9.25 volt. This results in highly consistent and repeatable performance of well-tuned code even when the batteries run low. The robot comes fully assembled with two micro metal gear motors, five reflectance sensors, an 8×2 character LCD, three user pushbuttons, all connected to the user-programmable Atmega328 microcontroller.

In addition, to compliment the performance of the 3pi robot, a company called mbed® produce a module using an NXP LPC1768 microprocessor. The NXP

LPC1768 is based on high performance ARM® Cortex™-M3 core, which runs at 96 MHz, together with 32 KB RAM and 512 KB FLASH memory. The module has several interfaces including USB Host and Device, built-in Ethernet, SPI, I2C, CAN, DAC, ADC, PWM and other I/O interfaces. The control unit is packaged as a small 40-pin DIP, 2.54mm pitch form-factor, making it convenient for prototyping using solder-less breadboards, stripboards, and through-hole PCBs.

Programming the module is as easy as using a USB Flash Drive because it includes a built-in USB programming interface. The USB drag & drop programming interface works with Windows, Mac OS X and Linux, which means updating the firmware does not require any drivers or a programming application. The binary programme can be easily compiled by using the “mbed Online Compiler”, or alternatively using any other standard off-line toolchain, such as: Keil uVision, Code Sourcery, Code Red, GCC, or IAR. A virtual serial port is also supported by using the same USB interface, enabling communication with a PC terminal running Labview, Matlab, or any other programming language that can operate a serial COM port.

2.2.1.4. Summary

Table 2. Comparison of robots

	ASURO	LEGO NXT 2.0	m3pi
Dimension (mm)	117x122x45	~168x168x56	Ø94 x 50
Weight (g)	165	>373	83
Velocity (m/s)	<0.79	0.498	1
Processor (bit)	ATmega8L (8bit)	ARMv7 (32bit)	ARMv7 (32bit)
Clock (MHz)	8	60	96
Cost (£)	34.00	230.00	93.00

As can be seen from the table, the m3pi generates the highest velocity, has the smallest dimension, lowest weight and fastest microprocessor clock speed.

It's not the cheapest module, but with its powerful ARM processor, there is no need to add cost on peripheral functions because of its high performance. For example, the 96 MHz clock frequency will allow the user to operate 2 channels of 20 KHz analog-to-digital conversion, together with the simple control of the electric motors, simultaneously on the same microprocessor. In comparison, ASURO and LEGO NXT will need support from external high speed ADC modules.

For these reasons, the m3pi was selected as the robot to be used as the platform for this project.

2.2.2. Mechanical design of recording platform

The mechanical parts of the recording platform were designed to ensure the stability of the neuronal recordings, as well as providing a physical connection to the two wheeled robot that includes mechanical vibration damping. It also made sure the electronic system was working under ideal environmental conditions, for example, being water protected, dust-proved and radio frequency noise tolerant.

2.2.2.1. Chassis

The chassis was designed to,

- 1) Fix the blowfly in the rotation centre of the platform
- 2) To minimize obstructions of the H1 receptive field.
- 3) To keep additional weight as low as possible

The chassis is composed of two parts, a disc and a rod. The disc accommodates the miniaturized electrophysiological devices (Fig 16). The rod in the centre is an extension of the disc used to mount the blowfly.

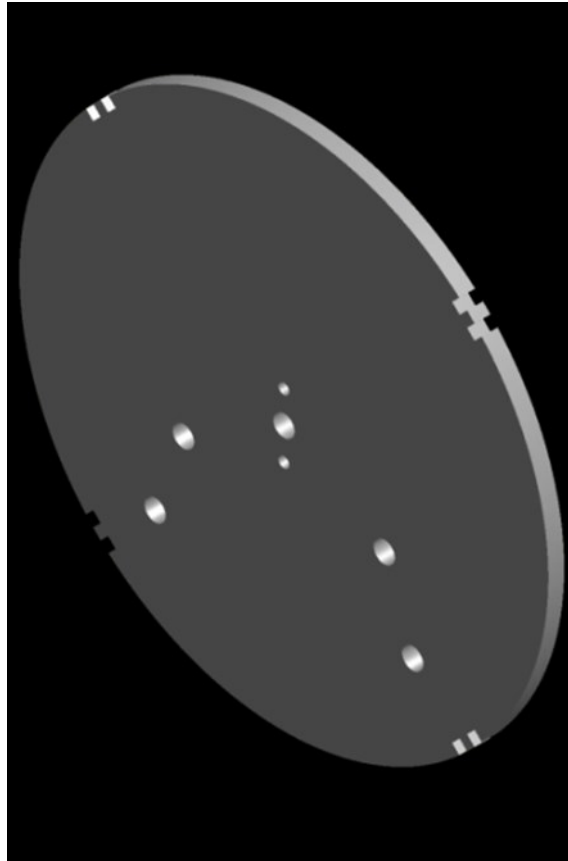


Figure 16. Chassis disc. It determines the distance between fly and electrodes.

The disc (Fig. 16) was cut from 3 mm aluminium sheet and its size matches the diameter of the 3pi robot. There are four pairs of notches on the edge of the disc, for connecting it with the robot, spaced at 90 degree intervals and three holes in the middle. A three millimetre hole in the centre was used for bolting on the central rod with a M3 screw. The adjacent two millimetre holes were positioned at the front and the back at a distance of 6 mm. These two holes were used for pivoting the disc and the rod, to provide mechanical stability during rapid angular accelerations of the disc. Mechanical stability is a necessary requirement for stable recordings. Any relative movements between the H1-cell, which is about 4-5 micrometre in diameter, and the sharp recording electrode placed right next to it may result in damages of the cell.

There are also two 4 mm holes used for mounting the holders for two small-scale micromanipulators.

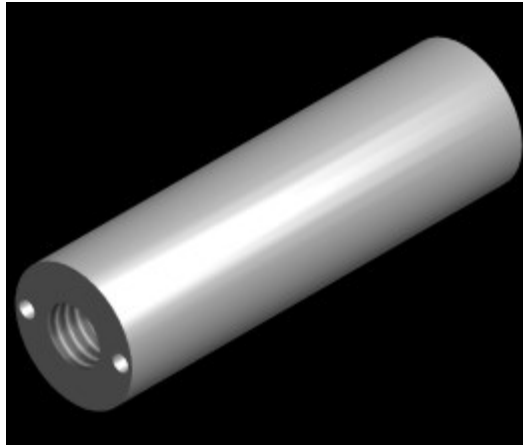


Figure 17. Chassis central rod. The component connects chassis and fly holder.

The blowfly will be mounted on the rod in the centre of the chassis disc. The H1-cell has a receptive field of approximately -45 to $+45$ degree in elevation (Fig 7). So the central rod (Fig. 17) was machined to 50 mm in length, which is the same as the radius of the chassis disc and prevents the ventral part of the cell's receptive field to be obstructed by the disc. For mounting, there are three holes on either end of the rod. The middle hole was threaded as M3, two 2 mm pivot holes on the sides were positioned to match the corresponding hole on the chassis disc. All holes are at least 10 mm deep.

2.2.2.2. Fly holder

A holder was built to position the fly in the centre of the chassis disc for electrophysiological recordings. It was made of four parts: a small Perspex tablet, a 2-way 2.54 mm interval standard pin header, two 2 mm banana plugs and a piece of wire (Fig. 18).

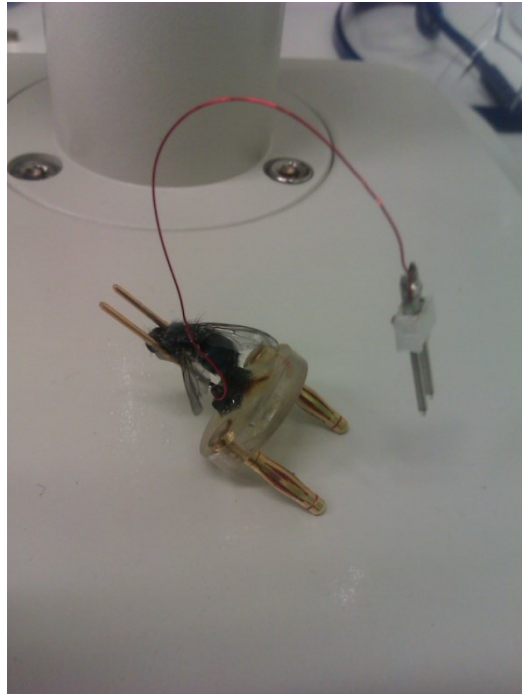


Figure 18. Fly holder. The component is used to fix a fly. The two pins also act as reference electrodes.

The fly holder (Fig. 18) serves two purposes:

- 1) Forms a mechanical connection between the blowfly and the chassis.
- 2) The wiring pins are used as reference electrodes while electrically isolating the blowfly from the chassis shielding.

The blowfly was waxed in between the pins, with its head in front and its thorax to the rear of the pins. The pins also serve as reference electrodes connected to a differential amplifier by half submerging it into the blowfly's haemolymph, avoiding a short circuit with the ground contact provided by the chassis.

2.2.2.3. *MM1-CR-XYZ micromanipulator*

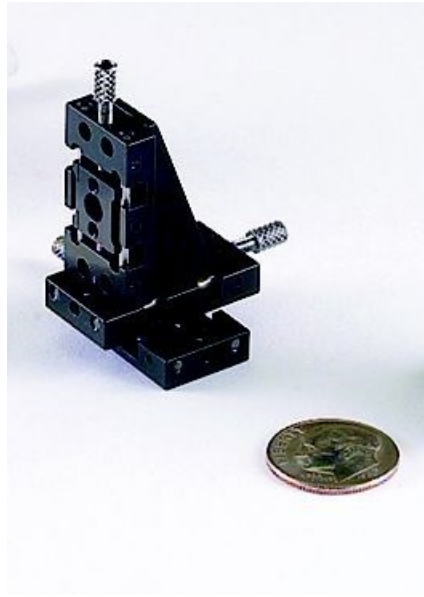


Figure 19. NAI® MM1-CR-XYZ micromanipulator. This small NAI® micromanipulator is much smaller and lighter than the Narishige® MX-2 model used in our lab. But this micromanipulator is much more difficult to operate as its light weight and small scale design is achieved at the expense of its mechanical stability.

The MM1-CR-XYZ micro manipulator is manufactured by National Aperture Inc. Due to its small size, this micromanipulator is highly sensitive to imprecise hand movements when operated. In order to minimize the effect of potentially damage the neuron by during handling, the manipulator block for thrust movement needed to be mounted onto a solid frame onto which the animal was mounted as well.

It was important to mount the thrust part of the micromanipulator to a solid surface, which reduced unwanted movements generated when using the knob screws for electrode placement. From measurement, 1 degree of knob rotation moves the sliding block 0.8 μm .

2.2.2.4. *Electrode holder*

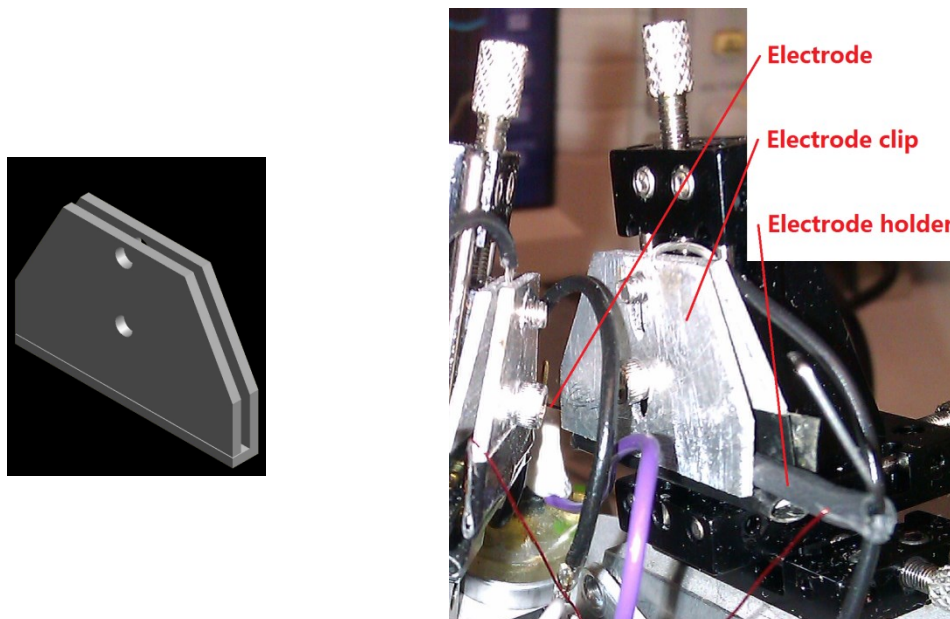


Figure 20. Electrode clip. (Left) This component clips the electrode holder and mounts onto the micromanipulator. (Right) The positions of electrode, electrode holder and electrode clip after assembled.

The electrode holder was made of two parts: the electrode socket (Fig. 20 Right) and the electrode clip (Fig. 20) both of which provided both stability for the electrode in position and provide electrical shielding.

The electrode socket was constructed by modifying one of the sheaths holding the electrodes in place within the original packaging (FHC® 3 M Ω tungsten electrodes, FHC Inc., Bowdoin, ME, USA), and simplifying their handling. Such an electrode sheath looks like a small metal tube with two slots on the side, wrapping around the electrode base, and a tungsten tail that is attached on the other end for handling. An electrode sheath was modified to an electrode holder which fits into the electrode clip, and electrically isolates it from the grounded electrode clip with electrical tape.

2.2.2.5. *Micromanipulator holder and amplifier enclosure*

To enable placement of the electrode within the fly head capsule the micromanipulators had to be raised to roughly the same level as the fly holder. I designed a base for the micromanipulators that serves two functions: (i) as

mentioned above, it levels the micromanipulator with the fly holder and (ii) by enclosing the amplifier it serves as an electrical shielding device. The micromanipulator base is a chunk of aluminium, with a 27 degree slope on the top. The angle is adjusted to prevent collisions of the electrode tip with the blowfly thorax when inserting the electrode into the brain. There are four threaded holes for 0-80 screw on the top, arranged to mount MM1-CR-XYZ micromanipulator. And two threaded holes for M4 screw on the bottom of the micromanipulator base, to mount it on the chassis.

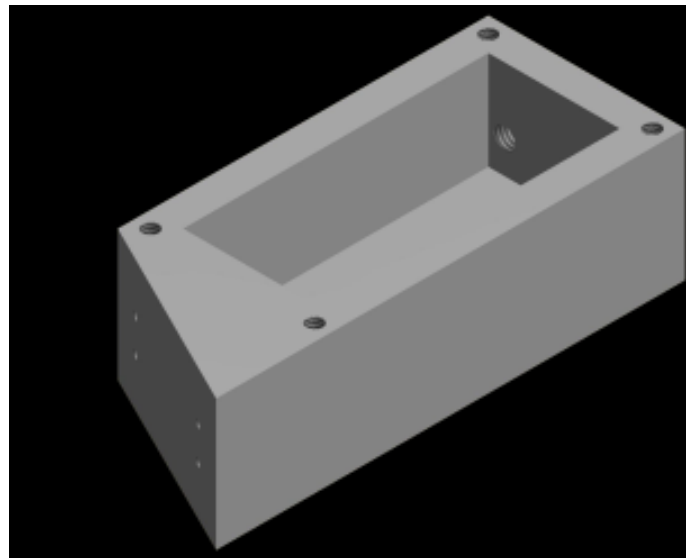


Figure 21. Micromanipulator holder. This component is the connection between chassis and micromanipulator. It also serves as a faraday cage of miniaturized amplifier.

The micromanipulator holder (Fig. 21) is hollowed for two reasons: for one, it reduces the weight of the recording platform and thus limits the loss of the robot's dynamics. Secondly, it serves as a Faraday cage for the amplifier and reduces dust contamination. The hollowed space within the micromanipulator base is 20mm x 30mm x 15mm in volume, which set the size constraints for the customized PCB including the amplifier (appendix 1).

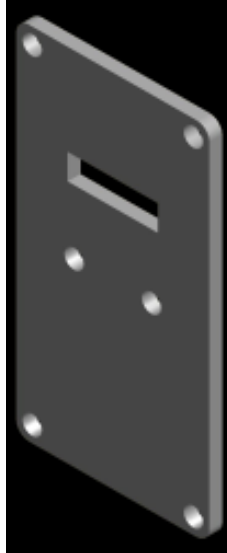


Figure 22. Amplifier enclosure lid. This component holds the miniaturized amplifier and mounts onto the micromanipulator holder.

The lid (Fig. 22) for the micromanipulator base was made from a 2 mm thick aluminium sheet to cover the hollowed space, as well as supply mechanical support for the PCB (section 2.2.3.2). It was fitted onto the micromanipulator base by 3 mm screws on the corners. Two 3 mm holes in the centre were aligned with the PCB mounting holes and a slot cut-out for amplifier input/output connector.

2.2.2.6. *Stabilizing beam*

The stabilizing beam is a machined aluminium component that connects to the central rod and micromanipulator bases on the upper side. This part tightly connects the fly holder and electrode holder to provide additional stability.

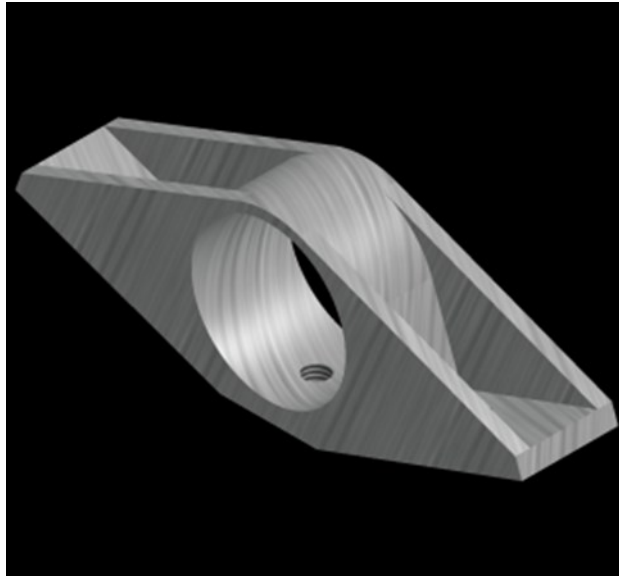


Figure 23. Stabilizing beam. This component is used to tighten the central rod and two micromanipulator holders.

The beam (Fig. 23) has a ring in the middle and two wings, one on each side. The ring has the same diameter as the central rod, and a three millimetre threaded hole on the anterior side of the ring was used to tighten the beam to the rod. There are 2 three millimetre holes on the wings for fixing them to the micromanipulator holders. The beam provides additional mechanical stability to the setup.

2.2.3. Electrical design of recording platform

2.2.3.1. Amplifier design specification

The electrical part of the project was mainly concerned with the design of the amplifier system. To be useful for electrophysiological recordings on a small robotic platform four general specifications had to be met: (i) small size, (ii) single power supply, (iii) low power consumption, and (iv) high gain.

As described above, space for an amplifier system inside the micromanipulator base was limited. The size of the PCB needed to be restricted to 20 mm x 30 mm and the height of the components should not be more than 15 mm. As conventional through-hole components were too large to be squeezed into the available space, surface-mount electronic components were the best choice.

The single supply operation was necessary because the robot requires 0-5V battery power. It was more efficient to use the same battery for both, the robot and the amplifier rather than employing two separate power supplies. A single supply amplifier works the same way as conventional dual supply amplifiers, but instead of an output signal range from -10V to +10V (0V as reference), the single supply amplifier output signal ranges from 0 - 5V (2.5V reference).

The power consumption of the amplifier needed to be as low as possible to sustain its function throughout closed-loop experiments on the robot when both amplifier and motors will draw current.

The gain of the amplifier was required to be approximately 10^4 in total, since the electric field potential generated during an action potential is in the range of $10^{-5} - 10^{-4}$ Volts and the analog-to-digital converter on the robot was also powered by the 5 Volt battery.

2.2.3.2. Amplifier system

With the specifications in hand, the task was then to select suitable components and assemble them in correct order to build an adequate amplifier system.

I used the structure of the conventional amplifier, a pre-amplifier followed by a secondary gain stage amplifier. This was necessary because it would have been difficult to reach a gain of 10^4 by using only one amplifier, due to noise, stability and bandwidth limitations. According to the required specifications, and after testing several options, I used off-the-shelf chips INA333 and AD8607 cascaded together with a gain of 10^2 each. (The circuit schematic is attached in the appendix.)

The INA333 uses FETs (Field-Effect Transistor) as input rather than BJTs (Bipolar Junction Transistor). The FET is driven by the gate electric field to control the conductivity of a channel, which requires much less current than the BJT transistor. By testing amplifiers using BJT transistors as input stage I found that they do not enable the recording of neuronal electric field potentials (e.g., AD8223). The INA333 instrumentation amplifier has bandwidth up to 3

KHz, which covers most of the frequency spectrum of neuronal action potential. This is in agreement with the low pass filter setting of commercial amplifiers (NPI) at 3 KHz.

AD8607 and OPA2333 were suitable as the secondary amplifier because their 40 dB (gain of 100) cut off frequencies were both around 4 KHz.

The design of the whole system was miniaturized to meet the tight space limitations. Both instrumentation amplifier and secondary amplifier were placed adjacent to each other. The neuronal field potential was fed into the INA333 through decoupling capacitors, plus a precise 2.5V bias voltage generated by an AD1582 component. After initial amplification the signal was passed on to the AD8607 for the second amplification to achieve an overall gain of 10^4 .

2.2.4. Systems for verification

After all the electrical and mechanical components of the miniaturized recording platform were assembled, the next step was to verify the functionality of the system.

To this end I recorded the neural activity of the H1-cell (see section 1.1.2.5) under two different conditions and compared the results (a) between the different conditions and (b) with previously published data. In one condition I tested the recording platform while the fly was mounted on a stepper motor and rotated around the vertical axis within a cylinder lined with a visual grating pattern. In the second condition the fly was kept stationary but the grating pattern was rotated around the fly. Under both conditions the relative motion between the fly's compound eyes providing the input to the H1-cell and the visual pattern were identical. The difference, however, was that the vibration from the stepper motor would reach the fly and electrode when the fly is rotated, but would not when the pattern is rotated. These two experimental conditions therefore allowed me to evaluate whether or not vibrations might have an impact on the recording of the H1-cell to visual motion.

The experimental setup used here included two stepper motors, one on the bottom to rotate the blowfly and the recording platform, the other on the top to rotate the visual stimulus. Both of the stepper motor systems were controlled by a computer which was also used to analyse the recorded data.

2.2.4.1. Stepper motor system

The stepper motor was a high power, high frequency electrical device which had to be shielded to avoid interference with low power precision analog devices, such as the electrophysiological recording system. The whole stepper motor system, together with its driver and power supply were enclosed in a 250mm x 250mm x 100 mm aluminium die-cast box which was connected directly to the electrical ground.

Inside the box, the stepper motor (QSH5718-76-28-189, Trinamic®) is controlled by a stepper motor driver (P808A, Astrosyn®). The driver translates the direction and frequency pulse signals to 4-way stepper motor control sequences. It supports micro-stepping up to 50 KHz. The stepper motor and its driver were powered by an AC/DC converter with 48 Vdc / 3 A outputs. The inputs to the stepper motor driver were buffered by two hex-inverters (74HCT04) used as a Schmitt trigger, to be compatible with low current input.

After the aluminium box lid was closed, it became a sealed aluminium box with two BNC socket providing pulsed signal inputs (one for direction, the other for frequency) and the torque output from the stepper motor shaft.

The input signals to the stepper motor driver were delivered from analog outputs of a data acquisition card, NI-DAQ (NI-USB-6215, National Instruments Corporation, Austin, TX, USA). The NI-USB-6215 is a device that can be configured as a high speed signal source from a computer through a USB port. The signal sequence data were transferred to the NI-DAQ from the computer and buffered inside its internal memory. Triggered from the computer, the NI-DAQ was reading out the signal sequence data from its buffer memory controlled by its interior high speed clock and played it back from its DA convertor.

2.2.4.2. *Pattern cylinder clip and internal LED ring light*

The grating pattern used for visual stimulation was clipped to the wall of a cylinder. It consisted of vertical black and white stripes at a fundamental spatial wavelength of 30 degrees.

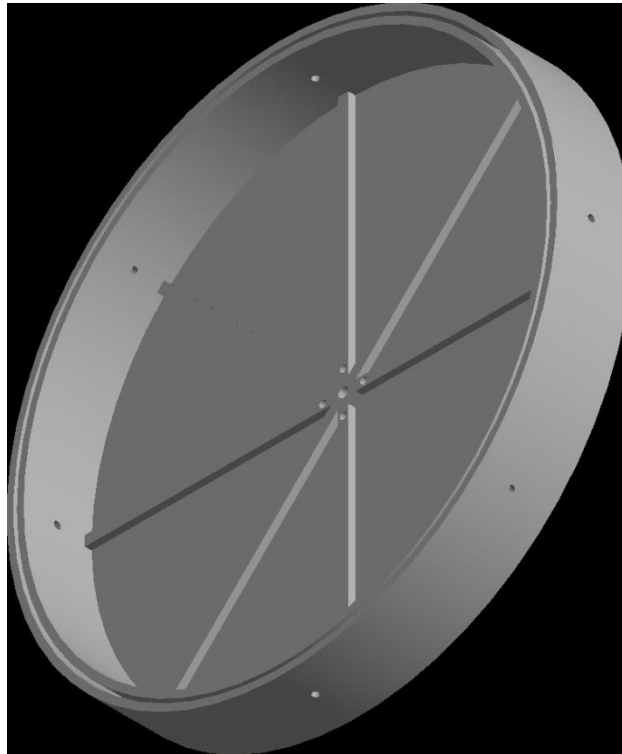


Figure 24. Pattern cylinder clip. This component clips paper pattern cylinder and mounts onto a stepper motor shaft.

The pattern cylinder clip (Fig 24) was manufactured by 3D printing in plastic.

To illuminate the visual grating pattern an LED ring was made by white adhesive LED stripes (Maplin® N91NA). They were assembled to build a homogeneous ring light and fixed to the pattern clip. The LEDs were powered by a 9V battery.

2.2.4.3. Assembly and shielding of systems

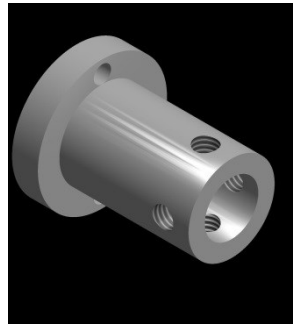


Figure 25. Motor shaft connector. This component connects the platform chassis and pattern clip to the stepper motor shaft.

The recording platform and the pattern clip were both connected to the stepper motor shaft through a steel component as shown in figure 25.

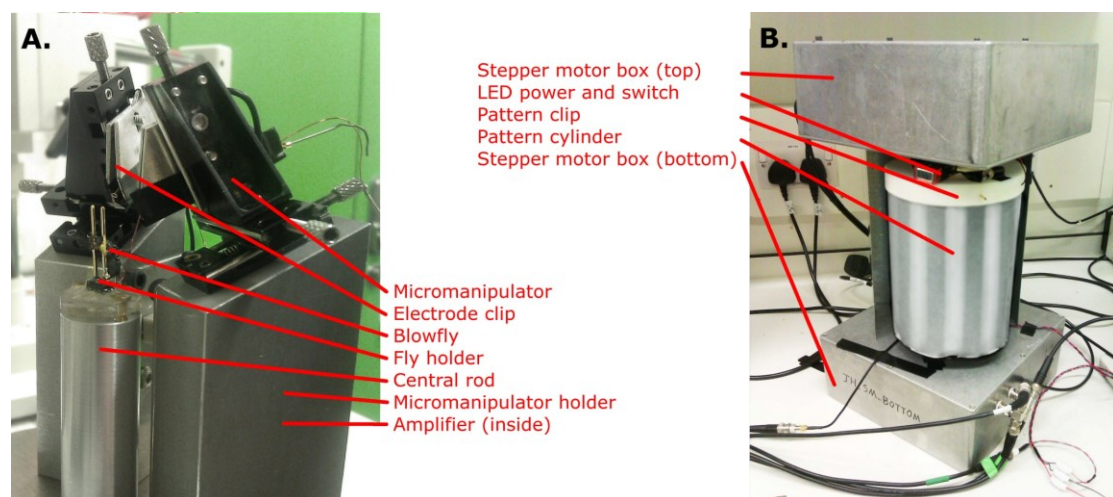


Figure 26. Fully assembled recording platform. (A) The fly is mounted so that a recording electrode can be inserted to the lobula plate from back of the head. **(B)** Experimental test setup. The recording platform is mounted on top of a stepper motor shaft (bottom). The surrounding grating pattern (special wavelength = 30 deg) is connected to the shaft of the top stepper motor. (Huang and Krapp, 2013)

The recording platform was assembled as shown in figure 26A. It was connected with the stepper motor on the bottom. The pattern clip was connected with the stepper motor on the top, as is shown in figure 26B. A metallic spacer was placed in between the two stepper motor boxes. The gap below the pattern cylinder was helpful when aligning the blowfly in the centre of the pattern cylinder.

All metal pieces were grounded, avoiding any ground loops, and connected to the amplifier reference.

2.2.4.4. Blowfly preparation

Female blowflies, *Calliphora vicina*, aged between 4 and 11 days were chosen for H1-cell recording. They were bred in the lab under a 12:12 hour's light-dark cycle.

Blowflies were inserted into Perspex tubes and immobilized/anesthetized by placing them in a mixture from water and ice for several minutes. The wing hinges were blocked by applying small amounts of bee-wax. The blowflies were then placed ventral side up on a small board with double sided adhesive tape. Legs and proboscis were removed and the resulting wounds were sealed with wax to prevent desiccation. The openings of the respiratory system, spiracles, were left unblocked. The animals were then placed on the fly holder (see Fig 18) by sliding the neck in between the two metal pins. The fly's head was aligned with the horizontal plane based on the pseudopupil method (Franceschini, 1975), before waxing it to the pins of the holder. The thorax was then pushed down and fixed to the sides of the pins to expose the rear head capsule.

The head capsule was opened under 40 x magnification of a stereo microscope (Stemi 2000, Zeiss©) using a micro scalpel. Fine forceps were then used to remove the cuticle on both sides of the rear head capsule. Ringer solution [for recipe see (Karmeier et al., 2001)] was applied to keep the tissue moist. Fat tissue, muscle tissue and air sacks were removed until the web of tracheae – the tubular ducts of the respiratory system – became visible.

The placement of the recording electrode was guided by the characteristic branching pattern of the major trachea within the lobula plate which related to the location and orientation of H1-cells.

2.2.4.5. Programming and experiment sequences

The stepper motors are controlled by custom-written software programmed in Python v2.7 under windows XP sp3 environment, together with the Python

extension package including numpy, scipy and nidaqmx. The source code is attached (cf. appendix 2a).

The micro-stepping frequency of the stepper motor driver was set to 50,000 steps per 360 degree, which enables the smoothest performance of the system. The analog output sampling frequency of NI-USB-6215 was set to 200 KHz, corresponding to the highest stable output frequency. The NI-DAQ would theoretically drive the stepper motor at angular velocity of 4 revolutions per second, which is equivalent to an angular velocity of 1440 deg/s.

When quantifying the speed of the motion stimulus, the temporal frequency, f , has to be considered as the relevant parameter which takes into account the spatial wavelength of the visual pattern:

$$f = \frac{\Omega}{\lambda}$$

Where Ω is the angular velocity, and λ gives the spatial (angular) wavelength.

Since the spatial wavelength used here is 30 deg, an angular velocity of 300 deg/s corresponds to 10 Hz temporal frequency.

To reduce any detrimental impact sudden angular accelerations and decelerations of the stepper motor may have on the stability of the electrophysiological recordings, changes in angular velocity were sinusoidal. The stimulation protocol used during the recordings from the H1-cell, lasted 10 seconds per trial and included the following 4 sequences

1. 0.5s no motion (H1-cell fires spontaneous spike rate).
2. 3s stimulation of null direction motion (H1-cell is inhibited).
3. 3s stimulation of preferred direction motion (H1-cell is excited).
4. 3.5s of no motion.

The null direction motion and preferred direction motion were presented at the same angular velocities.

During an experiment temporal frequencies in the range from 1 Hz to 10 Hz were delivered in a shuffled order. This order was mirrored for another 9

repeated trials (Fig.28 A). After 10 repetitions of trials where the fly was rotated, the same sequence was applied again, but this time while the fly is stationary and the grating pattern was rotated. This stimulation protocol was used throughout the experiments reported in this thesis, if not specified differently.

2.3. Results

2.3.1. Instantaneous recording stability analysis

Figure 27 shows typical results of an experiment where the fly was rotated, demonstrating that the miniaturized recording platform is indeed suitable for stable recordings of extracellular neural signals. In this specific experiment, the H1-cell spikes were recorded from the axon in the right lobula plate, while visual motion is presented to the left compound eye. The time course of the angular velocity of the recording platform is shown in Figure 27A, which, in this case, reached a maximum 270 deg/s in the counter-clockwise and the clockwise direction, respectively. Figure 27B shows the neural response of the H1-cell. The extracellularly recorded large action potentials (spikes) could be easily differentiated from the background noise. To visualize the shape of individual spikes Figure 27C presents the section marked by the two vertical black lines in Figure 27B, at higher time resolution. The signal to noise ratio (SNR) in this recording, which is the peak potential of the action potential compare to the envelop of the noise level, was high enough to detect individual action potential by using a simple voltage threshold criterion (horizontal red line, Fig. 27B) rather than a computationally expensive spike sorting algorithm. To compute a time-continuous measure of the neural response the instantaneous spike rate was calculated which is based on the inter-spike intervals (ISI) between consecutive action potentials. The instantaneous spike rate corresponds to the inverse of the time interval between two spikes (ISI), multiplied by one second.

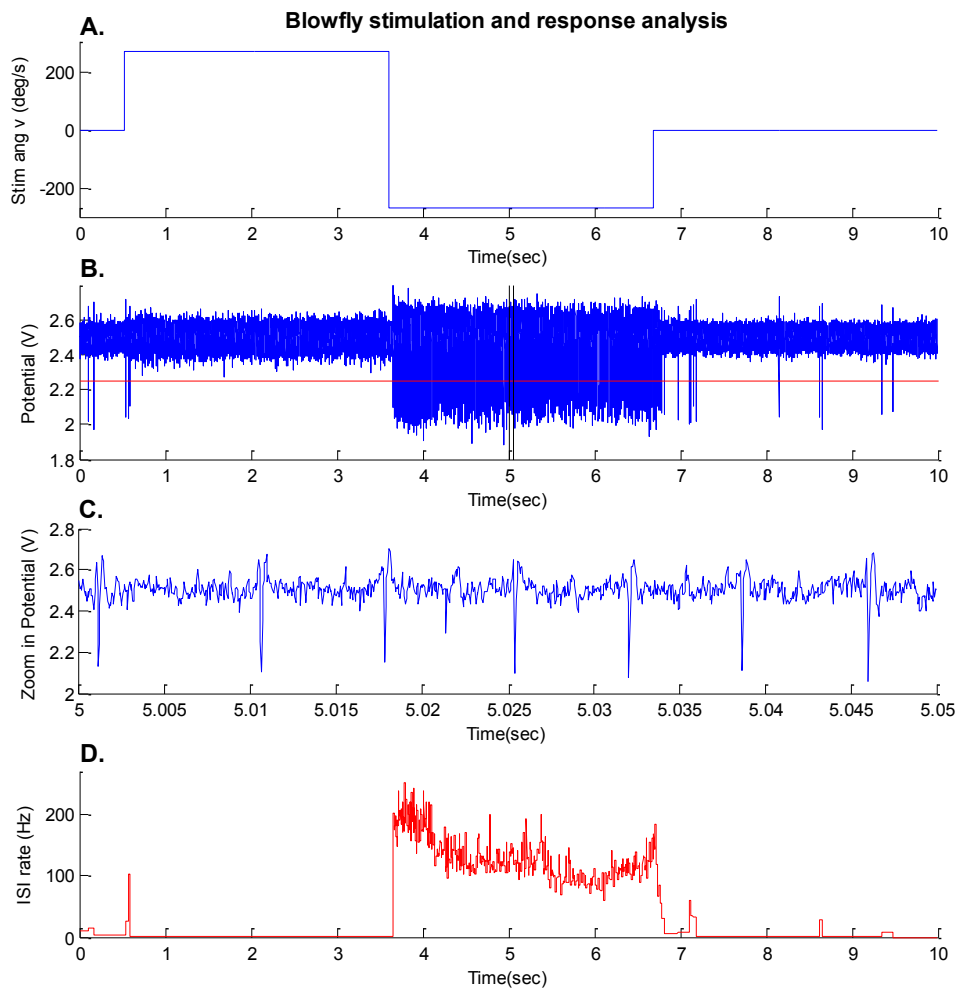


Figure 27. Stimulation and response during a 10 second H1-cell recording. (A) The angular velocity curve of stimulation (here, positive and negative angular velocities refer to motion in the anti-preferred and preferred direction of H1-cell, respectively). (B) The action potentials generated by the H1-cell under stimulation as described in A. The red horizontal line indicates the threshold potential for the spike sorting. The black window marks the section of the data magnified in C. (C) The zoom-in plot of the H1-cell action potential sequence described in B. (D) The spike rate of H1-cell, calculated from the time interval (inter spike interval, ISI) between two consecutive action potentials.

The responses of the H1-cell under these stimulus conditions were in agreement with previous studies (Jung et al., 2011). During counter-clockwise rotation the grating pattern moves from front-to-back over the left eye. (As mentioned in section 2.1.2.5) the H1-cell is inhibited during front-to-back motion which clearly is the case in this experiment. During the 3 seconds of counter clockwise rotation the H1-cell hardly generated any spikes – except for a few transient ones at the beginning of the rotation (Fig 27B and D). If the fly is rotated in the opposite direction and the relative motion between the

grating pattern and the left compound eye is from back-to-front, the H1-cell generates spikes at rates exceeding 200 spikes/s in the initial phase (Figure 27B and D). When no relative motion occurs between the grating pattern and the fly, the spike rate assume low values around 25 spikes/s, a value that is well within the variability range commonly observed across different flies (Egelhaaf et al., 2001).

In the context of this work the results presented in Figure 27 are of particular significance because: The spike amplitudes of the H1-cell did not change over the course of the trial despite the rotation of the platform. This demonstrates that the recoding platform provides sufficient mechanical stability to sustain high quality extracellular recording. Otherwise, had any relative movements between the electrode and the cell during the recoding occurred – even at the micro meter scale – the spike amplitude would have changed as a result of an increased or decreased distance between electrode and cell. The constant spike amplitude and thus the SNR indicate that this was not the case.

Secondly, the instantaneous spike rate shown in Figure 27D increased to around 200 Hz when the rotation switched from null direction to preferred direction, and adapted to around 100 Hz while the rotation continued at a constant angular velocity. The spike rate never exceeded 400 Hz throughout the entire recording. Spike rate above 400 Hz are generally indicative of an unphysiological state of the neuron, which could be the result of damage caused by the electrode. Together, these observations suggest that the recordings were stable and the cell was in a healthy physiological state.

2.3.2. Prolonged recording stability analysis

So far I presented evidence that a stable recording would be achieved over a period of 10 seconds. In the following I will show data obtained throughout an entire experiment lasting over 30 minutes.

Figure 28A shows the temporal frequencies (y-axis) applied over the duration of the experiment (x-axis). Each dot represents the temporal frequency of the stimulus presented in each 10 seconds recording. The sequence was shuffled

and kept in the same order for another 9 times. Recordings during which the fly was rotated are shown in red, blue symbols indicate experiments where the pattern was rotated.

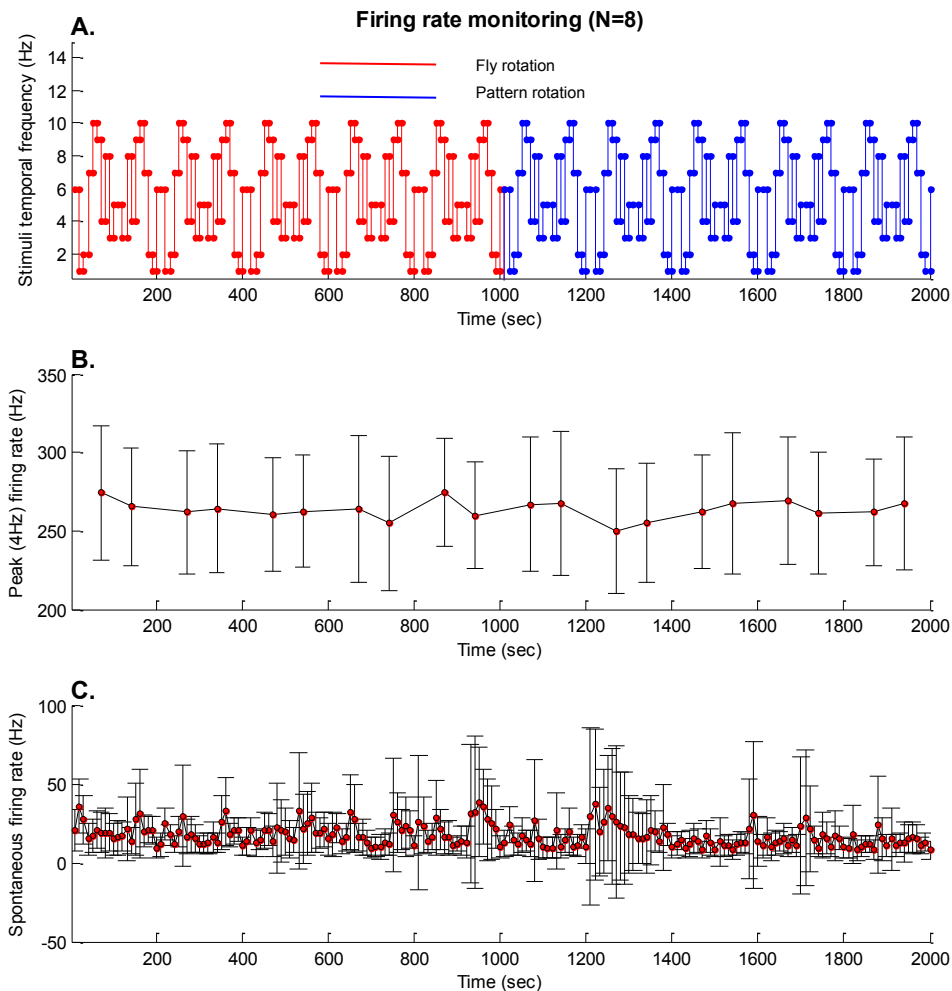


Figure 28. Experimental stability analysis. (A) The sequence of temporal frequencies of the stimulus used in the experiment. (B) Mean and standard deviation of spike rate at 4 Hz temporal frequency. (C) Mean and standard deviation of spontaneous spike rates. (N=8) (Huang and Krapp, 2013)

Figure 28B shows the mean peak spike rate and standard deviation over the whole experiment for responses obtained at a temporal frequency of 4 Hz (see section 2.1.1.2). In agreement with previous studies (Jung et al., 2011; Maddess and Laughlin, 1985) my experiments shown maximum peak spike rate when the H1-cell responds to a temporal frequency of 4 Hz. The averaged peak spike rates are all between 250 to 300 Hz for each repetition of the given temporal frequency, with similar standard deviation.

Figure 28C shows the averaged spontaneous spike rate based on 8 animals throughout the whole experiment. Except for a few temporary increases, from the start until the end of the experiment the spontaneous activity stays at about the same level.

The H1-cell is 1200 micrometer long, connecting the left and the right lobula plates in the fly brain by an axon that has a diameter of about 5 micrometer. The tungsten electrode tip is around 1 micrometer and needs to be placed right next to the neuron to achieve a good signal noise ratio. From experience we know, if the electrode tip is too far away from the neuron, the recorded signal amplitude will be very small. If the electrode tip is too close to the axon, the cell membrane may be damaged. A damaged neuron generates excessively high rates of action potentials due to a massive depolarization of the membrane potential which caused voltage gated sodium and potassium channels to open. If the membrane damage is small enough, the cell may regain a normal physiological state after a while when the membrane is still able to reassemble and seal any holes. But if the membrane damage is severe, and the cell won't be able to recover, the amplitude of the action potentials will become smaller over time, until the cell eventually dies.

The stable averaged peak- and spontaneous spike rate observed in the experiments tells us that no damage on the cell was inflicted during the whole experiment period. At no time did the peak spike rate reach 400 Hz, which would have been the case had the cell membrane been injured. The fairly constant spontaneous spike rate at about 20 to 30 Hz also indicates a healthy state of the cell. And finally, throughout the experiment the cell was responding to the stimulus in a directionally selective way which also reflects a proper physiological state. A few bursts of the spontaneous spike rate occurred, but a normal activity level was reached right afterwards. Bursting activity was thought to reflect internal activity modulations associated with the attempt of the fly to change its locomotor state, a phenomenon that is well documented in the literature (Longden and Krapp, 2010). Altogether the results suggest that the mobile platform enables stable recordings from the H1-cell over an extended period of time in all the experimental animals tested. (a link to a video is supplied in appendix 3). The data shown here were only

meant to demonstrate recording stability, the entire set of results will be presented in chapter 4.

2.4. Summary

The goal of the work described so far was to design, manufacture and test a miniaturized mobile platform that enables stable extracellular recordings from motion sensitive neurons in a blowfly.

On the wing, the blowfly is highly manoeuvrable, though, due to its small size, it is virtually impossible to study the neural mechanisms underlying its multisensory flight control while the animal is freely moving. Rather than embedding a recording system in a blowfly's brain, the present attempt is a first step towards the development of an experimental platform that will eventually enable neural recordings under closed-loop conditions. . Whether or not this goal will be achieved depends on a number of prerequisites which include the choice of an appropriate robot, the miniaturization of electrophysiological equipment and the demonstration that stable recordings can be achieved on a moving platform.

As far as the mobile robotic platform is concerned, out of three candidate systems the m3pi was chosen, the specifications of which suggest it to be better suited for the task than the ASURO or the Lego NXT robots. In particular its fast speed, light weight and powerful controller were the reasons to favour the m3pi over the other robots. Accordingly, the design of the miniaturized recording platform was based on the dimensions of this robot.

The design of the recording platform was constrained by both mechanical and electrical considerations. Except for the micromanipulators, which were off-the-shelf, the mechanical components were optimized to enable high recording stability without adding too much inertia to the system, in which case the dynamics of the robot would be further reduced. The electrical components had to comply with the size constraint given by the limited space inside the shielding micromanipulator base. A customized PCB was designed to accommodate a stage amplifier on a small scale that achieves a gain of 10^4 .

To test the performance of the miniaturized recording platform a computer-controlled stepper motor system was built. It allowed me to assess the stability while monitoring extracellular spiking activity in a directional selective interneuron. I carried out experiments under conditions where either the fly was rotated within a patterned cylinder or the fly was kept stationary and the pattern was rotated. The results obtained under both conditions demonstrated that the platform enabled prolonged high quality recordings without inflicting any damage to H1-cells studied in eight different animals.

In next chapter, the H1-cell of the blowfly will be characterized on top of a stepper motor with this verified recording platform.

3. H1-cell response characterization using the miniaturized recording platform

In this chapter, I will describe experiments on the H1-cell performed to assess the cell's suitability for robotic control. As mentioned in the previous chapter, the responses of the cell to visual motion were recorded under two different stimulus conditions: 1) during wide-field motion stimulation by rotating the fly within a stationary grating pattern, and 2) during wide-field motion stimulation by rotating the grating pattern around the stationary fly. These two stimulus conditions also allowed me to investigate whether or not mechanoreceptive systems modulate the responses of the H1-cell. Because of its obvious significance for closed-loop control, the stimulus parameter I studied in these experiments was temporal frequency. I identified the range of temporal frequencies within which a near linear relationship between the speed of pattern motion and the cell's responses exists.

3.1. Introduction

In order to learn how the blowfly utilizes the responses of its lobula plate tangential cells (LPTCs, cf. chapter 2) for flight control, a fundamental requirement is a quantitative analysis of the cell's responses as a function of visual stimulus parameters.

The H1-cell is one of the most popular LPTCs, the response properties of which have been characterized over many decades. H1-cell activity has been studied more than the activity of any other LPTCs, not only regarding its role in the control of optomotor behavior. It had also been studied in the context of applying information theory to work out the "neural code" used in the nervous system (Lewen et al., 2001), or to study circadian changes in sensory information processing (Bult et al., 1991) and finally, of course, to learn about the properties of the elementary motion detector (Lindemann and Egelhaaf, 2013). It is readily accessible for electrophysiological recordings and responds

to horizontal wide-field motion which a ground-based mobile platform is likely to generate.

In this chapter, recordings of H1-cell activity are presented that were performed under two conditions: 1) the fly was rotated within a stationary cylinder lined with a panoramic, vertical stripe pattern, and so experienced visual motion as well as mechanoreceptive stimulation – which we refer to as the “fly rotation” condition later; and 2) the pattern was rotated around the fly, and so it experienced visual motion – which we refer to as the “pattern rotation” condition. In the fly rotation condition, the halteres and other mechanoreceptors are stimulated in addition to the motion vision pathway, while in pattern rotation condition, it is only the motion visual pathway that is stimulated.

With the possibility of moving either the fly or the visual pattern, we can perform experiments to investigate how mechanoreceptors affect visual sensory in gaze-stabilization. We also have the potential to explore how the fly’s sensory systems can be integrated to usefully control its movements.

I performed four sets of experiments:

In the first experiment, I characterize the temporal frequency tuning of an H1-cell. The purpose of this experiment was to validate the functionality of the recording platform, by comparing tuning curves generated from data measured with my miniaturized equipment to results obtained using conventional setups reported in the literature (Jung et al., 2011).

The aim of the second set of experiments is to establish whether the simultaneous stimulation of mechanosensory systems alters the temporal frequency tuning of the H1-cell. To do this, I derived the temporal frequency tuning from the response measured when the fly was rotated, and compared the results to those obtained in stationary flies. I then repeated the experiments on flies the halteres of which had been removed.

In walking and flying flies, the temporal frequency tuning of LPTCs is modulated (Chiappe et al., 2010; Jung et al., 2011). Potentially, this modulation could reflect the impact of mechanosensory signals. Moreover,

some neck motor neurons which receive input from the LPTCs only generate action potentials if visual motion stimuli are combined with haltere stimulation (Huston and Krapp, 2009). Therefore, my experiment would help to find out whether halteres directly or indirectly modulate the responses of the LPTCs, in this case, the H1-cells.

In the third set of experiments, I characterized the responses of different sizes of the visual patterns. I was concerned that the cell's dynamic output range would be limited by potential size-dependent saturation non-linearities. Therefore, I decreased the area of the motion stimulus, by reducing the height of the visual grating to 2%, and compared the temporal frequency tuning curves derived from rotating the fly or the pattern with those obtained using the larger patterns.

In the fourth set of experiments, I investigated the impact of motion adaptation on the H1-cell responses. In flying or walking flies, motion adaptation affects the impact of locomotion on the temporal frequency tuning of the cell (Jung et al., 2011; Longden and Krapp, 2009). I therefore measured the temporal frequency tuning before and after the cell had been adapted to visual motion.

3.2. Experiment 1: H1-cell temporal frequency tuning

In this experiment, I investigated the H1-cell activities when mechanoreceptive systems on top of the motion vision pathway were stimulated and when the fly was presented only with a visual motion stimulus. As mentioned above, these two stimulus conditions were achieved by either rotating the fly or rotating the grating pattern. Another important purpose of these experiments was to demonstrate that the miniaturized recording platform enables stable extracellular recordings while the whole platform is moving at high angular velocities, a necessary condition for the application in autonomous robot control.

3.2.1. Method

H1-cell activity was recorded using the mobile recording platform introduced in the chapter 2. A vertical black and white visual grating was placed around

the blowfly. The responses of the H1-cell were recorded during fly rotation and pattern rotation.

For the recording, 4 - 11 day-old blowflies were chosen, immobilized using ice, and then fixed to a fly holder using bee wax. The cuticle of the back of the head capsule was removed. Fat tissue and muscles covering of the lobula plate were also removed, but the tracheae on the surface of the lobula plate were left intact.

To perform the recordings, a tungsten electrode was inserted into the lobula plate. I used the pattern of tracheae as visual landmarks to identify appropriate recording sites. The tip of the electrode was placed close to the estimated location of the axons of the contralateral H1-cell. The signal-to-noise ratio, i.e. the ratio between the amplitude of the H1-cell action potential peak to the amplitude of the background activity, was always higher than 2:1.

The recording platform was mounted on the shaft of a stepper motor positioned below the platform. A cylinder lined with a visual grating surrounding the fly was suspended from above and connected to a second stepper motor. The visual grating consisted of black and white vertical stripes with a spatial wavelength of 30° , printed on 200 g/m^2 A4 paper. For illumination, the cylinder was lit by 14 white LED (Maplin®: N91NA) as a circular light clipped on the top inside of the cylinder. The room light was turned off with the beginning of the experiments.

The blowfly has wide field of view in this arrangement. The view covers more than -90 deg to $+90 \text{ deg}$ in azimuth, and from -45 to $+90$ in elevation.

In order to derive the temporal frequency tuning curve, I stimulated the cell with pattern motion at angular velocities from 0 to 300 deg/s . In this experiment, temporal frequencies are from 1 Hz to 10 Hz, due to the spatial wavelength of 30° . Each temporal frequency stimulus was applied in a shuffled order and repeated 10 times, which was mirrored at each repetition, using alternating sequences to cancel any results caused by stimulus order.

H1-cell was first recorded during rotation of the fly, then the fly was kept stationary and the pattern was rotated. An entire experiment lasted for at least 2000 seconds (or 33 minutes 20 seconds).

A NI-USB-6215 data acquisition card was used for stimulus control and to store recorded neural signals on a PC. Software programmes controlling both processes were custom written in Matlab (Mathworks®). The motors were driven by a P808A stepper motor driver, which was controlled by an analog output channel of the data acquisition card. The neural signals were amplified by on-board amplifiers inside the recording platform (cf. chapter 2) before being sampled by the analog digital converter of the NI-USB-6215.

3.2.2. Result

After the recordings, the H1 spike trains were compared with a threshold to obtain the information about spiking events over time. The spike rate was calculated by averaging the number of action potentials generated during three seconds of visual stimulation in the cell's preferred direction (Fig. 27). The resulting rate was then averaged across 10 stimulation repetitions within one animal. To plot the overall temporal frequency tuning curve, the data from eight blowflies were collected to calculate the interindividual mean and standard error (Figure 29).

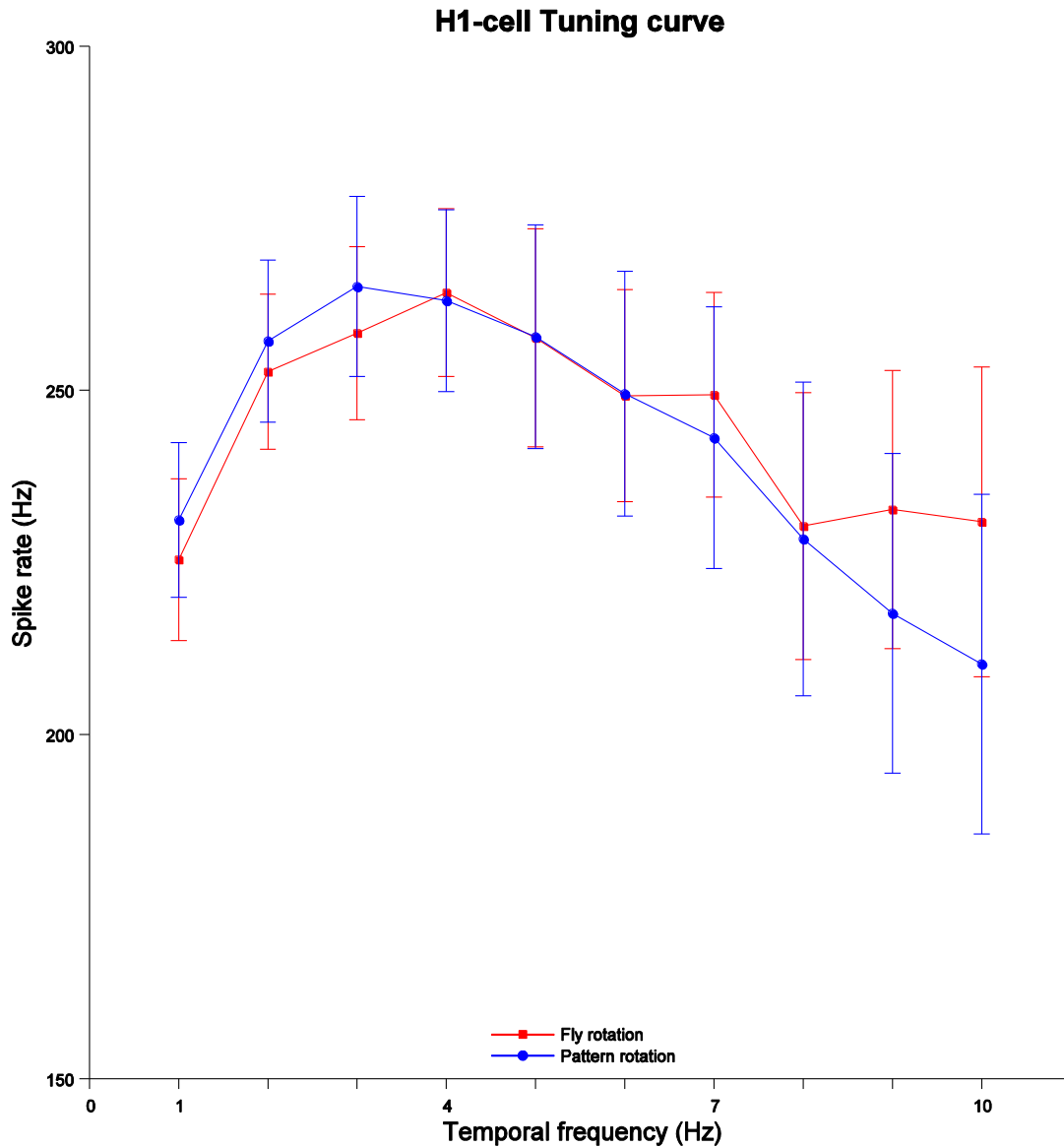


Figure 29. The H1-cell temporal frequency tuning curves under both fly rotation and pattern rotation conditions. The results are based on data from eight blowflies. Error bars give the standard error of the mean.

The shape of H1-cell temporal frequency tuning curves shown in Figure 29 was found to be similar for both rotation of the fly and rotation of the pattern. Although the average responses upon rotations of the fly at high frequency are slightly higher, there was no statistical difference. Altogether the optimum-shaped temporal frequency tuning of the H1-cell derived with the miniaturized recording platform is comparable with results obtained in previous studies where conventional equipment was used (but see discussion).

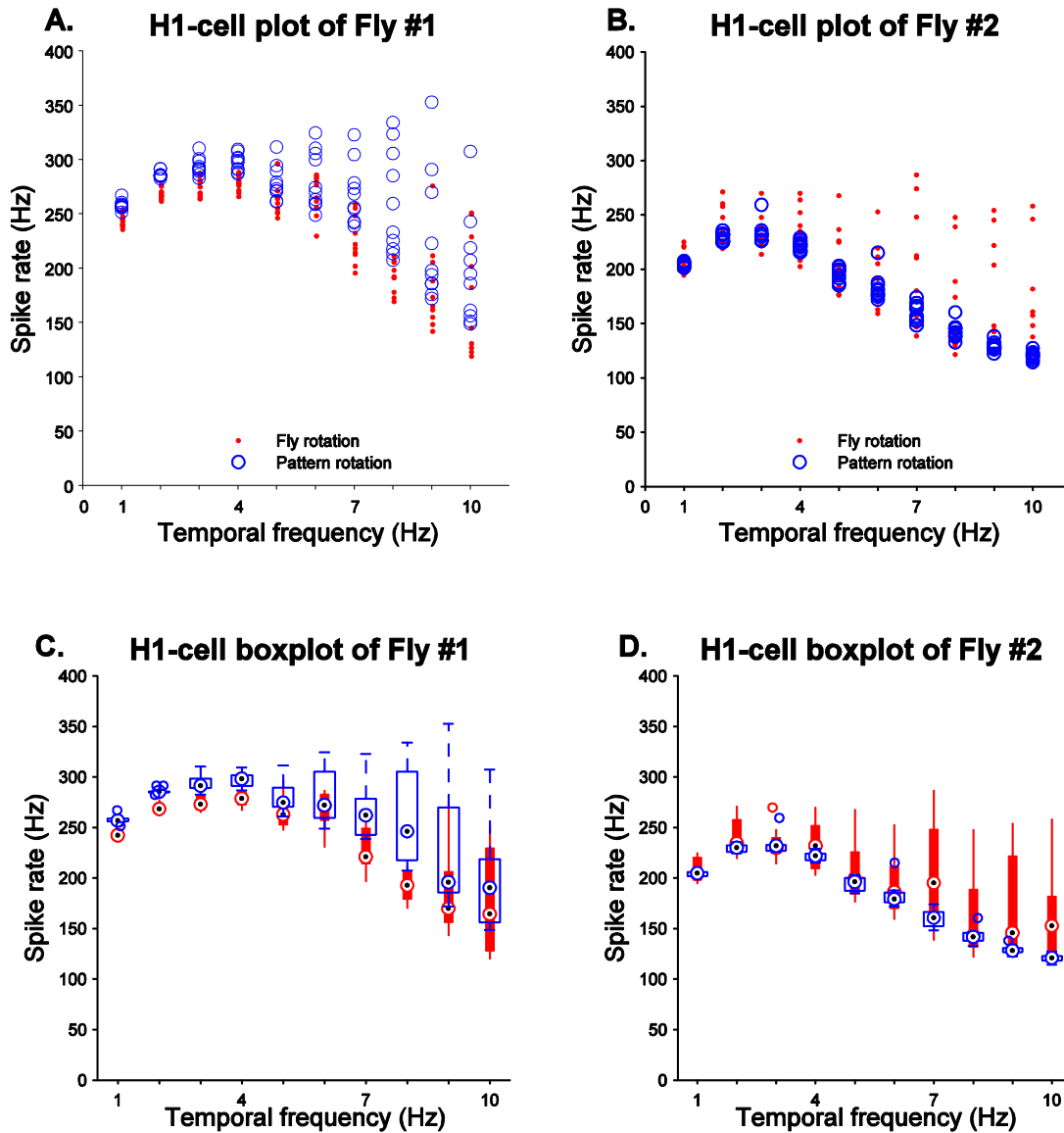


Figure 30. Extreme results obtained from individual animals: (A) The plot of individual trials of fly #1, where the variability of the spike rate is higher in pattern rotation condition. (B) the plot of individual trials of fly #2, where the variability of the spike rate is higher in fly rotation condition. (C) The boxplot of fly #1, showing similar mean spike rate to B. (D) the boxplot of fly #2, showing similar mean spike rate to C.

While the average results presented in Fig 29 appear to be consistent with data reported in the literature, the responses of individual flies to the range of tested temporal frequencies can be rather different. This is shown in Figure 30. For example: fly one (Fig. 30, left panels) had a higher spike rate variability in the responses to high temporal frequencies during pattern motion, while fly two (Fig. 30, right panels) had a higher variability of spike rates at high temporal frequencies during the rotation of the fly. Nevertheless, from the boxplot, both flies generated similar averaged spike rates for both experimental conditions.

3.2.3. Discussion

The results of this experiment allow for two conclusions: first, and most importantly, the custom-designed recording platform works as efficient as a conventional recording setup to obtain the H1-cell temporal frequency tuning. Second, as far as the mean temporal frequency tuning of the H1-cell is concerned, there is no differences between responses obtained under visual wide-field stimulation upon fly rotation and pattern rotation.

Temporal frequency tuning curves of blowfly H1-cells have been investigated in previous researches where commercial equipment was used (Jung et al., 2011; Longden and Krapp, 2010; Maddess and Laughlin, 1985). The H1-cell tuning curves show peak spike rates at a temporal frequencies between 1-5 Hz, in cases where the fly is fixed to a setup that delivers a local visual by 58 deg in circular angle (Maddess and Laughlin, 1985).

Here, the H1-cell responses were first recorded during pattern motion at temporal frequencies from 1 Hz to 10 Hz, where the peak temporal frequency was found at 4 Hz under wide field visual stimulation. The resulting tuning curves were virtually the same as those reported in previous studies (Jung et al., 2011; Maddess, 2001). This means the custom designed mobile recording platform works as good as the conventional recording setup.

I have already shown in the previous chapter that the gain and bandwidth of the miniaturized amplifier are properly tuned and that the system enables stable recordings. The experiment presented here further proves that the different settings in my mobile recording platform regarding angular extent and luminance do not produce H1-cells temporal frequency tuning curves which are qualitatively different from those obtained with conventional setups.

Secondly, H1-cell activity was recorded under wide-field motion stimulation induced by rotating the fly, where the visual grating was kept stationary. In this case, the blowfly experienced the same optic stimulation as it did during pattern rotation, but in addition mechanoreceptors – for instance the halteres or antennae – were stimulated. From a comparison of the respective tuning

curves (Fig 29), we can see that the H1-cell responses upon the rotation of the fly are similar to those during pattern rotation. It could be inferred that under the experimental conditions applied no mechanoreceptive signals altered the responses of H1-cell.

Additionally, the means of spike rate is slightly higher in the fly rotation condition than the rate in the pattern rotation condition. One of the assumption is due to the internal locomotor state change, when the fly was trying to take off (Jung et al., 2011; Longden and Krapp, 2009) after some mechanoreceptors were stimulated at high velocities.

On the other hand, an interesting finding of this study was that the variability of spike rates increased at high temporal frequencies. Two extreme cases have been presented (Fig 30), which shown that such increased variability occurred in both cases, during fly rotation and pattern rotation. This suggests that the temporal frequency-dependent increase in response variability is not related to whether or not mechanoreceptive stimuli were accessible to the fly.

The H1-cell is part of the network of horizontal LPTCs including the HS-cells (Borst and Haag, 2002b) which are the output cells from the lobula plate connecting to descending neurons. H1-cells are therefore indirectly involved in optomotor responses and gaze stabilization both of which compensate for rotational deviations from an equilibrium point. But the other function of HS cells studied by the Lindemann et al. (Lindemann et al., 2005) is to estimate relative distance during translational sections of flight. This function is of potential interest for robot control.

3.3. Experiment 2: Halteres removed

In this experiment, the H1-cell activities were recorded before and after removal of the halteres. An unspecific activation of the halteres during neck motor neuron recordings has shown an interaction between motion vision and haltere signals (Huston and Krapp, 2009). The high degree of variability at high temp frequencies found in the previous experiments could potentially reflect such unspecific interaction. After all, as halteres operate best in the

high velocity range. By removing the halteres, I made sure they would not provide any signals that could modify the H1-cell activity.

3.3.1. Method

The blowfly dissection, preparation, and recordings were performed in the same way as described in the previous section. But contra-lateral H1-cell activities were measured only under conditions where the fly was rotated with halteres kept intact or with halteres removed.

The range of temporal frequencies applied for stimulation was increased to 20 Hz. The angular velocity profile of the stepper motor was kept the same, from 0 to 300 deg/s, but the spatial wavelength of the pattern was reduced from 30 degree to 15 degree. Ten temporal frequencies were applied: 0.2 Hz, 1 Hz, 3 Hz, 4 Hz, 5 Hz, 8 Hz, 11 Hz, 14 Hz, 17 Hz and 20 Hz. These temporal frequencies were delivered in a shuffled sequence, which was alternated in mirrored order between repetitions. Each set of experiments was repeated 10 times.

During the first set of experiments, the H1-cell activities were recorded with intact halteres. After the recording, the halteres were pulled out by a pair of tweezers under the microscope. The second set of experiments was conducted using the same stimulus parameters, only in flies without halteres.

Four sets of experiments were applied on one blowfly. In the first two sets of experiments H1-cell activities were recorded by rotating the fly in the stationary pattern cylinder with and without halteres. The second two sets of experiments were performed using the laboratory environment as visual stimulus.

3.3.2. Result

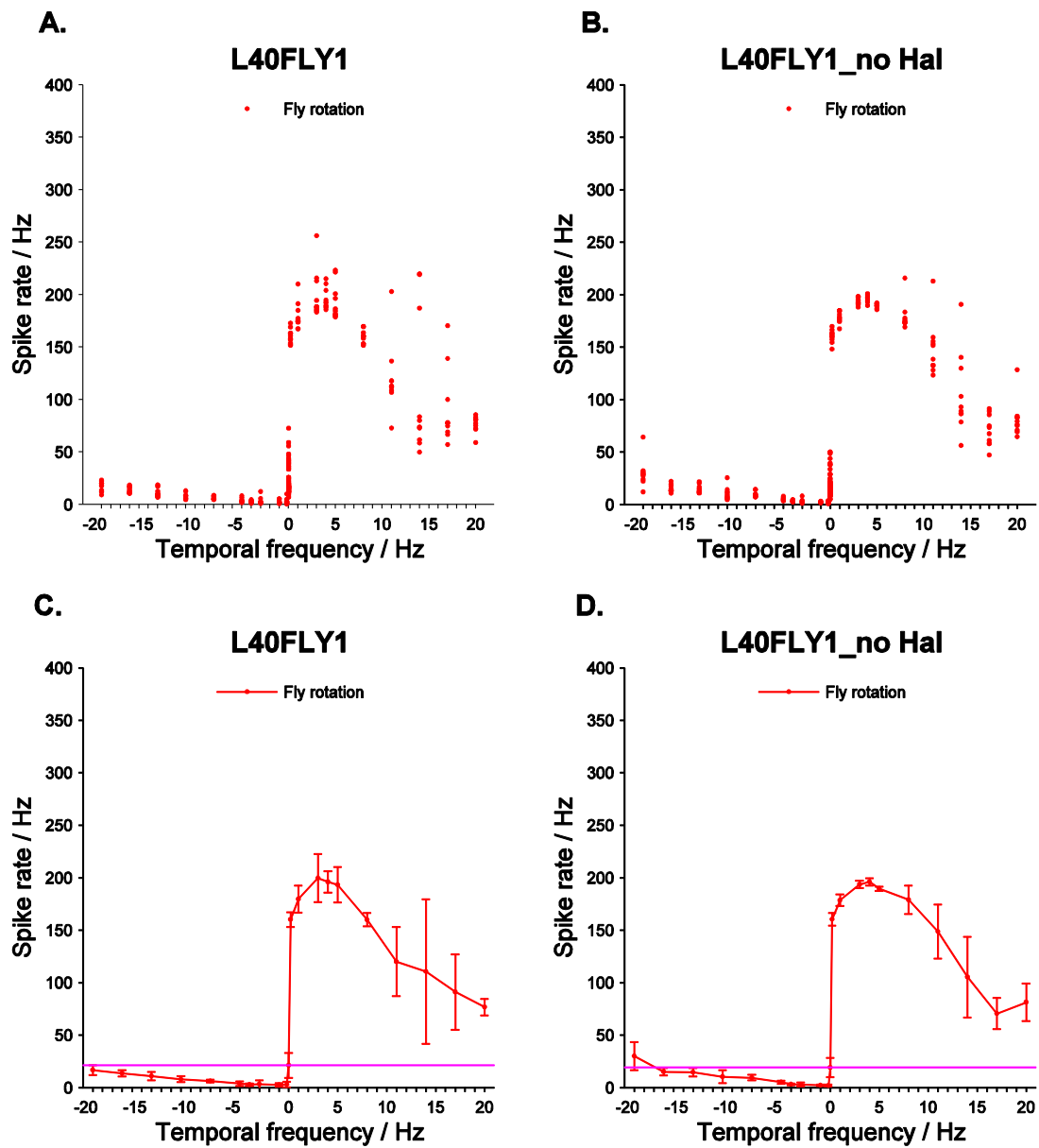


Figure 31. H1-cell temporal frequency tuning curves obtained with vertical black and white stripe pattern with and without halteres. Plots A, B are trials of stimulations at various temporal frequencies. Plots C, D are means and standard deviations of the H1-cell temporal frequency tuning (N=1). Plots A, C are obtained from blowflies with halteres; Plots B, D are based on experiments in blowflies without halteres. Positive and negative temporal frequencies correspond to visual stimuli in the preferred and anti-preferred direction of the H1-cell, respectively. The straight purple lines in plots C, D indicate the overall mean spontaneous spike rate.

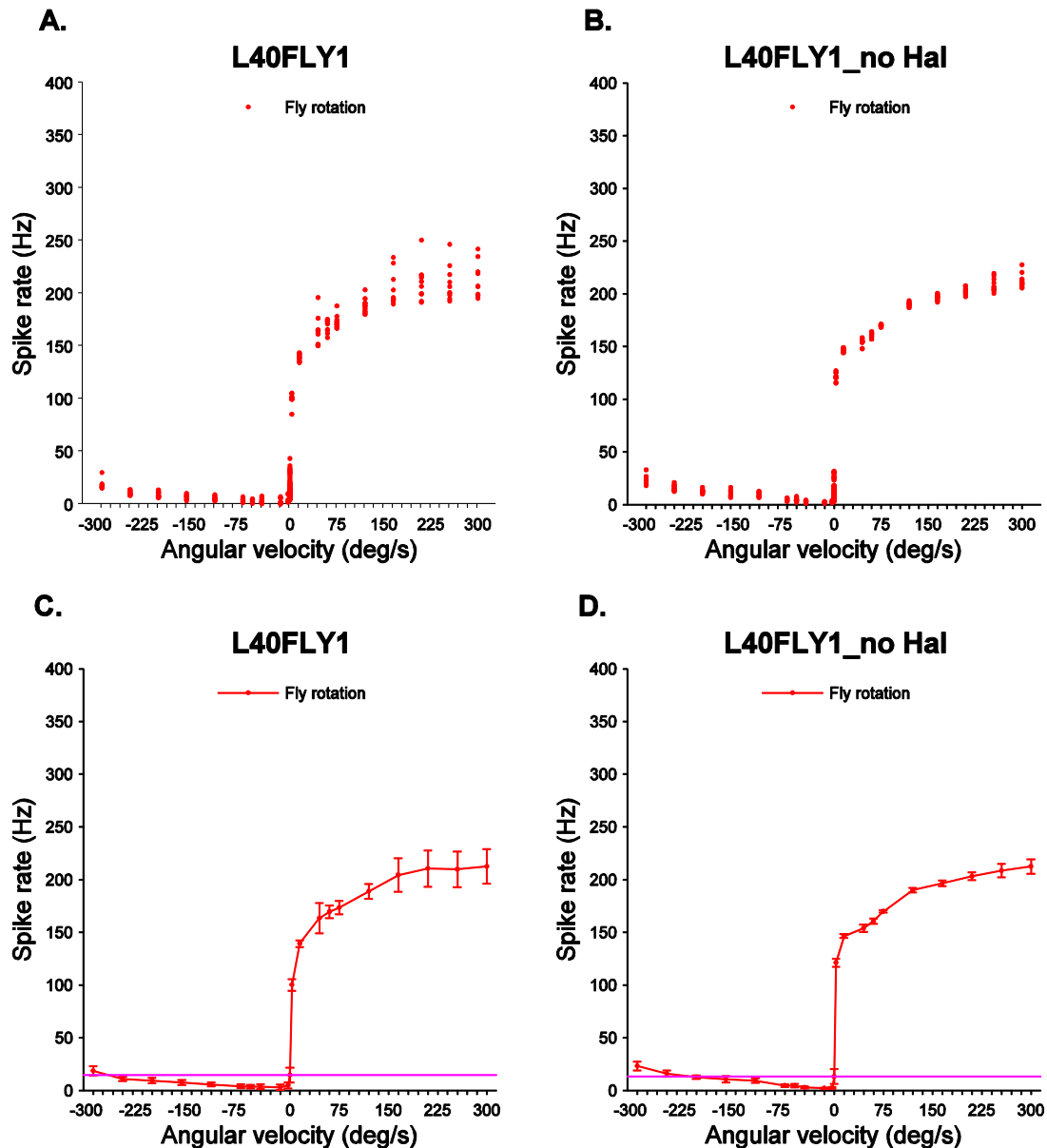


Figure 32. H1-cell temporal frequency tuning curves obtained with and without halteres in the laboratory environment. Plots A, B are trials of stimulations at various temporal frequencies. Plots C, D are means and standard deviations of the H1-cell temporal frequency tuning. Plots A, C show data from blowflies with halteres; Plot B, D present data for blowflies without halteres. As in the previous figure, negative and positive temporal frequencies indicate stimulation in the cell's preferred and anti-preferred direction, respectively. The straight purple lines in plots C, D indicate the overall mean spontaneous spike rate.

Figure 31 and figure 32, show no significant differences between the H1-cell temporal frequency tuning curves with and without their halteres. The variability without halteres seems to be slightly smaller than with halteres upon grating stimulation and the lab environment.

The most intriguing result of this experiment was the marked difference in shape of the temporal tuning curves obtained under the two visual stimulation

conditions. In comparison with the visual grating, using the laboratory environment as a visual stimulus resulted in a monotonic H1 temporal frequency tuning as opposed to an optimum curve and a reduced variability of the responses to high temporal frequencies.

Altogether, three flies were recorded grating stimulus and have similar temporal frequency tuning as Fig. 31, both with and without halteres. Only one fly was studied using the laboratory environment as a visual stimulus.

3.3.3. Discussion

In this experiment, the removal of the halteres did not change the shape of the temporal frequency tuning curve of the H1-cell.

The mean spontaneous activity of the H1-cell stayed at around 25 Hz before and after the removal of the halteres. Previous research has shown that haltere activity does not necessarily induce changes in the activity of LPTCs (Rosner et al., 2009). Neither does the rotation of the fly in my experiments. Other mechanoreceptive systems, including sensory hairs and antennae, are not affecting the H1-cell activity either. On the other hand, removal of halteres seems to reduce the variability in the H1-cell tuning curve. It is still not clear, however, which mechanism have affected the variability in the spike rate of the H1-cell, possibly due to the internal state changes (Jung et al., 2011; Longden and Krapp, 2009).

There is plenty of evidence from earlier studies that the optomotor pathway is receiving input from mechanoreceptive systems such as halteres (Huston and Krapp, 2009). The result of the experiment described here suggests that the integration of signals from horizontal cells and halteres is likely to happen in the optomotor pathway downstream of the H1-cell.

Figure 31 and 32 show two interesting results: (a) the visual stimulus conditions have an impact on the tuning (grating pattern and lab environment) and (b) the variability with and without halteres at high angular velocities in the lab environment may be different (smaller without halteres).

The laboratory-induced tuning curve shows a monotonic increase from 0 to 300 deg/s angular velocity, while the tuning curve derived from the grating

stimulus decreases for temporal frequencies higher than 4 Hz (60 deg/s in angular velocity). This is likely to be the consequence of the integration of a broad range of temporal frequencies as a result of the wide range of spatial wavelengths present in the laboratory environment.

Data reported by Lewen et al. (Lewen et al., 2001), show the spike rate of H1-cell under naturalistic visual stimulation to peak at around 1000 deg/s. The monotonic shape of the H1-cell temporal frequency tuning curve under I obtained in the lab environment is comparable with Lewen's data for the velocity range from 0.5 to 300 deg/s.

In a natural environment, the biggest spatial wavelength possible would be 360 deg. If the spatial wavelength in the grating I used was increased from 15 deg to 360 deg, i.e. 24 times bigger, then the angular velocity at which the peak spike rate in the tuning curve should occur, would be 24 times higher than 60 deg/s, which is 1440 deg/s. Unfortunately, this would be beyond the maximum angular velocity of the stepper motors I used in my experiments.

Regarding the variability, the variability with and without halteres at high angular velocities is slightly different in the lab environment.

Why does the H1-cell always peak at 4 Hz when a visual grating is used for stimulation? A possible answer could be related to the common observation that during evolution sensory systems have adapted to the input distribution they are most likely to encounter in their natural habitat. The maximum spatial wavelength visual systems may be confronted with in nature is 360 degrees. Blowfly can rotate at angular rates up to 1700 deg/s (Bomphrey et al., 2009), which means the maximum temporal frequency they may have to deal with is around $1700 / 360 = 4.72$ Hz. The fly is less likely to experience higher temporal frequencies than this in nature.

The variability of spike rate is always small when the temporal frequency is below 4 Hz as the data in figure 31 and the results from my previous experiments (Fig 30). Based on the assumption above, if the spike rate always peaked at 4 Hz temporal frequency, the bigger spatial wavelength, the higher angular velocity 4 Hz will become. When the spatial wavelength

becomes 360 deg (e.g. laboratory environment), the 4 Hz temporal frequency achieves 1440 deg. This may be the reason why the temporal frequency tuning curve in Fig 32 is monotonic and less variable in the range of 0 - 300 deg/s under laboratory environment.

The finding that the H1 tuning curve obtained in the laboratory environment is monotonic in the angular velocity range from 0 to 300 deg/s and shows only small variability, may prove helpful in designing robust robotic feedback control laws.

3.4. Experiment 3: Pattern size dependence

Besides the temporal frequency the response of LPTCs depends on a couple of other stimulus parameters which have been studied in the past (Hausen, 1984). Most of the parameters are directly related to the functional structure of the EMDs introduced earlier (Buchner, 1984). Pattern size, a parameter immediately relevant for robotic applications in different environments with varying spatial frequency compositions had been investigated both in behavioural (Reichardt et al., 1983) and electrophysiological (Haag et al., 1992) experiments before, although in experimental setup different from the one I have described here. A theoretical account on dendritic gain control in LPTC dendrites proposed a combination of the phenomenological EMD model and a biophysical model of the electrical properties of the LPTCs to explain some interesting experimental observations (Borst et al., 1995). Beyond a certain size of the stimulus pattern the behavioural and electrophysiological responses assumed plateau values that stayed constant even if the pattern size was further increased (Borst et al., 1995; Hausen, 1984; Reichardt et al., 1983). The observed plateau values were dependent on pattern velocity and could not be explained by a simple output saturation of the system. Based on their modelling approach Borst et al. (Borst et al., 1995) came to the conclusion that the gain control mechanism underlying the experimental results could be explained by a velocity dependent activation of excitatory and inhibitory membrane conductance which determines the plateau level of the responses. Ever since, the response of the LPTCs were believed to pattern

size-invariant – at least beyond a certain threshold size – which benefitted the encoding of image velocity.

As the experiment described above where the lab environment was used as the visual stimulus produced results qualitatively different from those obtained with the grating patterns I revisited the size parameter in my experiments. Especially in view of vision-based robotic control in arbitrary environments studying the size-dependent responses of the H1-cell would potentially provide useful information for the design of robust feedback algorithms.

In the experiment described below, the H1-cell was stimulated by visual gratings the size of which was varied by changing their extent along elevation.

3.4.1. Method

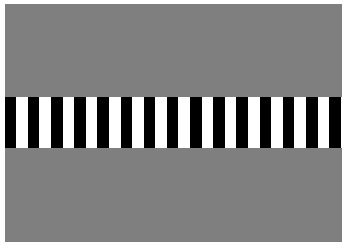
The blowfly dissection and recording procedures were the same as described in sections. H1-cell activities were recorded under both fly rotation and pattern rotation conditions.

Since the radius of the pattern cylinder (or the distance from the fly to the pattern surface) was fixed at 78.3 mm the angular extent of the pattern from the position of the fly could be calculated using by:

$$\theta = 2 \times \arctan \frac{w}{2r}$$

where: θ is the angular extent, w is the height of pattern and r is radius of the pattern cylinder.

Table 3. Angular extent of the stimulus grating

Pattern sample	Pattern height (mm)	Angular extent (deg)
	3	2.18
	10	7.30
	45	32.12
	85	56.94
	210	106.57

The vertical extent of the gratings used in my experiments is given in table 4. The sequence at which the different gratings were presented to each animal was random.

Temporal frequencies applied were 0.2 Hz, 1 Hz, 3 Hz, 4 Hz, 5 Hz, 8 Hz, 11 Hz, 14 Hz, 17 Hz and 20 Hz. Those temporal frequencies were presented in a shuffled sequence as described before including 10 repetitions. Five blowflies have been recorded in total.

3.4.2. Results

Angular Extent vs Spike Rate (pattern rotation)

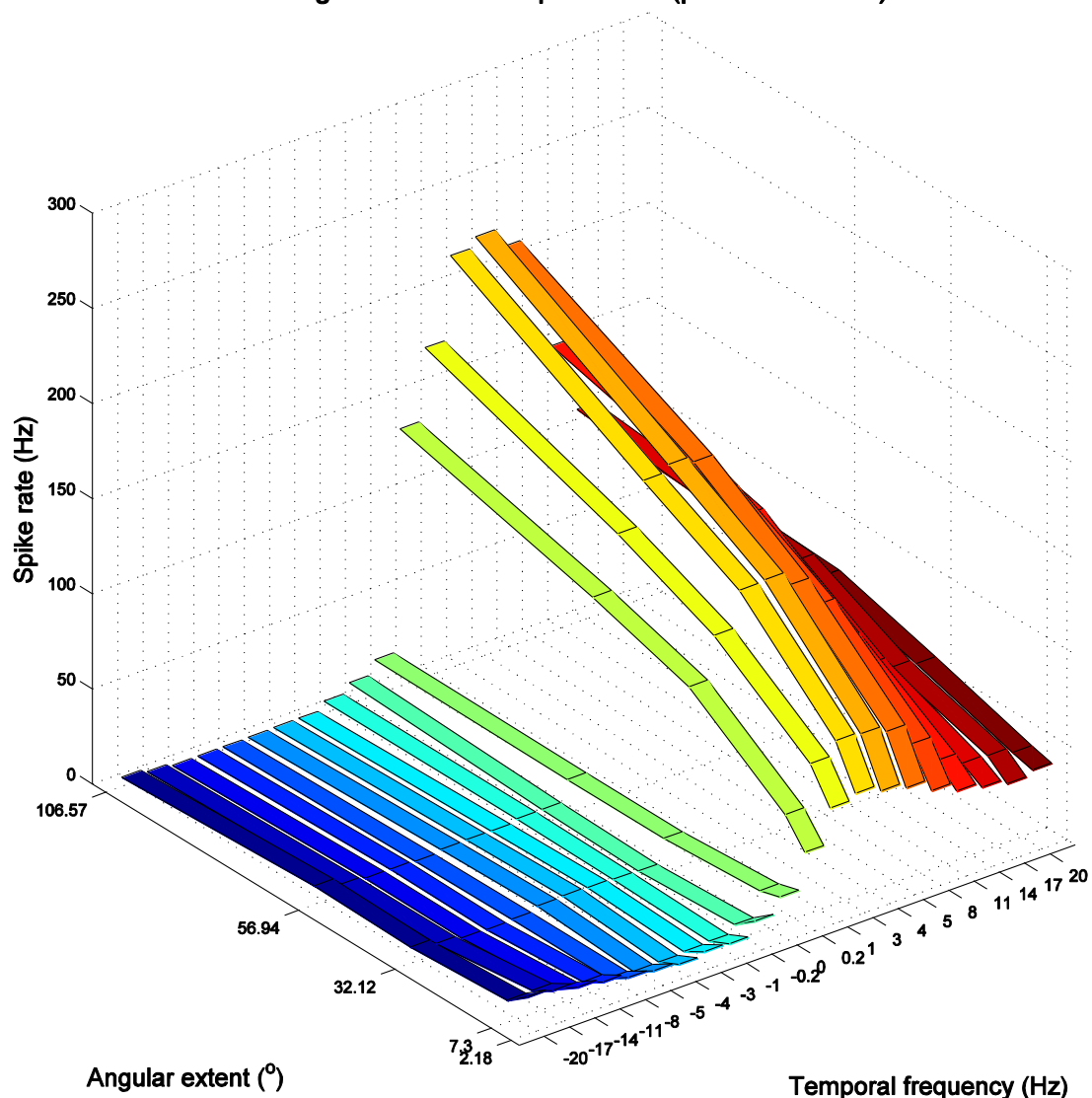


Figure 33. Temporal frequency tuning curves as a function of angular extent of the grating during pattern rotation. Each ribbon represents the angular extent dependent spike rate for a given temporal frequency. The middle green ribbon at 0 Hz temporal frequency shows the overall mean spontaneous spike rate. Negative and positive temporal frequencies correspond to motion in the anti-preferred and preferred direction of the cell, respectively. (The plot include averages of data from 5 animals.)

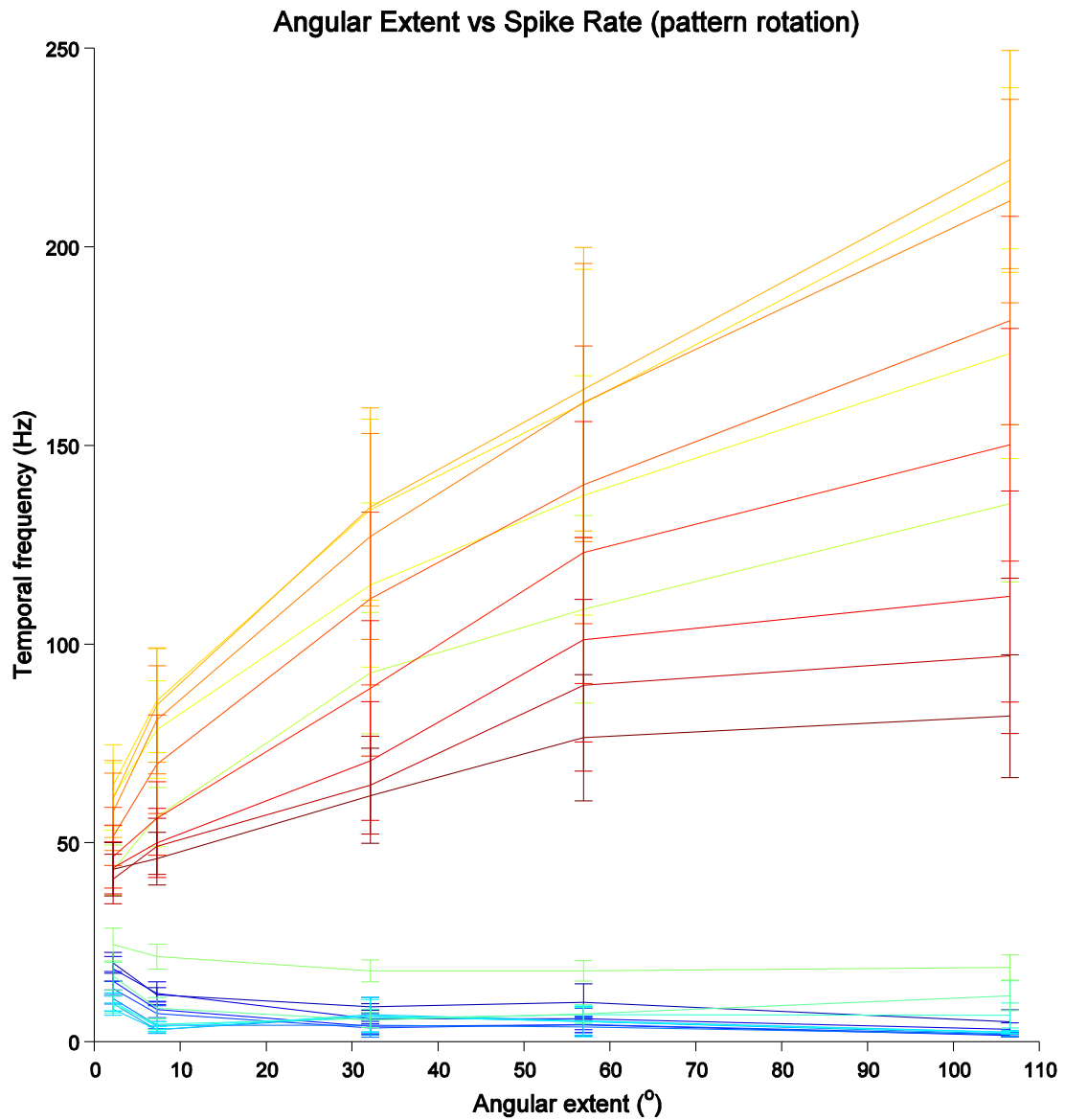


Figure 34. Side view of data shown in figure 33. Each curve shows the angular extent dependent response for one temporal frequency obtained upon pattern rotation. The blue lines give responses to null direction motion, where neurons are inhibited. The red lines give responses to preferred direction motion, where neurons are excited. (N=5)

Angular Extent vs Spike Rate (fly rotation)

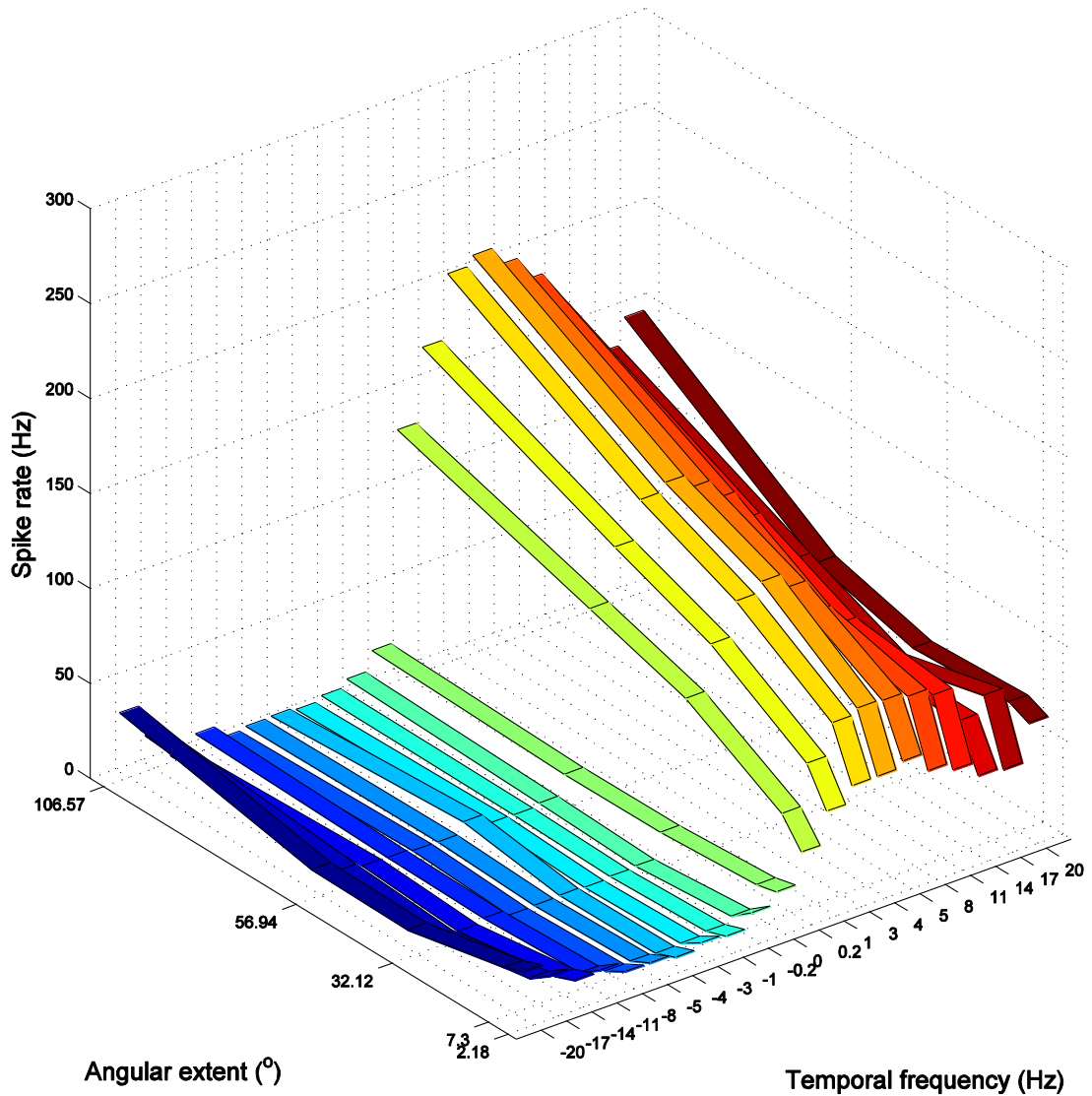


Figure 35. Temporal frequency tuning curves as a function of angular extent of the grating during fly rotation. The data were gathered from the same animals (N=5) which were used to obtain the results presented in figure 33, but here the animals were rotated in the centre of the stationary pattern.

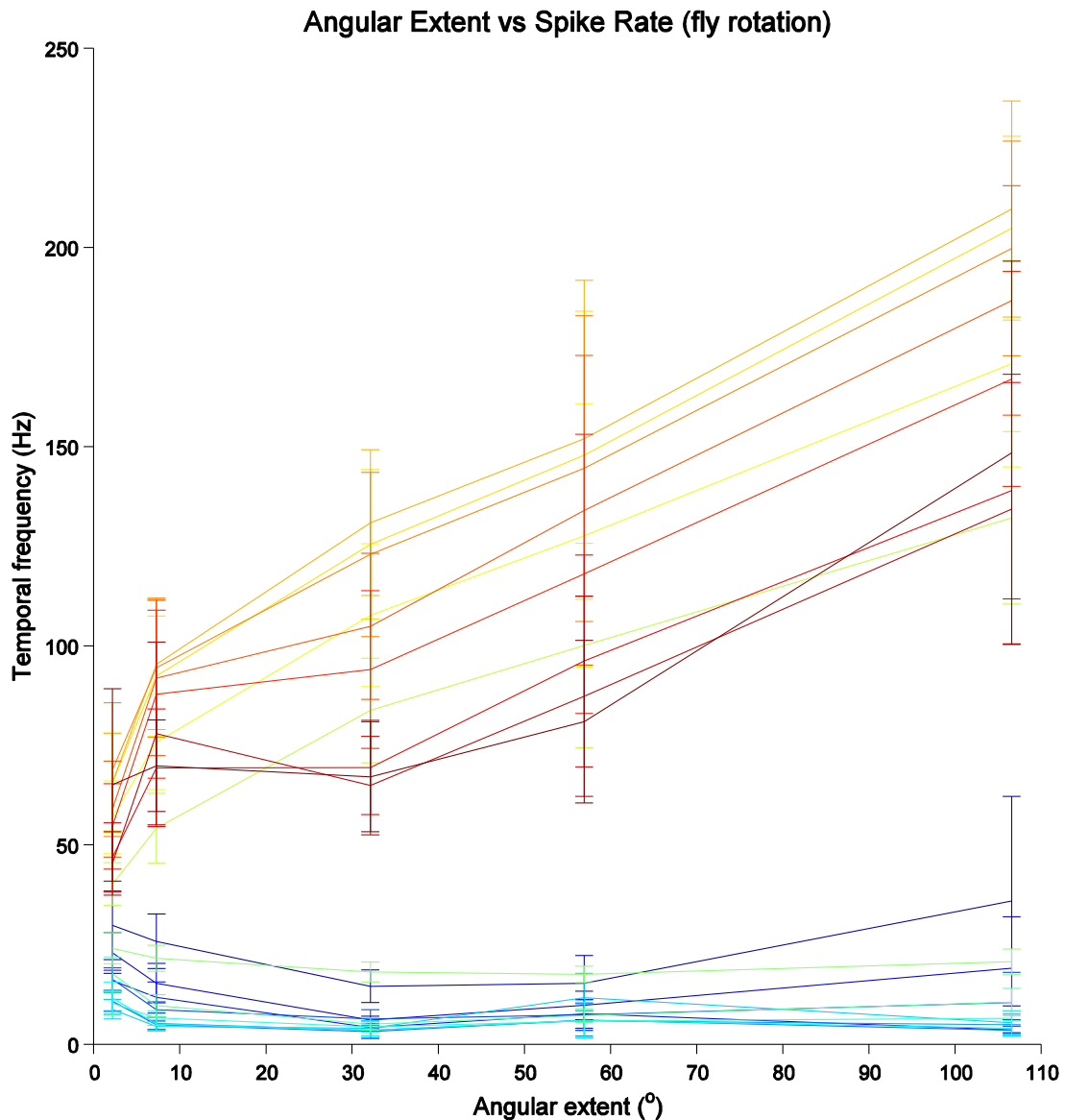


Figure 36. The side view of the results shown in figure 35. It is the same way of presenting the data as in figure 34. Note that for angular extents greater than 32.12 deg, there is a linear relationship between pattern size and spike rate for all positive temporal frequencies.

The H1-cell tuning curves obtained upon pattern rotation using gratings of five different angular extents are plotted in 3D format in figure 33, while the corresponding result obtained during fly rotation are given in figure 35. Side views of the two data sets are presented in figure 34 and 36, respectively, for an easier inspection of the relationship between angular extent and response.

The spike rates measured while the fly was rotated were higher than those obtained during pattern rotation for all angular extents above 32.12 degree (Fig 36).

3.4.3. Discussion

In this experiment, the results shows: (1) the spike rates of H1-cells are almost proportionally related to the angular extent of the visual grating, which is different from on size-dependent responses of LPTCs published before (Borst et al., 1995; Hausen, 1982). (2) a detailed inspection of the plots reveals that spike rate and angular extent are related more closely by a straight line when the fly is rotated as opposed to the grating for angular extents greater than 32.12 degrees (Fig 36).

As mentioned above, size dependent response of other LPTCs, for instance the HS-cell had been studied before (Hausen, 1982). But in those experiments the responses assumed different plateaus levels which depended on pattern velocity. That shows the responses are nearly independent of size beyond a certain extent of the stimuli (Hausen, 1982). My results, however, show that the H1-cell shows a linear relationship between angular extent and spike rate. A possible reason for this discrepancy could be the application of different visual stimulus. The stimuli in Hausen's experiments were presented through a 50 deg x 32deg aperture that was placed 30 deg in azimuth. And the pattern size was changed within this aperture. In my experiment, the blowfly had a field of view of at least ± 90 degree azimuth angle, and -45 to +90 degree elevation angle. The azimuth and elevation range are far bigger than Hausen's experiment.

However there are evaluated curves where the membrane potential of the HS-cell was plotted against angular extent in Hausen's publication (Hausen, 1982), which did not settle at a constant value with increasing pattern size, evaluated from other experimental data from the same experiment. Considering the stimulation parameters 1.5 Hz temporal frequency and 32 degree maximum angular extent along elevation in Hausen's experiment, the evaluated curves are quite comparable to the result in Fig 34.

It is not clear why the linearity between H1-cell spiking rate and angular extent of the pattern is more pronounced when the fly is rotated (Fig 36).

The linear size-dependence of the H1-cell activity I found might potentially support distance estimation in the context of collision avoidance (Lindemann

et al., 2005) on a robot, because an object is normally smaller and slower in distance than in front of eyes.

3.5. Experiment 4: Bi-lateral H1-cells adaptation

Motion adaptation is another property of visual system that could change the H1-cell spike rate. In this section I report experiments to investigate the responses of H1-cells before and after visual motion adaptation. For the robot, the controller needs to know whether the change of the spike rate is caused by adaptation, and compensate the change if necessary.

3.5.1. Method

The blowfly dissection and recording procedures are the same as for the previous experiment. The electrode is inserted into the right lobula plate and placed at a position where both ipsilateral and contralateral H1-cell spikes can be recorded with signal noise ratio greater than 2:1. Three flies were recorded.

The visual stimulation protocol in this experiment contained two parts, where the direction of stimulus motion was swapped. During both rotations in the clockwise and counter-clockwise direction of the pattern one of the H1-cells is excited, while its contralateral counterpart is inhibited, as shown in Fig 37.

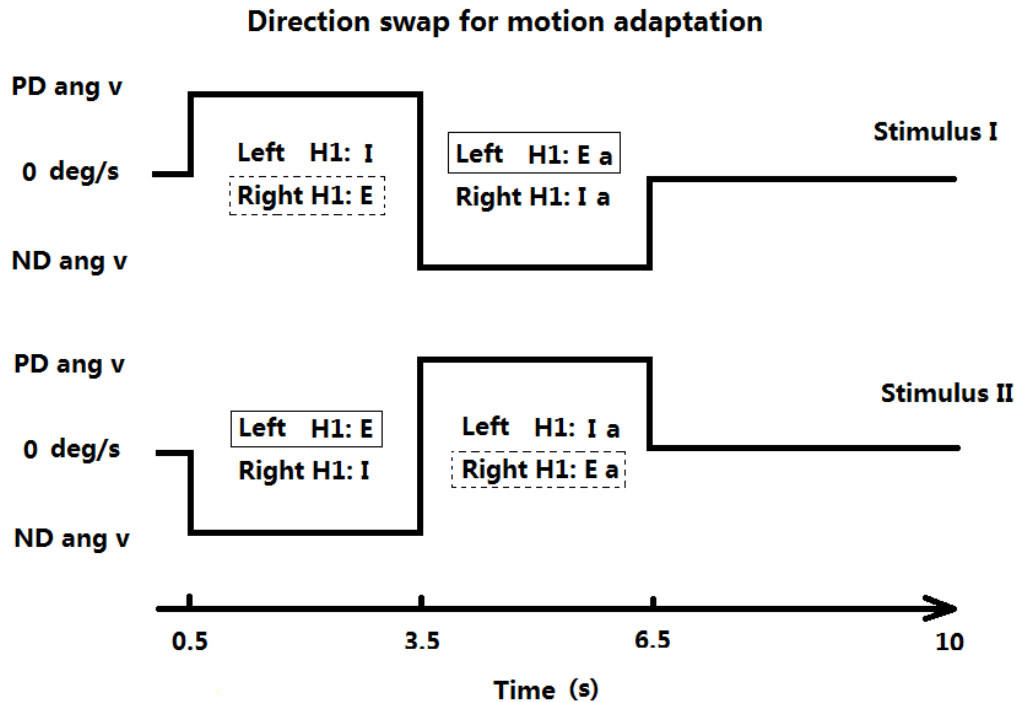


Figure 37. Motion adaptation experiments. The electrode was placed in the right lobula plate of the blowfly to record the activity of the contralateral H1-cell. The first stimulation sequence consists of 0.5 second without motion, 3 seconds anticlockwise rotation (view from dorsal side of the blowfly), 3 seconds clockwise rotation and 3.5 seconds without motion. The second stimulation sequence has 0.5 second without motion, 3 seconds clockwise rotation, 3 seconds anticlockwise rotation and 3.5 seconds without motion. This protocol guarantees that both H1-cells are excited by motion in the anti-preferred direction before and after motion adaptation. “E” stands for excitation, “I” for inhibition, “a” for motion adapted.

Each recording lasts for 10 seconds. The temporal frequency is the same for both clockwise rotation and anticlockwise rotation. A different temporal frequency is then applied during the next 10 seconds of the experiment. Ten different temporal frequencies were used: 0.2 Hz, 1 Hz, 3 Hz, 4 Hz, 5 Hz, 8 Hz, 11 Hz, 14 Hz, 17 Hz and 20 Hz. They were applied in a shuffled sequence. Each set of experiments was repeated 10 times.

3.5.2. Result

After the experiment, the H1-cell spike rates were calculated by averaging the number of action potentials within a 3-second time interval of clockwise or anticlockwise rotation (each symbol in Fig. 38A, 38B). H1-cell spike rates obtained during 10 repetitions of the same stimulus conditions were used to calculate the means and standard deviations for each temporal frequency (in Fig. 38C, 38D).

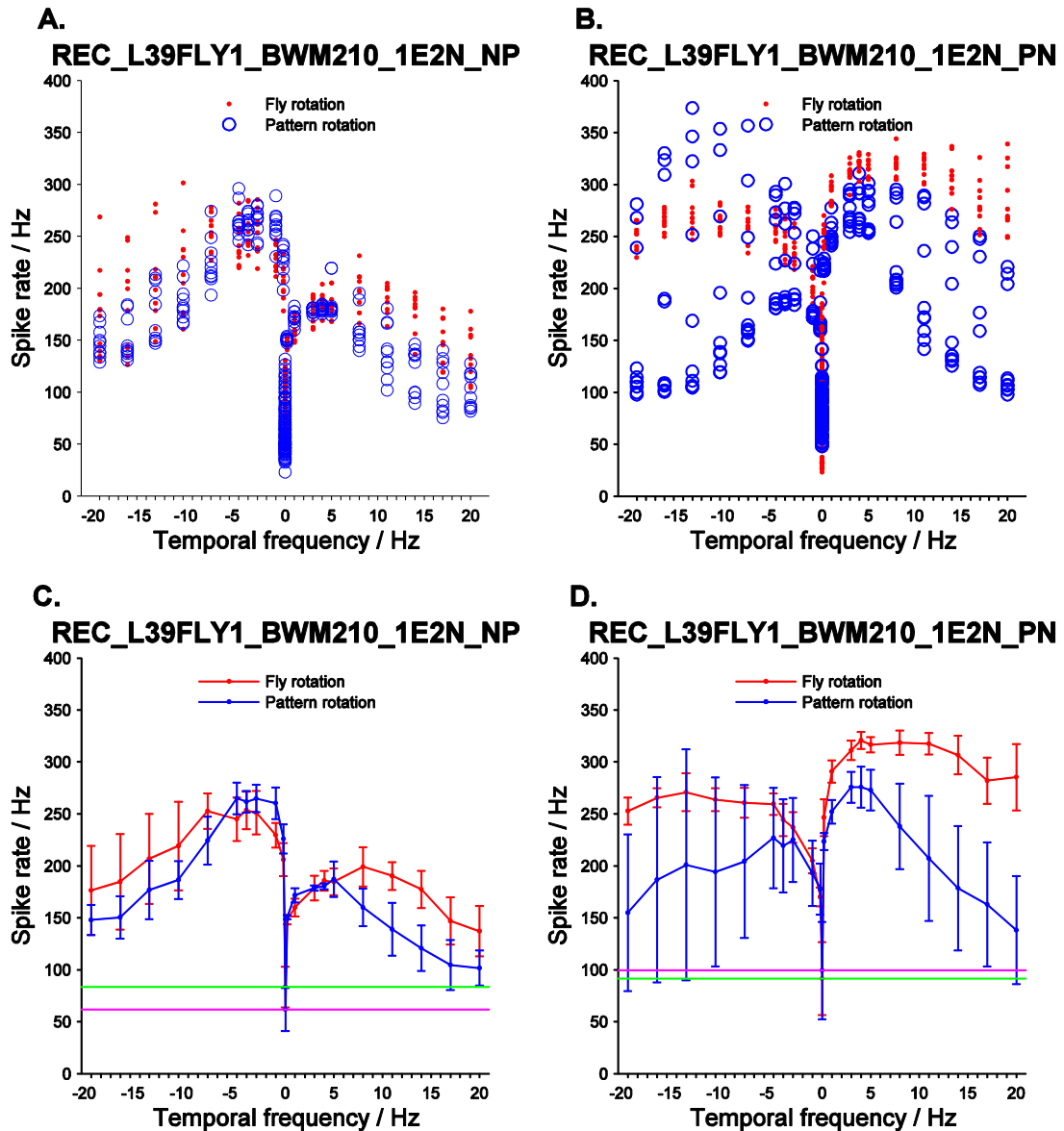


Figure 38. Dual H1-cell recordings in asymmetric temporal frequency tuning curves after adaptation. The electrode is recording both H1 neurons in the right hand side of the lobula plate. Data presented in plots A, C were recorded under CCW-CW stimulation. The tuning curve of the contralateral (left) H1 (motion adapted) is plotted over positive temporal frequencies while the the tuning curve of the ipsi-lateral (right) H1-cell is plotted against negative temporal frequencies. Data presented in plot B, D were recorded under CW-CCW stimulation. The tuning curve of the contralateral (left) H1-cell is plotted against positive temporal frequencies. While the tuning curve of the ipsi-lateral (right) H1-cell (motion adapted) is plotted against negative temporal frequencies. The green line indicates the overall mean spontaneous spike rate in between pattern rotations, the magenta line shows the overall mean spontaneous spike rate in between fly rotation.

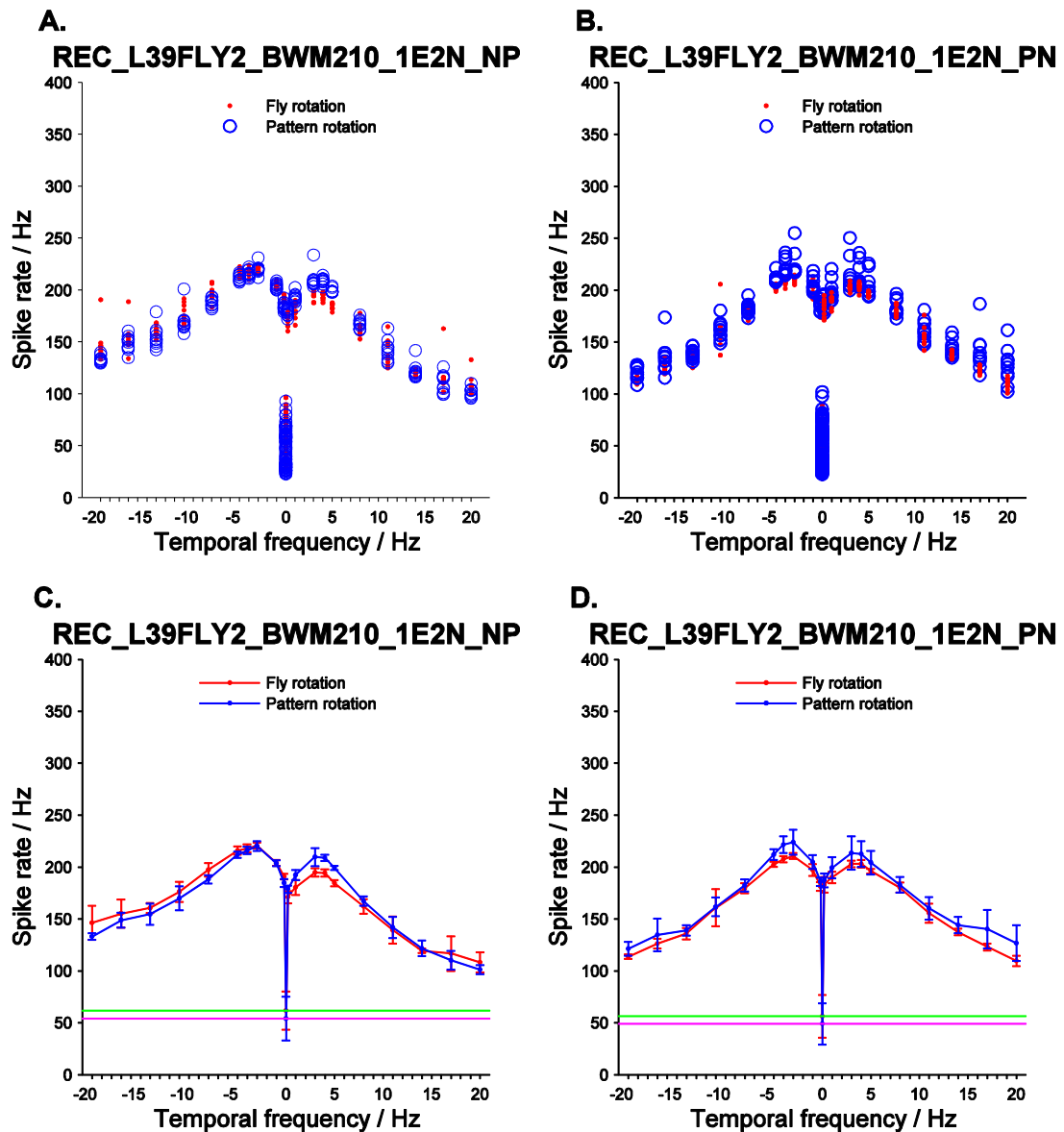


Figure 39. Dual H1-cell recordings show symmetric temporal frequency tuning curve with adaptation. Same experimental conditions as described in figure 38, but recorded from a different blowfly.

The H1-cell spike rate is affected by motion adaptation. The adapted cell generates a lower spike rate than the non-adapted cell under both conditions, i.e. when pattern is rotated and when the fly is rotated.

The peak spike rates shown in Figure 38 and 39, have to be viewed in relation to the cell's spontaneous activity. The spike rates recorded before and after motion adaptation are more different, when the overall mean spontaneous activity is around 50 Hz for both cells. There is hardly any difference in spike rates recorded before and after motion adaptation, when the overall mean

spontaneous spike rate of each H1-cell is around 25 Hz (average of two H1-cell spontaneous rates which is 50Hz from Figure 39).

3.5.3. Discussion

Adaptation does change H1 spike rate, the higher the level of motion adaptation in the cell, the lower the spike rate it generates. In this experiment, we can see the temporal frequency tuning curve affected by adaptation when the fly is rotated and when the pattern is rotated (Fig 38).

Here I present – for the first time in this study - un-adapted temporal frequency tuning curves derived from experiments using the miniaturized recording platform (Fig 38). All experiments described in previous sections were carried out on H1-cells subjected to motion adaptation, where 3 seconds of null direction motion were followed by 3 seconds of motion in the preferred direction. The justification for this protocol was based on the observation that airborne or walking blowflies, on average, translate in the forward direction. In this case the H1-cells would be stimulated by motion in their anti-preferred direction. Regarding the comparison with previous studies on motion adaptation in H1-cell (Maddess, 2001), the two temporal frequency tuning curves of a fixed blowfly before and after adaption in his work were similar to the frequency tuning curves in my experiment (Fig 38).

In a special case, the H1-cell responses were almost identical before and after adaptation (Fig 39). Here, the frequency tuning curves of both the contralateral and ipsilateral H1-cells were almost perfectly mirror symmetrical. And the variability of the spike rates is low. Considering the low spontaneous spike rates, one assumption, based on research into state-dependent information processing in LPTCs (Jung et al., 2011; Longden and Krapp, 2009), could be that this fly's (Fig 39) activity was recorded while it was in a passive locomotion state. In such a case the responses of the H1-cell would be minimum, where adaptation cannot reduce the spike rate any further.

The other important outcome of the experiment described in this section is that it shows the feasibility of performing simultaneous extracellular double recordings from both H1-cells on the miniaturized platform using only one electrode. In the future, spike peak potentials from different H1-cell can be

distinguished if carefully select the position of recording location. This could potentially simplify the design of the brain machine interface implemented for closed-loop robotic control, or to potentially record the V1-cell using the second electrode.

For robotic control, monitoring of the spontaneous activity would be useful as it indicates the state of the blowfly.

3.6. Summary

In this chapter, I described the characterization of the H1-cell responses in blowflies using a miniaturized recording platform under different stimulus conditions. The H1-cells were recorded either when the fly was rotated within a cylinder lined with a visual grating or when the grating was rotated while the fly was stationary. The major goals of this work were (a) to demonstrate that the novel miniaturized recording equipment is suitable for stable recordings even if the whole platform is rotated at different angular velocities, (b) to investigate the potential impact of mechanoreceptive systems on the responses of the H1-cell, and (c) to show that the results obtained with the novel platform are in agreement with those obtained using conventional electrophysiology equipment in previous studies. Overall the results suggest that the platform I designed is well suited to be used for the closed-loop control of a wheeled robot.

Four experiments have been carried out to characterize H1-cell responses during fly or pattern rotation:

In the first experiment I recorded the H1-cell responses under both conditions to temporal frequencies in the range between 1 and 10 Hz. The results show no substantial differences between the temporal frequency tuning curves of H1-cell derived from fly and pattern rotation and that the tuning curves are in agreement with earlier results reported in the literature. This indicates that the designed recording platform has equivalent functionality to commercially available equipment. The finding that the tuning curves do not show any statistically significant differences between the fly rotation and pattern rotation

stimulus conditions also indicates no sizable impact of mechanosensory systems on the H1-cell activities within the range of tested temporal frequencies.

In the second experiment H1-cell responses were recorded upon stimulation with temporal frequencies from 1 to 20 Hz in rotated flies with and without halteres. From these experiments similar H1-cell temporal frequency tuning curves were derived. The results suggest that the integration of visual motion and halteres information (Huston and Krapp, 2009) does not occur at the level of the H1-cell, i.e. within the lobula plate. The integration probably happens in downstream elements of the optomotor pathway, possibly at level of the neck motor neurons. An interesting additional finding was that the H1-cell responses obtained during rotations of the fly in the laboratory environment shows a monotonic dependence on angular velocity up to 300 deg/s. This response property of the H1-cell, which was in agreement with previous studies (Lewen et al., 2001), will benefit the design of robust control laws for closed-loop experiments on a mobile robot.

The third experiment was meant to characterize the H1-cell temporal frequency tuning as a function of the vertical angular extent of the visual grating used for motion stimulation. The results show, from 32.12 deg vertical pattern extent, a nearly proportional relationship between angular extent and the spike rate of the H1-cell for all positive temporal frequencies tested. Under the stimulus condition when the fly was rotated, I observed an almost linear dependence of the neural response on the angular extent of the grating. The linear dependence on pattern size is in contrast with previous studies suggesting size-invariant responses of LPTCs (Borst et al., 1995; Hausen, 1982) might be caused by the different stimulus extents along the azimuth.

The fourth experiment included simultaneous double recordings from both H1-cells. The activity of the two H1-cells was recorded by using only one electrode. The impact of motion adaptation was demonstrated by comparing the spike rates of both H1-cells. H1-cells adapted by visual motion were shown to generate lower spike rates than non-adapted H1-cells (Maddess and Laughlin, 1985). I also found evidence that motion adaptation and

spontaneous spike rate may be correlated and might possibly depend on the animal's internal locomotor state (Jung et al., 2011; Longden and Krapp, 2009).

The experiments in this thesis were focussed on the aspects mentioned above: temporal frequency, mechanosensory integration, angular extent and motion adaptation, which are influenced by motion. Although there are other factors which have been shown to impact on the spike rate of the H1-cell, including ambient temperature (Egelhaaf et al., 2001), circadian rhythm (Bult et al., 1991), age (Whim and Evans, 1989) and nutritional state (Ishida and Ozaki, 2011), those factors are not directly related to motion stimulation, and may be investigated at a later stage.

The next step will be to mount the novel miniaturized recording platform on a two-wheel robot.

4. H1-cell to robot interface

In this chapter, the results of H1-cell characterization from previous chapter are used to establish an H1-cell interface between the cell and the controls of a ground based two-wheeled robot. at a first step the dynamic properties of the robot have to be characterized. These two tasks are necessary to create a functional closed-loop platform to study multisensory integration.

4.1. Introduction

Brain machine interfaces are implants that connect the nervous system to a machine by means of electrodes, which enable some sort of task-specific communication (Jebari, 2013). By its bare nature, a brain machine interface requires both the application of neurophysiological expertise and engineering technologies.

In this thesis, the brain machine interface consists of a connection between the H1-cell in the fly motion vision pathway and a robot As mentioned in the previous chapters the H1-cells is one of the motion sensitive tangential cells located in the fly lobula plate and responds to horizontal motion in a directional selective way. The spike rate of the H1-cell will be used in to control the trajectory of a 3pi®, a two-wheel ground based educational robot (Fig. 15).

In order to establish a robot-based experimental system suitable to study multisensory integration under closed-loop conditions, two requirements have to be met: (i) the response properties of the sensor system should allow for a robust feedback control of the robot. This aspect has been dealt with in previous chapters. (ii) the kinematics of the robot should enable movements which cover the dynamic input range of the sensory systems under study. The latter aspect requires a proper characterization of the robotic system. The results of this characterization together with (a) an analysis of the relationship between input a pulse width modulation signal (PWM) and output angular

velocity of the robot, (b) as well as programmes to control the interface on the microcontroller, will be presented in this chapter.

The 3pi® robot has been chosen as the actuator in the brain machine interface described here because it has some advantages over competing two wheeled robots, including: high speed DC motors, high frequency microcontroller clock rate, and economical price.

The first requirement is developing a method to characterize the speed of the robot. As per its specification the robot is supposed to achieve a turning rate of 1500 deg/s, which has a considerable overlap with angular velocities observed in freely flying blowfly's (max: 1700 deg/s) (Bomphrey et al., 2009). The speed of the robot is regulated by PWM. It is essential to characterize the speed / voltage relationship. This will show whether the DC motor behaves linearly over the entire speed range and will indicate the influences of frictions. A linear motor operation with PWM input would make the motor a time invariant transfer function in the control loop.

The second requirement is to program the interface. Since the blowfly is mounted on top of the robot, movements of the robot will induce relative motion – optic flow – between the fly and the visual environment. This will, through the motion vision pathway provided by the compound eyes, modulate the activities of the H1-cells which will be used to steer the robot by differentially driving the motors of the wheels. In this interface configuration the H1-cell is effectively used as an optic flow sensor that provides closed-loop feedback signals. To this end the analog H1-cell spikes need to be recorded, amplified, filtered and converted into time-continuous digitized signals for further on board processing and the generation of motor control signals. While signal recording, amplification and filtering have been outlined previously (cf. chapter 3), in the following I will describe the remaining signal processing tasks, including: data acquisition, spike detecting and spike rate-to-velocity conversion to the robot. The spike rate-to-velocity converter is the key part in this system, which is based on the characterization of the H1-cell responses. Similarly studies have been performed on an interface between neck motor nerves in the silkworm with a robot based on the integration of

olfactory and visual signals (Minegishi et al., 2013). In contrast to the work on the silkmoth robot interface, the fly robot interface here will be configured to control the robotic motion based on visual information but at a considerable higher dynamic range.

4.2. Experiment 1: robot angular velocity calibration

4.2.1. Method

The 3pi® is equipped with a limited number of sensors when purchased. It has no on-board accelerometer, tachometer or odometer. Therefore its angular velocity cannot be directly or indirectly measured. There are many ways to measure angular velocities, for instance by using an inertial measurement unit (IMU). To minimize the measurement error, I eventually used high speed videography to extract the robot's angular velocity from image sequences taken at a rate of 500 frames per second.

Effectively, the angular velocity of the robot was obtained by differentiating the angular orientation of the robot over time which required high contrast image.

In order to achieve good image contrast and thus simplify further processing, white paper was used to cover the top of the 3pi® robot and two labels were added: 1) a black circle, indicating the centre of the robot's rotation 2) a black cross on the edge of the robot, to indicate its orientation. The robot was then placed on the A0 size white matte paper on the floor. A black triangle was painted on the white paper approximately 70 mm away from the robot's centre of rotation as an external reference point (Fig. 42).

A Photron® SA3 high speed video camera was mounted on a tripod. The optical axis was pointing downwards right at the robots centre of rotation. Recordings were triggered by a push button. Imagery was saved to the camera hard drive in bitmap format (*.bmp) for further off-line analysis

The robot was programmed to change its yaw angular velocity by means of a periodic step-up and step-down pulse width modulated (PWM) voltage profile as illustrated in figure 40. The PWM voltage is described by 8 bits, which has 256 levels. It started from level 0, and stepped up to level 250 by increments of 50. The step-down sequence started at level 255 and decreased to level 5

by decrement of 50. The same voltage output sequences were then repeated, but with the robot rotating in the opposite direction.

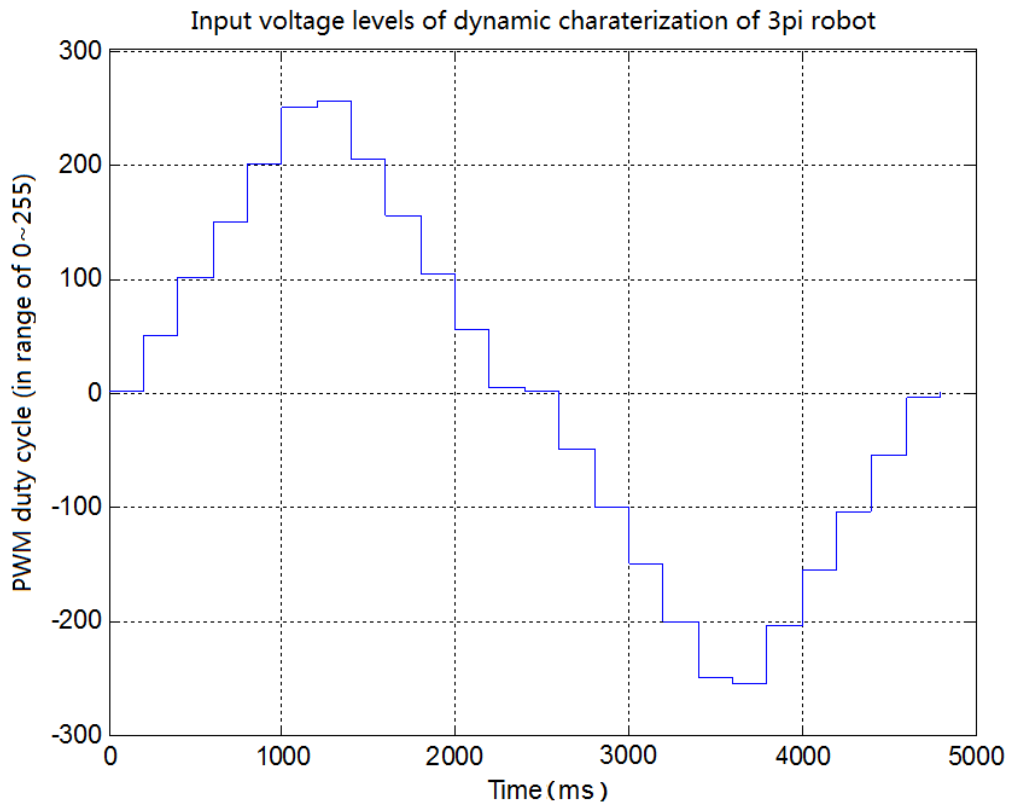


Figure 40. Input voltage levels for dynamic characterization of 3pi robot. The input voltage is regulated by an 8 bit PWM generator. Levels 0 to 255 are equivalent to 0V to 9.25V, which are applied to the DC motors driving the wheels of the robot.

4.2.2. Result

From the stored image sequences the rotation angle of the robot was extracted using customize software written in Matlab.

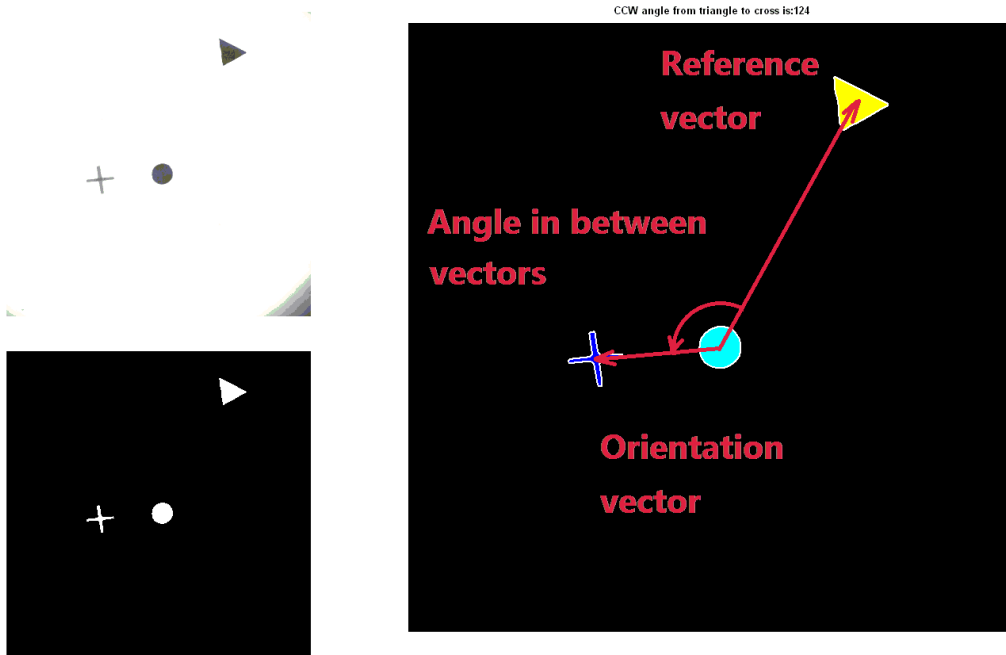


Figure 41. Image processing for analysing angular orientation. The top left image is the original image, where the robot is in the middle of the image with the black dot indicating the rotating centre and the black cross marking the robot edge. The black triangle is the reference mark on the ground. The bottom left shows a high contrast (black and white) image after noise removal and contrast saturation. The image on the right shows the result of the analysis where the angular orientation has been calculated with respect to the coordinates of the patterns. The vector from dot to cross represents the orientation of the robot. The vector from dot to triangle is the reference vector. The angle calculated is defined by the counter clockwise angle between the reference vector and the vector describing the robot orientation.

The data processing is based on a pattern recognition algorithm applied to the high speed camera images. In the original images a region of interest (ROI) was defined. Pixel values within the ROI were run through a threshold operation which effectively resulted in a black and white image, where all background pixels are black and those belonging to one of the labels (dot, cross, triangle) are white. Exploiting the different 'roundness' of the labels pattern recognition, commands from the Matlab image processing toolbox were used to obtain the pixel coordinates of the centres of the different labels. Once those coordinates were known, a vector connecting the dot with the cross (cr) provided the angular orientation of the robot relative to a reference vector defined by the pixel positions of the dot and the triangle (tr) (Fig. 41 right). The angular orientation of the robot, theta (θ), was computed from the three pattern coordinates by the following equation:

$$\theta = \cos^{-1} \frac{(x_c - x_d)(x_t - x_d) + (y_c - y_d)(y_t - y_d)}{\sqrt{(x_c - x_d)^2 + (y_c - y_d)^2} \times \sqrt{(x_t - x_d)^2 + (y_t - y_d)^2}}$$

Where (x_c, y_c) are the coordinate of the cross pattern, (x_d, y_d) are the coordinate of the dot pattern and (x_t, y_t) are the coordinate of the triangle pattern.

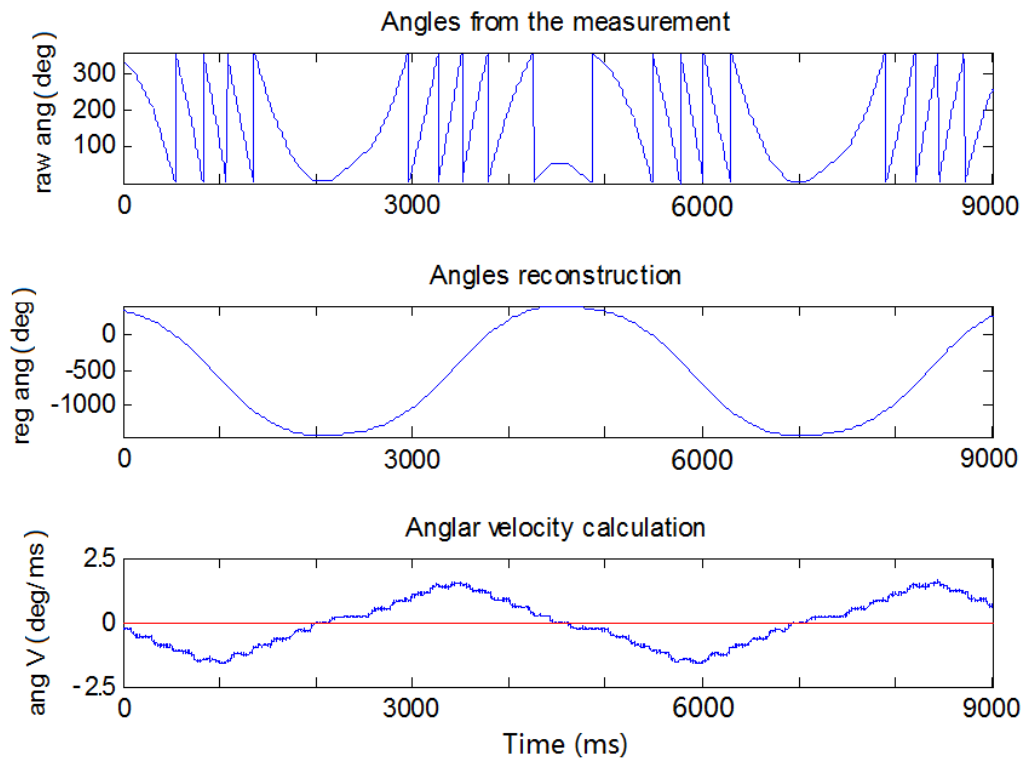


Figure 42. Robot angular velocity calculation. (Top) The angular orientations of robot measured from frames captured by a high speed camera. **(Middle)** Continuous representation of angular rotation. It shows the cumulative rotation angle covered by the robot over time relative to its initial angular position. **(Bottom)** Angular velocity of the robot, obtained from the temporal derivative of the angular position. The red line indicates 0 deg/ms.

After the robot angular orientations were extracted from images of high speed camera, the angular velocities were obtained from the temporal derivative of the angular orientations (Fig. 42). The angular velocity curve is based on the sequence of control signals shown in figure 40. The mean and standard deviation of the angular velocities at each step was calculated and are plotted in figure 43.

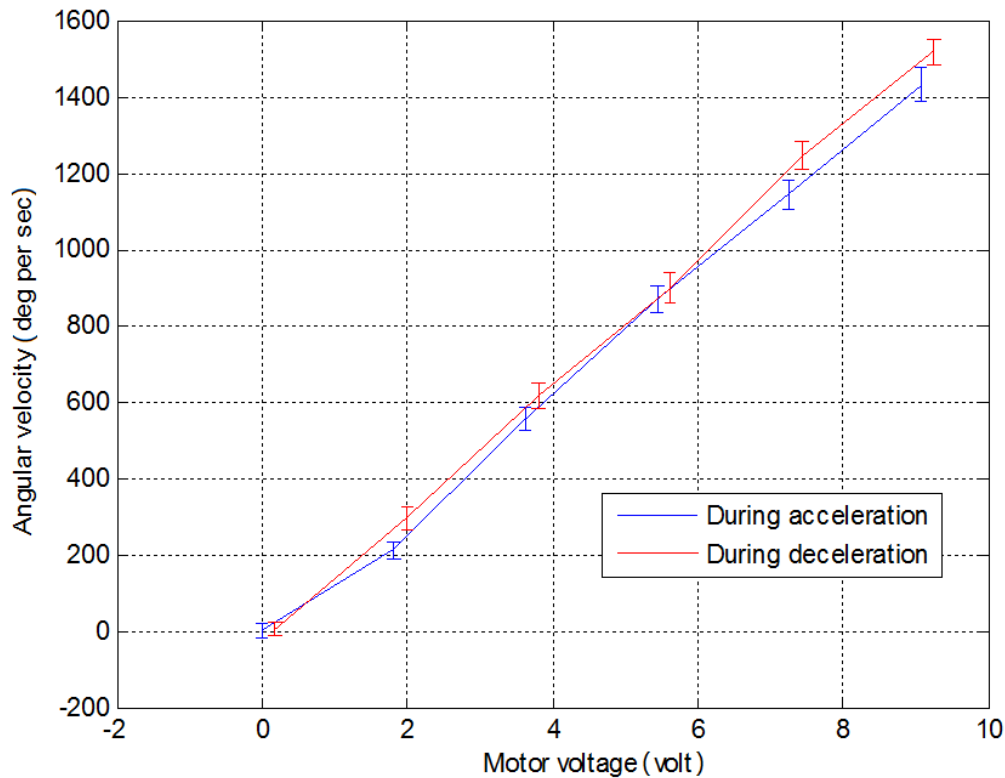


Figure 43. Angular velocity of the robot as a function of PWM voltage during acceleration and deceleration. The mean and standard deviation of each point was calculated from 100 angular velocity measurements.

The results show that the angular velocity of the robot is a linear function of the PWM voltage sent to the motors with a small hysteresis between acceleration and deceleration. These results will benefit the implementation on linear feedback control laws of the closed-loop robotic interface system.

4.2.3. Conclusion

The results of the robot characterization show that (a) the 3pi® is able to reach maximum rotation speeds of 1500 deg/s, and that (b) there is a linear relationship between PWM voltage input and angular velocity of the robot throughout the entire dynamic range. The measured peak angular velocity indicates that the rated DC motor power is high enough to overcome the power loss due to frictions in the gear box and the ball bearings caused by the robot weight and lubrication status. Should in the future more weight be added to the robot, a similar calibration procedure could be performed with dummy load. It is worth mentioning that for the Pololu®, the manufacturer supplies a collection of DC motors with higher rated speed and gear ratio which should

guarantee the required angular velocity range will be achievable even if the robot's payload is increased.

As was shown in semi-closed loop experiments on roll gaze stabilization in blowflies, haltere-induced compensatory head movements were maximum at thorax rotations of approximately 1000 deg/s (Hengstenberg, 1991). The maximum angular velocity of the robot of 1500 deg/s should be sufficiently high for effective haltere stimulation – a necessary condition to investigate multisensory integration at the level of the LPTCs.

Finally, the PWM voltage regulation improves the dynamics of low voltage operation of the DC motor, as well as increases electrical noise resistance. As mentioned above, the linear relationship between PWM voltage input and angular velocity output can be described as a simple transfer function in the system and eases the design of the control laws in closed-loop experiments.

4.3. Experiment 2: bi-lateral neuron machine interface

The ultimate goal of this project is to eventually control a robot by using the blowfly's H1-cell as a visual motion sensor. Here, recordings from both H1-cells are required to cover rotations in the counter clockwise and in the clockwise direction by the dynamic output range of the right and the left H1-cell, respectively. Then, an essential step is to build an interface between H1-cell responses and robot, by which the control loop is closed and the blowfly is enabled to steer the robot.

This experiment is only a proof of concept. It shows the possibility of generating linear control signals for rotations in clockwise and counter-clockwise direction using the spikes from the left and right H1-cell, respectively. All components are in place, e.g. recording platform, robot, microcontroller, interface programme, for more systematic studies in the future.

4.3.1. Method

In this experiment two separate electrodes were used to perform simultaneous double records from both, the H1-cell within the left and the right

lobula plate, respectively. The microcontroller (NXP® LPC1768) of the robot was programmed to be the brain machine interface, which converts the H1-cell spike rate from the blowfly into the motor angular velocity of the robot.

4.3.1.1. Dissection

A blowfly from the laboratory colony aged between 4 - 11 was anesthetized/immobilized using ice. The legs and proboscis were removed. The fly was fitted onto the designed fly holder, and the head is aligned with the horizontal plane based on inspection of the symmetrical deep pseudopupil (Franceschini, 1972). The thorax was pushed down and the mesopleuron part was waxed to the pins on the fly holder for exposure of the back of the head. The cuticle on the back of the head was cut open. Fat tissue and muscles covering the lobula plate were removed to expose the tracheas on the surface of the lobula plate, as guide lines of electrode allocation.

Two tungsten electrodes were inserted into the lobula plate one in each side of the brain. They were placed one at a time using the tracheae providing the lobula plate for visual guidance of the electrode placement. The left hand side electrode was recording the axon of the contralateral H1-cell, which obtain receives input from the right eye, and the right hand side electrode was recording the axon of the contralateral H1-cell, which receives input from the left eye. The ratio between the amplitude of H1-cell action potential peaks and the amplitude of the background noise envelope exceeded 2:1. The second electrode was inserted after retracting the first one, preventing neural damage from excessive mechanical tensions in the nervous tissue. After both H1-cells were localized, the two electrodes were carefully advanced into their recording position.

4.3.1.2. Interface programming

The mbed® microcontroller (NXP LPC1768) is based on an ARM cortex-M3 core, running at 96 MHz, with 512 KB flash. Its peripheral modules include an analog digital converter (ADC) module, which receives neural signals from the designed amplifier (cf. appendix 1), and transmit digitized neural signal to the microcontroller. It also sends processed velocity signal to robot via a universal asynchronous receiver/transmitter (UART). Together with its low power

consumption, which allows the microcontroller to be powered by battery, this device is an ideally suited component for building an on-board blowfly robot interface.

The firmware of the microcontroller has two subroutines in the main loop. The first subroutine implements the brain machine interface, which is continuously running in the background as a thread. It handles tasks, such as: neural signal sampling, signal processing (spike extraction, spike rate calculation, visual motor signal transformation) and robotic control signal generation. This subroutine is interrupted at 20 Hz, where the spikes over 50ms sampling period is averaged as spike rate for robot velocity conversion. The second subroutine establishes the UART communication, which is updating the control signal to the robot. The subroutine is called at 20 Hz as well.

Alternatively, the inter-spike interval (ISI) algorithm can be used to calculate the spike rate, which is based on the time between two adjacent action potentials. The advantage of using the ISI algorithm is short latency, but the disadvantage is its high sensitivity to noise. The ISI would be the algorithm of choice if short latency were critical for design of closed-loop control law.

The programme run on the NXP LPC1768 is compiled by an mbed® online integrated development environment (IDE) software, which can generate the firmware by an integrated ARM C compiler. The source code is provided in the appendix (appendix 2).

From the program, the sampling frequency of the ADC module is set to 5 KHz. Each sample of the recording is compared with a threshold voltage, which is determined from the oscilloscope before starting the experiment and programmed in to the robot. A positive crossing of the threshold value is regarded as a spike, which is used to generate the spike raster (action potential occurrences on time axis) as a binary vector. The raster is stored in a first in first out (FIFO) array with a size of 250 samples, which corresponds to a sampling interval of 50 ms. An estimation of the time-continuous spike rate is then obtained by averaging over the past time interval.

The next stage is to translate the spike rate estimate into a robot control signal. Based on the H1-cell response characterization described in the previous chapter, the cell's velocity tuning curve obtained in the laboratory as a visual environment (Fig. 32) is used as a input-output function of the controller. Instead of programming the slightly logarithmic relationship between spike rate and angular velocity, I programmed a linear relationship where 100 and 300 spikes/s correspond to the minimum and maximum angular velocity of the robot, respectively.

Finally, the PWM voltage signal for the robot motor control, which was derived from the time-continuous H1-cell spike rate and reflects the angular velocity of the robot, is calculated and transmitted to the robot through the UART.

4.3.1.3. System assembly

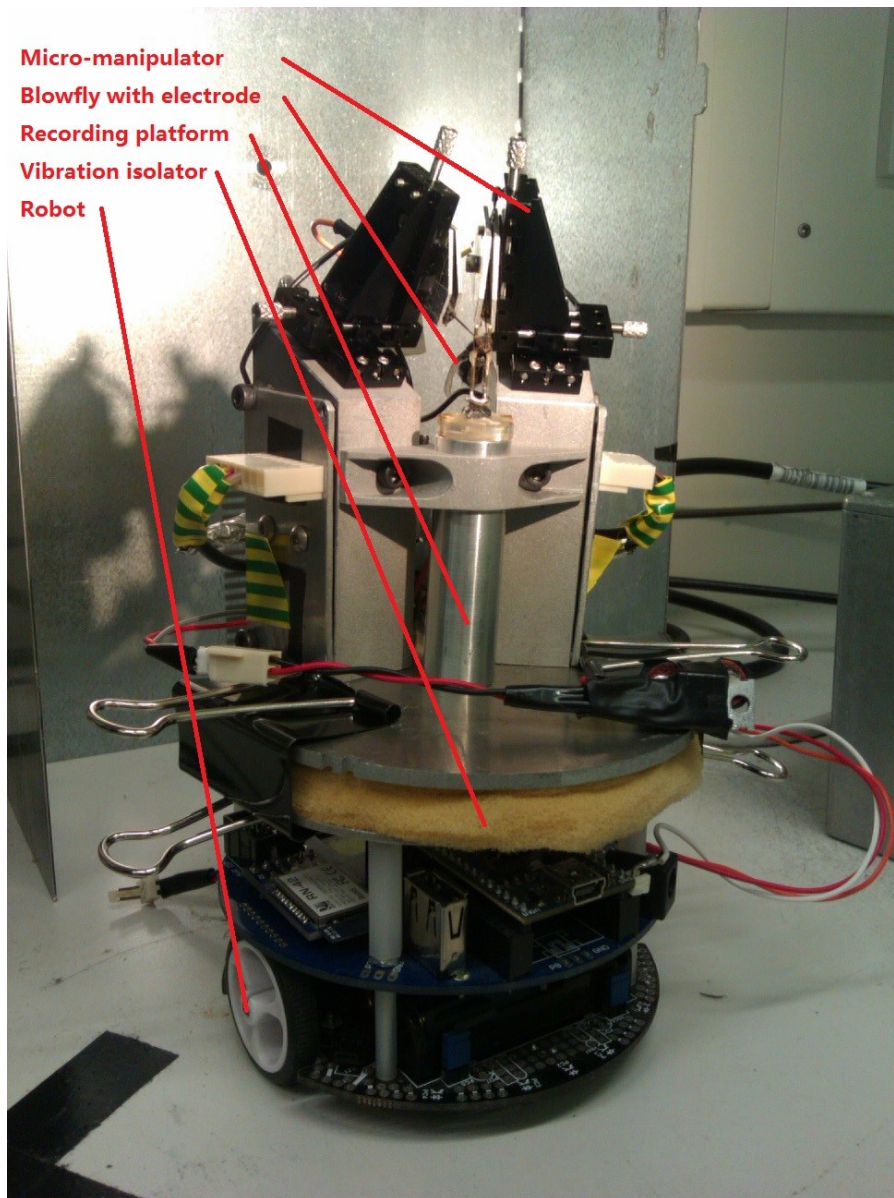


Figure 44. Full assembled fly-robot interface system. The mini-micromanipulators are used for electrodes placement. The blowfly is fixed in the rotating centre of the recording platform. The platform is insulated from mechanical vibrations of the motors driving the wheels by a damping layer made from a piece of sponge. The 3pi robot (diameter 94 mm) serves as spatial scaling reference in this figure.

After blowfly preparation and programming the robot interface, the two subsystems, i.e. the miniaturized recording platform and the 2-wheeled robot were combined (Fig 43). The sponge in between platform and robot is used to isolate the recording platform from the high frequency mechanical vibrations caused by the motors. Electrical connections for signal transmission between recording platform and robot are provided by 3.5 mm jack plugs and sockets.

4.3.2. Results

After two electrodes were inserted at appropriate recording positions, the amplifiers were properly working and transmitted spikes of both H1-cells. Unfortunately, an unexpected crosstalk issue arose, where each electrode was meant to record its contralateral H1-cell, but picked up the signals from both H1-cells when both amplifiers are powered. Spike detection by a simple threshold became problematic. Voltage peaks were not only generated as a result of spikes generated by the recorded H1-cell, but also due to the electrical cross talk between the amplifiers. This meant a simple threshold detection algorithm was not suited to selectively convert spikes of a given H1-cell into a specific set of unit pulses. Luckily, the cross talk signals had smaller amplitudes than the recorded spikes. So a simple sorting algorithm was used in addition to the threshold-based detection which took into account the peak amplitude to distinguish between the spikes of the two H1-cells.

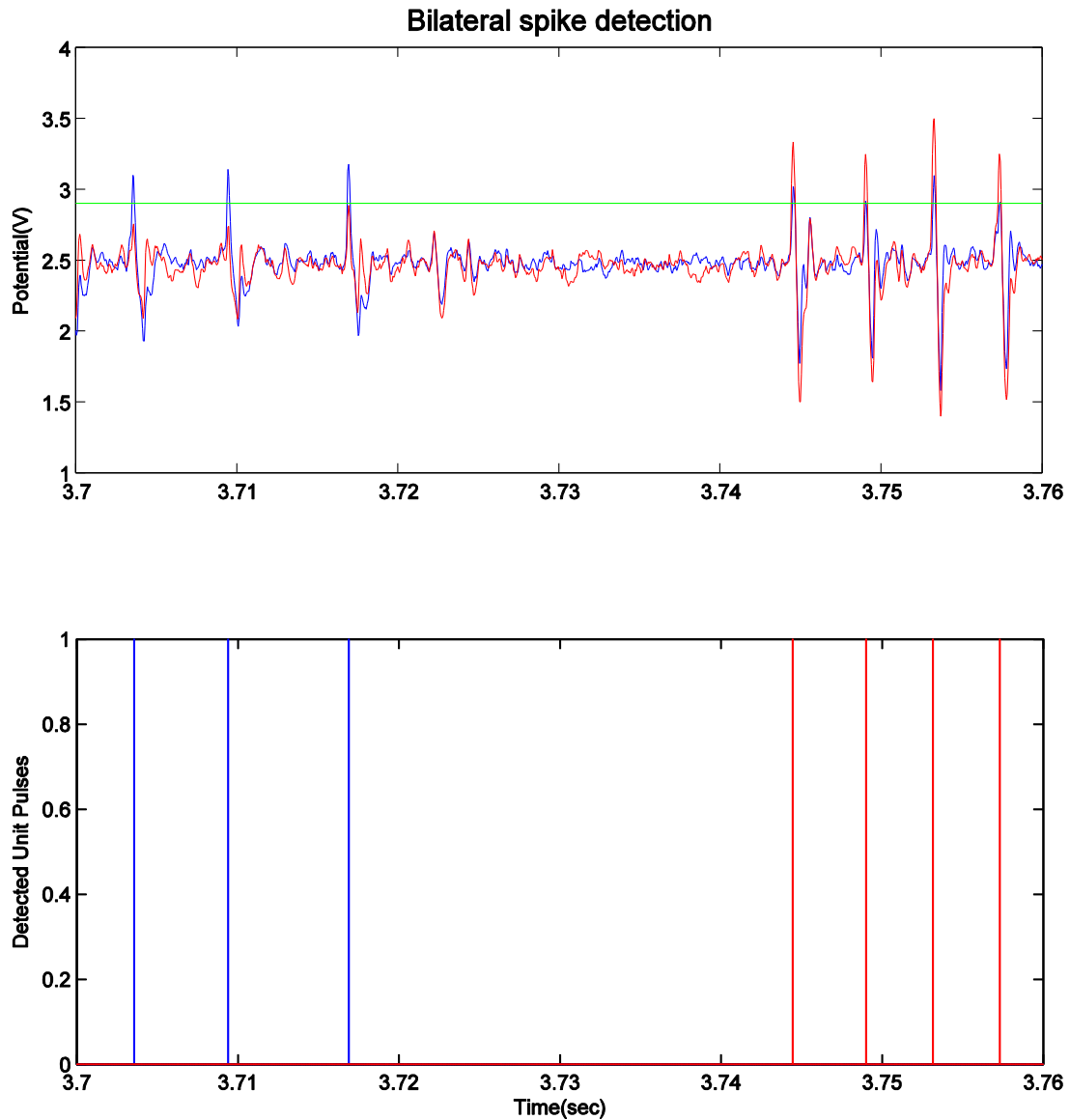


Figure 45. Bilateral H1-cell action potential detection. (top) The blue and red signals are recorded from different H1-cells. The green line is the threshold voltage for spike sorting. In this experiment crosstalk between the two recording channels occurred. Based on the different spike amplitudes of generated by the two H1-cells. The signals of the two cells could be separated in software. (bottom) The accurately detected spikes of the two H1-cells. Blue and red vertical lines indicated the detection of spikes of the ipsilateral and contralateral H1, respectively.

After sorting out the genuine H1-cell action potentials from cross-talk noise, each wheel of the robot could be rotated according to the spike rate from each corresponding contralateral H1-cell.

4.3.3. Discussion

In this experiment, the brain machine interface between the H1-cells and the robot was implemented, and tested under open-loop conditions.

The brain machine interface on the microcontroller allows the robot to rotate the wheels based on the ambient horizontal image motion, or optic flow experienced by the blowfly. The robot is capable of move forward when other objects are approaching laterally from behind. The rotating of the wheel was tested with robot being suspended. It is still an open loop condition, since the rotation of the wheel did not generate global optic flow and thus there was no feedback due to movements of the robot.

As a starting point of building an on-board blowfly robot interface, the transfer function of the interface is a relatively simple inverted model of the H1-cell velocity tuning obtained in the laboratory environment (Fig 32) as described in the previous chapter. Mechanosensory integration appears not to be reflected in H1-cell responses – at least not with respect to the average firing rate.

As VS-cells, on the other hand, are synaptically connected to descending neurons (Wertz et al., 2009), haltere signal integration may show an impact on the responses to visual motion in the spiking V1 cell –which has also been shown to reflect inputs to the ocelli system (Parsons et al., 2006). In the future H1-cell responses will be used for robotic control and V1-cell responses will be analysed regarding multisensory integration.

Regarding the crosstalk problem, one of the solutions would be to have two amplifier components, a head stage (pre-amplifier) and separate AC-amplifier stage, as realized in commercial amplifiers. The head stage amplifier would be a low gain stage placed as close as possible to the recording site, while the second amplifier stage provides high gain and would be placed as close as possible to the ADC module. The amplified microvolt signal in the cable is less likely to interfere with other pre-amplified signal through radio frequency.

In the future, more sophisticated interfaces could be implemented where, for instance, the flies will be mounted in a way that enables tethered flight, while recording the responses of LPTCs (*Drosophila*: (Maimon et al., 2010), *Calliphora*: (Jung et al., 2011)) on top of the robot. Such a setup would also permit to analyse the wing beat amplitude as a behavioural output parameter to close the loop between the fly and the robot. At the same time the behavioural output and the neuronal signals may be correlated while different

sensory systems are enabled or switched off. More details will be discussed in next chapter.

4.4. Summary

In this chapter, I have described the implementation of a basic brain machine interface as a proof of concept and tested it under open-loop conditions. I demonstrated that the wheels of a two wheel ground-based robot could be controlled independently by the neuronal signals of the two H1-cells in the left and right parts of the blowfly's visual system. Two experiments were carried out to assess the performance of the system.

The first experiment (section 4.2) established the relationship between the PWM signal and the angular rotation of the robot. To this end I used a high speed camera to monitor the angular velocity of the robot, while the robot was pre-programmed with a speed profile. The acceleration curve and deceleration curve, show a linear relationship between angular velocity of the robot and the input PWM signal. This is a good prerequisite for robotic closed-loop control, where the controller can treat its transfer function as a constant gain.

In a second experiment (section 4.3) I implemented a brain machine interface – including the required hardware and software components. An inverted model from H1-cell temporal frequency tuning was used for the transformation of spike rate into independent motor signals driving the two wheels. Future modifications of the amplifier circuits will have to be made to avoid crosstalk issues between the two amplifiers used which, in case of my experiment, could be resolved by means of a software solution.

5. Summary and future work

5.1. Summary

The main objective of this project was to establish a brain machine interface between a blowfly and a suitable 2-wheeled robot. My work provides the basis for an experimental platform that will enable studies on multisensory integration under closed-loop conditions.

The greatest challenge in this project was to reduce the size and weight of electrophysiological equipment commonly used from about 5 kg and 0.5m x 0.5m x 0.2m (Narishige® micromanipulators and NPI® amplifier) to the 500 g and Ø100mm x 50mm, respectively, so it could be mounted on top of an m3pi robot. To this end I designed a small platform which met the size and weight constraints while still providing sufficient mechanical stability and vibration damping enabling stable extracellular recording over extended periods of time.

The core part of the interface is a miniaturized extracellular recording platform, described in chapter 2. The amplifier was made by off-the-shelf components with a customized PCB, which is small, light-weight, low-power, cheap, while achieving sufficient gain and bandwidth to monitor spiking activity in the blowfly motion vision system. Using the platform, the H1-cell responses could be investigated while either the fly was rotated within a stationary visual pattern or the pattern was rotated around the stationary fly.

Stepper motors were used to test the recording platform. The H1-cell of the blowfly was recorded under two different conditions across various temporal frequencies up to 20 Hz. The data obtained upon pattern rotation were in agreement with previously published results regarding the cell's temporal frequency/velocity tuning (Jung et al., 2011; Maddess and Laughlin, 1985). Rotating an fly in a static visual environment was essentially a novel experimental condition where the fly could access both visual and mechanosensory information.

In chapter 3, I described four experiments to characterize H1-cell responses using the miniaturized recording platform as a function of stimulus parameters relevant for later closed-loop experiments, again upon fly rotation and pattern rotation. The first experiment showed the mean values of the temporal frequency tuning of the H1-cell (a) did not show differences between the two conditions and (b) were agreement with data found in the literature. The second experiment showed no difference on H1 temporal frequencies tuning before and after removal of halteres, although the velocity turning curves between grating stimulus and laboratory environment were found to be qualitatively different. In the third experiment I characterized the relationship between vertical angular extent of the visual pattern and H1-cell spike rate. It revealed a near-linear relationship between angular extent and H1-cell spike rate. The fourth experiment was a proof of concept. It shows the feasibility to generate linear control signals for rotating the robot using the spikes rate of the H1-cell.

While most of the results were in agreement with previous publications, in some cases the findings I obtained using my recording platform were in contradiction with theoretical predictions, for instance, regarding size-dependent responses of LPTCs in the fly motion vision pathway (section 3.4).

Finally, in chapter 4, the blowfly robot interface system is implemented. After angular velocity calibrations of the robot, the fly robot interface, which converts the output from the amplifier into signals for motor control, was developed based on velocity tuning curve (Fig. 32) and programmed into the microcontroller of the robot. The system was able to react to surrounding optic flow received by the blowfly's compound eyes in an approximation of a simple semi-closed-loop control test (appendix 3).

5.2. Future work

The final goal of this project is to study the neural mechanisms of multisensory integration supporting blowfly gaze and flight control.

5.2.1. Optomotor

Some previous work (Jung et al., 2011; Maimon et al., 2010) has shown the possibilities of combining behavioural and physiological experiment. In these experiments neural activity was recorded while monitoring motor activity the animals generated, for instance walking (Chiappe et al., 2010) or flying (Jung et al., 2011) under tethered conditions.

As I described earlier in my thesis, the bio-hybrid silkmoth robot (Minegishi et al., 2013) had implemented a closed-loop control, which is able to find odour sources by adjust its angular velocity with sensory feedbacks caused by its behaviour.

Closed-loop control is the next step of this project. A possible extension of the functionality of the miniaturized recording platform would be to modify the fly holder so that both electrophysiological recordings can be performed while simultaneously monitoring behavioural output parameters. The fly could be fixed in a way where only the head is immobilized, legs and wings are left free to move. The LPTC activity could still be recorded, but in addition the wing beat amplitudes could be monitored. Differences between the left and right wing beat amplitude are indicative of the yaw torque the fly tries to generate and could be used for closed-loop control as frequently done in *Drosophila* optomotor experiments (Frye, 2010; Tammero and Dickinson, 2002).

There are still unsolved questions in this thesis. Regarding to the angular extent experiment (section 3.4), my results are slightly different from those previously published. The spike rate increased linearly, when the angular extent was increased rather than assuming a plateau value that depends on image velocity as previously reported (Borst et al., 1995). Partly these contradictory results may be explained based on different wide-field stimulation arrangements between my experimental setup and those used in other studies. While in my experiments flies received input over an azimuthal range of ± 90 deg, effectively stimulating both eyes, other studies provided only monocular input within a limited azimuth range. The way to test this explanation would be to perform the same experiments in my setup again, but to cover the eyes except for an aperture of the size that was used in the

experiments by Hausen (Hausen, 1982). Along those lines, an experiment only covering one eye would show whether the linear relationship between H1-cell response and pattern extent is established by binocular interactions, which could be mediated by the heterolateral networks of horizontal cells.

Regarding to the adaptation experiment (section 3.5), it is still an open question that how does the motion adaptation work? And is it related to the locomotor state change? In future experiments, after the free wing beat recording and wing beat analyser are implemented, it will be easier to observe state change from behaviour activity, e.g. wing beat, and analyse the adaptation of visual cell activity at the same time.

In future, the parameters of open-loop experiments need more test. The experimental protocols are chosen to come closer to the expected closed-loop conditions. This could include experiments where the robot is following a left-right oscillatory trajectory and asymmetric distance distributions are systematically introduced by positioning visible objects at different distances while recording the activity of the H1-cells.

5.2.2. Multi-sensory integration

The multisensory integration experiments (section 3.3) of this thesis did not indicate a marked impact of mechanosensory systems on the activity of the H1-cell. Such impact which should have been revealed by differences in the results obtained during fly or pattern rotation.

A clear indication of multisensory integration has been shown for the V1 cell, another spiking LPTC which receives input from the VS-cells. Interactions between the two visual systems, compound eyes and ocelli, have been shown in extracellular V1 cell recordings (Parsons et al., 2006). They were interpreted as a result of the VS cells being electrically coupled to descending neurons (Strausfeld and Seyan, 1985) which receive input from several sense organs including the antennae, ocelli, and compound eyes. Descending neurons are very likely to be the major stage for multisensory integration (Taylor and Krapp, 2007; Wertz et al., 2008) and are connected to the neck

and the flight motor system. Motor neurons of the flight motor system had also been shown to integrate sensory information from more than one sensor system. As mentioned earlier, some of the NMNs, for instance, receive input from the motion vision pathway provided by the compound eye and from the halteres (Huston and Krapp, 2009). These inputs have to arrive simultaneously at the NMNs for them to generate action potentials, so they establish a non-linear gating function (Huston and Krapp, 2009).

It is very likely that V1 cell activity does reflect some aspects of multisensory integration. The cell can be recorded in the future in a similar way as the H1-cell was characterized in this thesis.

5.2.3. Closed loop control

There are two independent lines of evidence that the signals of LPTCs can be used for a potential closed loop control.

Firstly, studies from the Egelhaaf lab revealed that HS cell signals, if compared between the left and right cell, provide sufficient information for differential distance estimation. Simply put, the cell that shows higher activity during a translation phase indicates a closer distance to objects, information that could be used to generate a turn in the opposite direction (Karmeier et al., 2006; Lindemann et al., 2005). The relevance of the HS cells in distance estimation was proposed after the analysis of flight trajectories under semi-free flight conditions (Hateren and Schilstra, 1999). In a 0.4 m³ environment, *Calliphora* displayed a stereotyped flight pattern where phases of sudden yaw rotations were followed by phases of almost pure translations along a mixture from thrust and side-slip. During those phases where rotational optic flow is nearly zero, the integrated response of wide-field field optic flow processing LPTCs should be determined by two parameters: translation speed and the distance to objects in the environment (Dahmen et al., 2001; Franz and Krapp, 2000; Koenderink and Doorn, 1987; Krapp, 2000). As translation speed would be the same for cells in either half of the brain the remaining difference in the responses of the left and right HS cell would be due to different distances (Lindemann et al., 2005).

Secondly, research into the application of biological principles of optic flow processing (Krapp, 2000) for micro air vehicle control provided an independent proof of concept that the activity of LPTCs may be used to control distance to visual objects and other flight related parameters (Hyslop et al., 2010).

During a straight forward translation both H1-cells would be more or less entirely inhibited due to their motion preference for back-to-front motion. A pre-programmed forward translation component superimposed by a regular pattern of alternating left-right rotations can be a solution. The amplitude of the next rotation would be chosen depending on the H1-cell activity measured within a certain integration time window.

Such a strategy of 'active vision' would be inspired by free flight behaviour observed in *Calliphora* and *Lucilia* and may be an ideal starting point for addressing a number of outstanding questions which could not have been tackled before: (i) how are signals from multiple sensory modalities integrated under closed-loop conditions? – as posed before, (ii) is there any evidence for flies using forward-models when analysing optic flow information during self-motion? (A forward model is a prediction of the sensory consequences of a self-generated motor action. Such model could increase the efficiency of motor control strategies. Whenever there is a mismatch between the forward model and the actually measure sensory feedback, the resulting difference may be used as an error signal to adjust the gains of the motor commands (Wolpert et al., 1995)), and (iii) will flies in such a closed-loop setting adapt their neural responses to the changed dynamics of their self-motion?

Bibliography

Bausenwein, B., Dittrich, A.P., and Fischbach, K.F. (1992). The optic lobe of *Drosophila melanogaster*. II. Sorting of retinotopic pathways in the medulla. *Cell Tissue Res.* 267, 17–28.

Beersma, D.G.M., Stavenga, D.G., and Kuiper, J.W. (1977). Retinal lattice, visual field and binocularities in flies. *J. Comp. Physiol.* 119, 207–220.

Bomphrey, R.J., Walker, S.M., and Taylor, G.K. (2009). The Typical Flight Performance of Blowflies: Measuring the Normal Performance Envelope of *Calliphora vicina* Using a Novel Corner-Cube Arena. *PLoS ONE* 4, e7852.

Borst, A., and Egelhaaf, M. (1989). Principles of visual motion detection. *Trends Neurosci.* 12, 297–306.

Borst, A., and Haag, J. (1996). The intrinsic electrophysiological characteristics of fly lobula plate tangential cells: I. Passive membrane properties. *J. Comput. Neurosci.* 3, 313–336.

Borst, A., and Haag, J. (2002a). Neural networks in the cockpit of the fly. *J. Comp. Physiol. A* 188, 419–437.

Borst, A., and Haag, J. (2002b). Neural networks in the cockpit of the fly. *J. Comp. Physiol. A* 188, 419–437.

Borst, A., Egelhaaf, M., and Haag, J. (1995). Mechanisms of dendritic integration underlying gain control in fly motion-sensitive interneurons. *J. Comput. Neurosci.* 2, 5–18.

Buchner, E. (1984). Behavioural Analysis of Spatial Vision in Insects. In *Photoreception and Vision in Invertebrates*, M.A. Ali, ed. (Springer US), pp. 561–621.

Bult, R., Schuling, F.H., and Mastebroek, H.A. (1991). Circadian inputs influence the performance of a spiking, movement-sensitive neuron in the visual system of the blowfly. *J. Biol. Rhythms* 6, 55–69.

Chiappe, M.E., Seelig, J.D., Reiser, M.B., and Jayaraman, V. (2010). Walking Modulates Speed Sensitivity in *Drosophila* Motion Vision. *Curr. Biol.* 20, 1470–1475.

Dahmen, H.-J., Franz, M.O., and Krapp, H.G. (2001). Extracting Egomotion from Optic Flow: Limits of Accuracy and Neural Matched Filters. In *Motion Vision*, J.M. Zanker, and J. Zeil, eds. (Springer Berlin Heidelberg), pp. 143–168.

- Egelhaaf, M., and Borst, A. (1993). Movement detection in arthropods. *Rev. Oculomot. Res.* 5, 53–77.
- Egelhaaf, M., Grewe, J., Kern, R., and Warzecha, A.-K. (2001). Outdoor performance of a motion-sensitive neuron in the blowfly. *Vision Res.* 41, 3627–3637.
- Ejaz, N., Peterson, K.D., and Krapp, H.G. (2011). An Experimental Platform to Study the Closed-loop Performance of Brain-machine Interfaces. *J. Vis. Exp.*
- Ejaz, N., Krapp, H.G., and Tanaka, R.J. (2013). Closed-loop response properties of a visual interneuron involved in fly optomotor control. *Front. Neural Circuits* 7, 50.
- Franceschini, N. (1972). Pupil and Pseudopupil in the Compound Eye of *Drosophila*. In *Information Processing in the Visual Systems of Arthropods*, R. Wehner, ed. (Springer Berlin Heidelberg), pp. 75–82.
- Franceschini, N. (1975). Sampling of the Visual Environment by the Compound Eye of the Fly: Fundamentals and Applications. In *Photoreceptor Optics*, D.A.W. Snyder, and P.D.R. Menzel, eds. (Springer Berlin Heidelberg), pp. 98–125.
- Franz, M.O., and Krapp, H.G. (2000). Wide-field, motion-sensitive neurons and matched filters for optic flow fields. *Biol. Cybern.* 83, 185–197.
- Frye, M.A. (2010). Multisensory systems integration for high-performance motor control in flies. *Curr. Opin. Neurobiol.* 20, 347–352.
- Haag, J., Egelhaaf, M., and Borst, A. (1992). Dendritic integration of motion information in visual interneurons of the blowfly. *Neurosci. Lett.* 140, 173–176.
- Harris, R.A., O'Carroll, D.C., and Laughlin, S.B. (2000). Contrast Gain Reduction in Fly Motion Adaptation. *Neuron* 28, 595–606.
- Harrison, R.R., Fotowat, H., Chan, R., Kier, R.J., Olberg, R., Leonardo, A., and Gabbiani, F. (2011). Wireless Neural/EMG Telemetry Systems for Small Freely Moving Animals. *IEEE Trans. Biomed. Circuits Syst.* 5, 103–111.
- Hateren, J.H., and Schilstra, C. (1999). Blowfly flight and optic flow. II. Head movements during flight. *J. Exp. Biol.* 202, 1491–1500.
- Hausen, K. (1982). Motion sensitive interneurons in the optomotor system of the fly. *Biol. Cybern.* 46, 67–79.
- Hausen, K. (1984). The Lobula-Complex of the Fly: Structure, Function and Significance in Visual Behaviour. In *Photoreception and Vision in Invertebrates*, M.A. Ali, ed. (Springer US), pp. 523–559.
- Hausen, K. (1993). Decoding of retinal image flow in insects. *Rev. Oculomot. Res.* 5, 203–235.

- Heisenberg, M., and Buchner, E. (1977). The rôle of retinula cell types in visual behavior of *Drosophila melanogaster*. *J. Comp. Physiol.* *117*, 127–162.
- Hengstenberg, R. (1977). Spike responses of “non-spiking” visual interneurone. *Nature* *270*, 338–340.
- Hengstenberg, R. (1991). Gaze control in the blowfly *Calliphora*: a multisensory, two-stage integration process. *Semin. Neurosci.* *3*, 19–29.
- Hengstenberg, R. (1993). Multisensory control in insect oculomotor systems. *Rev. Oculomot. Res.* *5*, 285–298.
- Huang, J.V., and Krapp, H.G. (2013). Miniaturized Electrophysiology Platform for Fly-Robot Interface to Study Multisensory Integration. In *Biomimetic and Biohybrid Systems*, N.F. Lepora, A. Mura, H.G. Krapp, P.F.M.J. Verschure, and T.J. Prescott, eds. (Springer Berlin Heidelberg), pp. 119–130.
- Huston, S.J., and Krapp, H.G. (2009). Nonlinear Integration of Visual and Haltere Inputs in Fly Neck Motor Neurons. *J. Neurosci.* *29*, 13097–13105.
- Hyslop, A., Krapp, H.G., and Humbert, J.S. (2010). Control theoretic interpretation of directional motion preferences in optic flow processing interneurons. *Biol. Cybern.* *103*, 353–364.
- Ishida, Y., and Ozaki, M. (2011). A putative octopamine/tyramine receptor mediating appetite in a hungry fly. *Naturwissenschaften* *98*, 635–638.
- Jebari, K. (2013). Brain Machine Interface and Human Enhancement – An Ethical Review. *Neuroethics* *6*, 617–625.
- Jung, S.N., Borst, A., and Haag, J. (2011). Flight Activity Alters Velocity Tuning of Fly Motion-Sensitive Neurons. *J. Neurosci.* *31*, 9231–9237.
- Karmeier, K., Tabor, R., Egelhaaf, M., and Krapp, H.G. (2001). Early visual experience and the receptive-field organization of optic flow processing interneurons in the fly motion pathway. *Vis. Neurosci.* *18*, 1–8.
- Karmeier, K., Hateren, J.H. van, Kern, R., and Egelhaaf, M. (2006). Encoding of Naturalistic Optic Flow by a Population of Blowfly Motion-Sensitive Neurons. *J. Neurophysiol.* *96*, 1602–1614.
- Kirschfeld, K., Franceschini, N., and Minke, B. (1977). Evidence for a sensitising pigment in fly photoreceptors. *Nature* *269*, 386–390.
- Koenderink, J.J., and Doorn, A.J. van (1987). Facts on optic flow. *Biol. Cybern.* *56*, 247–254.
- Krapp, H.G. (2000). Neuronal matched filters for optic flow processing in flying insects. *Int. Rev. Neurobiol.* *44*, 93–120.
- Krapp, H.G., and Hengstenberg, R. (1996). Estimation of self-motion by optic flow processing in single visual interneurons. *Nature* *384*, 463–466.

Krapp, H.G., and Hengstenberg, R. (1997). A fast stimulus procedure to determine local receptive field properties of motion-sensitive visual interneurons. *Vision Res.* *37*, 225–234.

Krapp, H.G., and Wicklein, M. (2008). 1.06 - Central Processing of Visual Information in Insects. In *The Senses: A Comprehensive Reference*, R.H. Masland, T.D. Albright, T.D. Albright, R.H. Masland, P. Dallos, D. Oertel, S. Firestein, G.K. Beauchamp, M.C. Bushnell, A.I. Basbaum, et al., eds. (New York: Academic Press), pp. 131–203.

Land, M.F., and Eckert, H. (1985). Maps of the acute zones of fly eyes. *J. Comp. Physiol. A* *156*, 525–538.

Laughlin, S. (1984). The Roles of Parallel Channels in Early Visual Processing by the Arthropod Compound Eye. In *Photoreception and Vision in Invertebrates*, M.A. Ali, ed. (Springer US), pp. 457–481.

Lewen, G.D., Bialek, W., and de Ruyter van Steveninck, R.R. (2001). Neural coding of naturalistic motion stimuli. *Netw. Bristol Engl.* *12*, 317–329.

Lindemann, J.P., and Egelhaaf, M. (2013). Texture dependence of motion sensing and free flight behavior in blowflies. *Front. Behav. Neurosci.* *6*, 92.

Lindemann, J.P., Kern, R., Hateren, J.H. van, Ritter, H., and Egelhaaf, M. (2005). On the Computations Analyzing Natural Optic Flow: Quantitative Model Analysis of the Blowfly Motion Vision Pathway. *J. Neurosci.* *25*, 6435–6448.

Longden, K.D., and Krapp, H.G. (2009). State-Dependent Performance of Optic-Flow Processing Interneurons. *J. Neurophysiol.* *102*, 3606–3618.

Longden, K.D., and Krapp, H.G. (2010). Octopaminergic Modulation of Temporal Frequency Coding in an Identified Optic Flow-Processing Interneuron. *Front. Syst. Neurosci.* *4*.

Maddess, T. (2001). Dynamic Effects in Real-Time Responses of Motion Sensitive Neurones. In *Motion Vision*, J.M. Zanker, and J. Zeil, eds. (Springer Berlin Heidelberg), pp. 321–329.

Maddess, T., and Laughlin, S.B. (1985). Adaptation of the Motion-Sensitive Neuron H1 Is Generated Locally and Governed by Contrast Frequency. *Proc. R. Soc. Lond. B Biol. Sci.* *225*, 251–275.

Maimon, G., Straw, A.D., and Dickinson, M.H. (2010). Active flight increases the gain of visual motion processing in *Drosophila*. *Nat. Neurosci.* *13*, 393–399.

Minegishi, R., Takahashi, Y., Takashima, A., Kurabayashi, D., and Kanzaki, R. (2013). Modification in Command Neural Signals of an Insect's Odor Source Searching Behavior on the Brain-Machine Hybrid System. In *Biomimetic and Biohybrid Systems*, N.F. Lepora, A. Mura, H.G. Krapp, P.F.M.J. Verschure, and T.J. Prescott, eds. (Springer Berlin Heidelberg), pp. 167–178.

Nalbach, G. (1993). The halteres of the blowfly *Calliphora*. *J. Comp. Physiol. A* 173, 293–300.

Pack, C.C., and Born, R.T. (2001). Temporal dynamics of a neural solution to the aperture problem in visual area MT of macaque brain. *Nature* 409, 1040–1042.

Parsons, M.M., Krapp, H.G., and Laughlin, S.B. (2006). A motion-sensitive neurone responds to signals from the two visual systems of the blowfly, the compound eyes and ocelli. *J. Exp. Biol.* 209, 4464–4474.

Peterson, K.D. (2010). Development of a micro recording probe for measurements of neuronal activity in freely moving animals. Ph.D. Imperial College London.

Reichardt, W. (1987). Computation of optical motion by movement detectors. *Biophys. Chem.* 26, 263–278.

Reichardt, W., and Egelhaaf, M. (1988). Properties of individual movement detectors as derived from behavioural experiments on the visual system of the fly. *Biol. Cybern.* 58, 287–294.

Reichardt, W., Poggio, T., and Hausen, K. (1983). Figure-ground discrimination by relative movement in the visual system of the fly. *Biol. Cybern.* 46, 1–30.

Rosner, R., Egelhaaf, M., Grewe, J., and Warzecha, A.K. (2009). Variability of blowfly head optomotor responses. *J. Exp. Biol.* 212, 1170–1184.

Schilstra, C., and van Hateren, J.H. (1998). Using miniature sensor coils for simultaneous measurement of orientation and position of small, fast-moving animals. *J. Neurosci. Methods* 83, 125–131.

Shimojo, S., Silverman, G.H., and Nakayama, K. (1989). Occlusion and the solution to the aperture problem for motion. *Vision Res.* 29, 619–626.

Stevenson, R., Corbo, K., Baca, L., and Le, Q. (1995). Cage size and flight speed of the tobacco hawkmoth *Manduca sexta*. *J. Exp. Biol.* 198, 1665–1672.

Strausfeld, D.N.J. (1976a). The Atlas: Sections through the Brain. In *Atlas of an Insect Brain*, D.N.J. Strausfeld, ed. (Springer Berlin Heidelberg), pp. 57–115.

Strausfeld, N.J. (1976b). The Atlas: Sections through the Brain. In *Atlas of an Insect Brain*, N.J. Strausfeld, ed. (Springer Berlin Heidelberg), pp. 57–115.

Strausfeld, N.J., and Lee, J.-K. (1991). Neuronal basis for parallel visual processing in the fly. *Vis. Neurosci.* 7, 13–33.

Strausfeld, N.J., and Seyan, H.S. (1985). Convergence of visual, haltere, and prosternal inputs at neck motor neurons of *Calliphora erythrocephala*. *Cell Tissue Res.* 240, 601–615.

Takeuchi, S., and Shimoyama, I. (2004). A radio-telemetry system with a shape memory alloy microelectrode for neural recording of freely moving insects. *IEEE Trans. Biomed. Eng.* *51*, 133–137.

Tammero, L.F., and Dickinson, M.H. (2002). Collision-Avoidance and Landing Responses Are Mediated by Separate Pathways in the Fruit Fly, *Drosophila Melanogaster*. *J. Exp. Biol.* *205*, 2785–2798.

Taylor, G.K., and Krapp, H.G. (2007). Sensory Systems and Flight Stability: What do Insects Measure and Why? In *Advances in Insect Physiology*, J. Casas and S.J. Simpson, ed. (Academic Press), pp. 231–316.

Tuthill, J.C., Nern, A., Holtz, S.L., Rubin, G.M., and Reiser, M.B. (2013). Contributions of the 12 neuron classes in the fly lamina to motion vision. *Neuron* *79*, 128–140.

Wang, H., Ando, N., and Kanzaki, R. (2008). Active control of free flight manoeuvres in a hawkmoth, *Agrius convolvuli*. *J. Exp. Biol.* *211*, 423–432.

Warwick K, Gasson M, Hutt B, and et al (2003). THE application of implant technology for cybernetic systems. *Arch. Neurol.* *60*, 1369–1373.

Wertz, A., Borst, A., and Haag, J. (2008). Nonlinear Integration of Binocular Optic Flow by DNOVS2, A Descending Neuron of the Fly. *J. Neurosci.* *28*, 3131–3140.

Wertz, A., Haag, J., and Borst, A. (2009). Local and global motion preferences in descending neurons of the fly. *J. Comp. Physiol. A* *195*, 1107–1120.

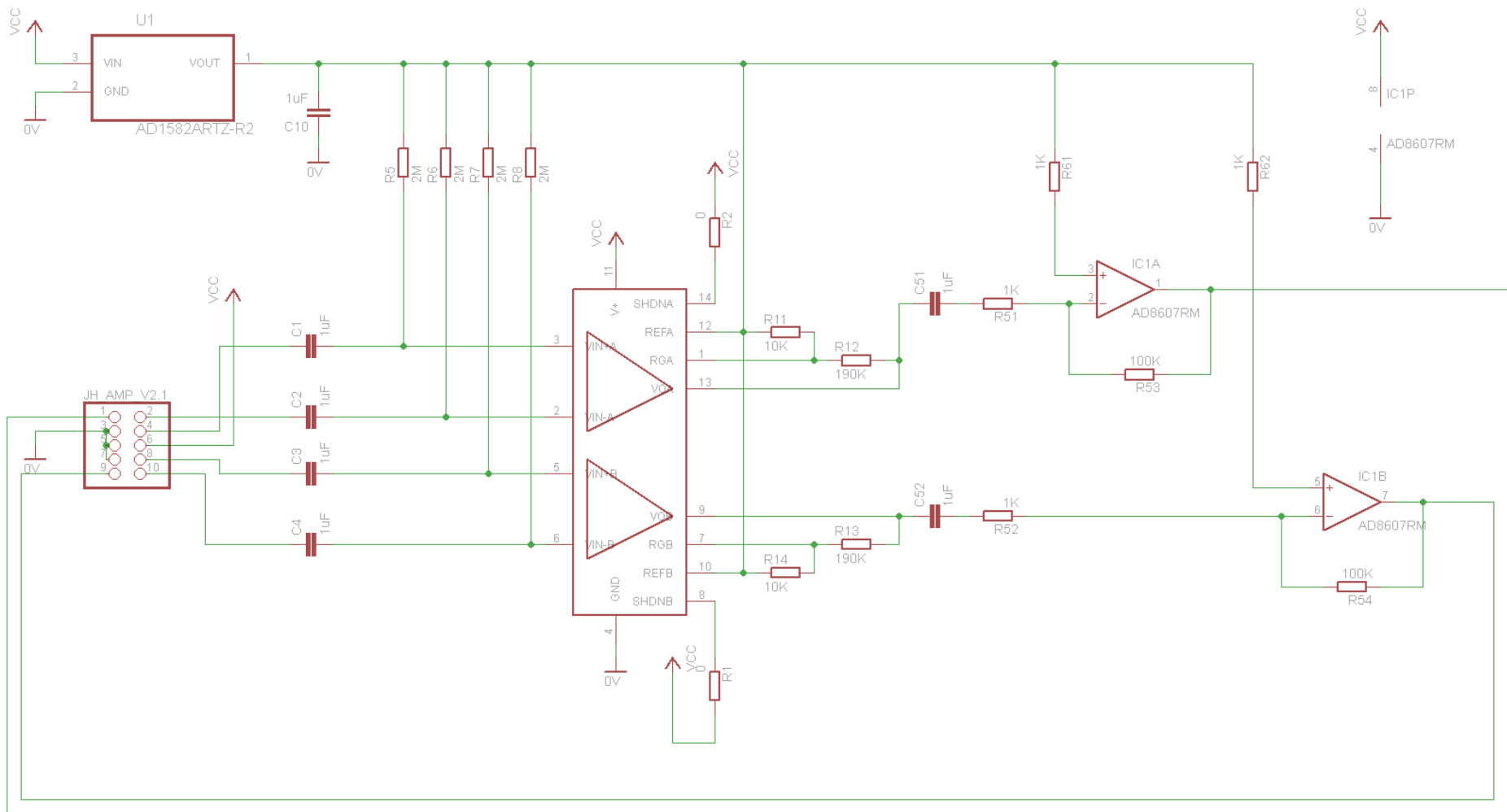
Whim, M.D., and Evans, P.D. (1989). Age-dependence of octopaminergic modulation of flight muscle in the locust. *J. Comp. Physiol. A* *165*, 125–137.

Wolpert, D.M., Ghahramani, Z., and Jordan, M.I. (1995). An internal model for sensorimotor integration. *Science* *269*, 1880–1882.

Zufferey Jean-Christophe Staff (2008). *Insect Inspired Flying Robots* (Boca Raton; Florence: C R C Press LLC Taylor & Francis Group [Distributor]).

Appendix

Appendix 1. Schematic of miniaturized amplifier



Appendix 2. Source code

- a. Stimulation protocol:

https://github.com/Blueasteroid/Blowfly-robot-interface/py_H1_3s_stim.py

- b. Fly-machine interface:

https://github.com/Blueasteroid/Blowfly-robot-interface/blob/master/m3pi_firmware_50ms-win-rate.cpp

Appendix 3. Video link

- a. H1-cell recording stability on top of miniaturized recording platform

Link: <https://www.youtube.com/watch?v=FAaEuLILbJM>

- b. Open-loop control of robot wheel by blowfly H1-cell robot interface

Link: <https://www.youtube.com/watch?v=PbTmX4bF3aU>